



University of
Stavanger

Faculty of Science and Technology

MASTER'S THESIS

| | |
|--|---|
| Study program/Specialization: Petroleum Technology /Reservoir Technology | Spring semester, 2016 Open / Restricted access |
| Writer: Ingrid Byberg | (Writer's signature) |
| Faculty supervisor: Karl Audun Lehne External supervisor(s): | |
| Thesis title Reservoir Characterization of the Skagerrak Formation in the Central North Sea | |
| Credits (ECTS): 30 | |
| Key words: Reservoir Characterization of three wells in the Central North Sea. | Pages: 143..... + enclosure: Stavanger, 15.06.2016 Date/year |

Table of Content

| | |
|---|-----------|
| Table of Content | 2 |
| 1 Acknowledgements | 9 |
| 2 Abstract..... | 10 |
| 3 Introduction | 11 |
| 4 The Skagerrak Formation | 12 |
| 4.1 General description of the Depositional Environment in the Skagerrak Formation | 13 |
| 4.1.1 Alluvial Fan..... | 13 |
| 4.2 Brief geological history and Depositional Environment..... | 15 |
| 4.2.1 The Skagerrak Lithology..... | 16 |
| 4.2.2 The Lithostratigraphy..... | 17 |
| 5 The Sleipner Area..... | 18 |
| 5.1 The Sleipner Øst Field and Well 15/9-9..... | 19 |
| 5.2 The Gungne Field and Well 15/9-15 | 19 |
| 5.3 The Loke Field and Well 15/9-17 | 20 |
| 6 Zonation of the wells | 20 |
| 7 Fluid Contacts | 22 |
| 8 Log Quality | 23 |
| 9 Geological Evaluation | 26 |
| 9.1 The Depositional Environment in the Skagerrak Formation..... | 27 |
| 9.1.1 Well 15/9-9, The Sleipner Øst Field | 27 |
| 9.1.2 Well 15/9-15, The Gungne Field | 31 |
| 9.1.3 Well 15/9-17, The Loke Field | 33 |
| 9.2 Well 6510/2-1 from Norwegian Sea, Mid Norway | 36 |
| 9.3 Correlation of Well 15/9-9, 15/9-15 and 15/9-17 | 38 |
| 10 Petrophysical Theory | 40 |
| 10.1 Petrophysical Parameters..... | 40 |
| 10.1.1 Clay Rich Formations..... | 40 |
| 10.1.2 Porosity | 43 |
| 10.1.3 Permeability..... | 44 |
| 10.1.4 Water saturation, Sw | 44 |
| 10.1.5 Formation Factor F and F* | 46 |
| 10.1.6 Cementation Exponent (m) and Tortuosity Factor (a) | 48 |

| | | |
|--------|--|----|
| 10.1.7 | The Archie's Equation | 48 |
| 10.1.8 | The Indonesian Equation | 50 |
| 10.1.9 | The Waxman Smits Equation | 50 |
| 10.2 | The Saturation Modelling | 52 |
| 10.2.1 | The Capillary Pressure..... | 52 |
| 10.2.2 | Interfacial Tension and Surface Tension..... | 53 |
| 10.2.3 | The Capillary Pressure Curve and Irreducible Water Saturation (Swirr)..... | 54 |
| 10.2.4 | The Free Water Level (FWL) and the Gas Water Contact (GWC)..... | 56 |
| 10.2.5 | The Leverett J-function | 57 |
| 11 | Well testing..... | 58 |
| 11.1 | Pressure Transient Test and Pressure Transient Analysis..... | 58 |
| 11.1.1 | Wellbore Storage (WBS) | 59 |
| 11.1.2 | Skin | 59 |
| 11.1.3 | Identification of the Infinite Acting Radial flow and kh | 60 |
| 11.1.4 | The Radius of Investigation | 60 |
| 11.2 | Permeability in Well Tests | 61 |
| 12 | Core Data Evaluation | 62 |
| 12.1 | Depth shift of core data..... | 62 |
| 12.2 | Grain density from cores | 63 |
| 12.3 | Overburden correction | 64 |
| 12.4 | Cementation exponent, m..... | 64 |
| 12.5 | Saturation exponent, n..... | 67 |
| 13 | Petrophysical Model..... | 69 |
| 13.1 | Clay Volume..... | 69 |
| 13.2 | Porosity | 70 |
| 13.2.1 | Cross plot derived from density- neutron logs..... | 70 |
| 13.2.2 | Effective Porosity Determination | 72 |
| 13.2.3 | Total Porosity Determination | 73 |
| 13.3 | The Permeability determination | 75 |
| 13.4 | Ratio of Vertical to Horizontal Permeability | 77 |
| 13.5 | Formation Temperature | 79 |
| 13.6 | Formation Water resistivity, R_w , determination | 79 |
| 14 | Water saturation model | 80 |
| 14.1 | Water saturation modelling from core and log data | 80 |
| 14.2 | Water saturation from log data..... | 81 |
| 14.3 | Water Saturation from core data | 83 |

| | | |
|--------|---|-----|
| 14.3.1 | Capillary Pressure Curves..... | 83 |
| 14.3.2 | Irreducible water saturation, Swirr | 85 |
| 14.3.3 | Normalisation of the Water Saturation..... | 86 |
| 14.3.4 | J-function and Water Saturation (Sw) from cores..... | 87 |
| 14.3.5 | Water saturation from cores in the reservoir | 90 |
| 14.4 | Water Saturation from combined method..... | 90 |
| 14.5 | The Swirr Equation determined from logs | 91 |
| 14.6 | Water Saturation from core method with adjusted Swirr from logs..... | 94 |
| 14.7 | Water Saturation where J-function and normalised Sw created from logs | 94 |
| 14.8 | Method with Swr | 96 |
| 15 | Evaluation of DST from well 15/-9-15,Gungne Field..... | 98 |
| 15.1 | Introduction | 98 |
| 15.2 | Interpretation of DST 1 | 99 |
| 15.3 | Testing of different fault models..... | 101 |
| 16 | Result | 106 |
| 16.1 | Geology | 106 |
| 16.2 | Porosity, Permeability and Cut offs..... | 107 |
| 16.3 | Averages from Cut offs | 110 |
| 16.4 | Results from Water Saturation Modelling | 113 |
| 16.5 | Result of DST Evaluation..... | 118 |
| 17 | Conclusion..... | 119 |
| 18 | Nomenclature | 120 |
| 19 | References | 122 |
| 19.1 | Written references | 122 |
| 19.2 | Oral References | 125 |
| 19.3 | Software | 125 |
| 19.4 | Illustrations used in the thesis..... | 125 |
| 20 | Appendix CPI-Plot..... | 126 |
| 20.1 | Appendix Geological Data | 130 |
| 20.1.1 | Correlation of the Skagerrak Formation..... | 130 |
| 20.2 | Appendix Petrophysical Data | 132 |
| 20.2.1 | Plots of Core Porosity vs. Permeability with Vclay..... | 132 |
| 20.2.2 | Averages from Cut off..... | 134 |
| 20.2.3 | Vclay Averages | 136 |
| 20.3 | Water saturation methods | 137 |
| 20.3.1 | Swirr from Indonesia, Archie and Waxman Smits..... | 137 |

| | | |
|--------|---|-----|
| 20.3.2 | Swn determined from logs | 141 |
| 20.3.3 | Determination of B in the Waxman Smits Method | 142 |

List of Tables

| | | |
|------------|--|---|
| Table 6-1 | Zonation of all three well in the Sleipner Area | 21 |
| Table 7-1 | Contacts in the wells..... | 22 |
| Table 8-1 | Bit size used in all three wells in the Skagerrak Formation [1]..... | 24 |
| Table 9-1 | Correlating zones in well 15/9-15 and 15/9-17 | 38 |
| Table 10-1 | Contact angles and Interfacial tension | 54 |
| Table 12-1 | Depth shift of core data, well 15/9-15 and well 15/9-17..... | 63 |
| Table 12-2 | Grain density values from Well 15/9-9, 15/9-15 and 15/9-17 | 64 |
| Table 12-3 | a, m and n values used in Skagerrak evaluation | 68 |
| Table 12-4 | a, m* and n* determination in all wells..... | 69 |
| Table 13-1 | used Gamma ray values in Vclay determination..... | 70 |
| Table 13-2 | Input for the total porosity calculations | 74 |
| Table 13-3 | Correlations from core permeability vs. core porosity used in the KLOGH evaluation..... | 76 |
| Table 13-4 | Formation temperatures in Skagerrak Formation | 79 |
| Table 13-5 | Rw determination..... | 80 |
| Table 14-1 | Waxman Smits Qv, B, T..... | 82 |
| Table 14-2 | Regression constants from the Swn core equation in well 15/9-15 and 15/9-17 | 89 |
| Table 14-3 | Parametes in J res equation..... | 91 |
| Table 14-4 | a and b for the SWIRRR equation for logs, well 15/9-15, Gungne Field..... | 91 |
| Table 14-5 | a and b for the SWIRR equation for logs, well 15/9-17, Loke Field | 92 |
| Table 14-6 | Swirr a and b..... | 93 |
| Table 14-7 | a and b determined from log methods, well 15/9-17..... | 95 |
| Table 15-1 | Perforation interval for DST 1 and DST 2 in well 15/9-15 | 99 |
| Table 15-2 | Input data for the interpretation [ref] well test report PL 046 RFT, DST no 1 and No. 2 Well 15/9-15 LET-SVG february 1983. Engineer K.Kviljo..... | 99 |
| Table 15-3 | The results from DST 1..... | 101 |
| Table 16-1 | Average permeability values for the Skagerrak Formation..... | 108 |
| Table 16-2 | Average values by using cut off values $k > 0.05$ and $\phi > 0.1$ | 111 |
| Table 16-3 | Average values by using cut off values $k > 0.05$ and $\phi > 0.1$ | 111 |
| Table 16-4 | Average values by using cut off values $k > 0.05$ and $\phi > 0.1$ | 112 |
| Table 21-1 | Average values by using cut off values $k > 0.05$, $\phi > 0.1$, $V_{cl} = 0.5$, well 15/9-9 | 134 |
| Table 21-2 | Average values by using cut off values $k > 0.05$, $\phi > 0.1$, $V_{cl} = 0.5$ 15/9-15..... | 134 |
| Table 21-3 | Average values by using cut off values $k > 0.05$, $\phi > 0.1$, $V_{cl} = 0.5$ 15/9-17 | 135 |
| Table 21-4 | Swirr determined from core and log methods | 140 |
| Table 21-5 | a and b determined from log methods, well 15/9-15..... | 142 |
| Table 21-6 | Coring interval, well 15/9-9, Sleipner Øst | Feil! Bokmerke er ikke definert. |
| Table 21-7 | Coring interval, well 15/9-15, Gungne Field | Feil! Bokmerke er ikke definert. |
| Table 21-8 | Coring interval, well 15/9-17, Loke Field | Feil! Bokmerke er ikke definert. |

List of Figures

| | |
|---|----|
| Figure 4-1 Map of Southern North Sea [1] | 12 |
| Figure 4-2 Schematic channels and plains of braided river system, CPI from Zone 5 in well 15/9-15, Gungne Field | 14 |
| Figure 4-3 Meandering rivers and plain, CPI from Zone 4 in well 15/9-15, Gungne field | 15 |
| Figure 4-4 Lithostratigraphy of Skagerrak Formation [1]..... | 18 |
| Figure 5-1 Map over the Sleipner Area, Central North Sea [1] | 19 |
| Figure 7-1 RFT pressure data [13] from well 15/9-15 and well 15/9-17 | 23 |
| Figure 8-1 Caliper vs. RHOB vs. NPHI, well 15/9-9 | 24 |
| Figure 8-2 Caliper vs. RHOB, vs. NPHI, well 15/9-15..... | 25 |
| Figure 8-3 Caliper vs. RHOB vs. NPHI, well 15/9-17..... | 26 |
| Figure 9-1 Core samples and CPI from upper part of the Skagerrak Formation, well 15/9-9 [1] | 29 |
| Figure 9-2 Core samples and CPI from lower part of the Skagerrak Formation, well 15/9-9 | 31 |
| Figure 9-3 Core sample and CPI from Zone 5 in Skagerrak Formation, Well 15/9-15..... | 33 |
| Figure 9-4 core sample and CPI from Top of the Skagerrak Formation, zone 8, well 15/9-17..... | 34 |
| Figure 9-5 Core sample and CPI from 15/9-17 | 35 |
| Figure 9-6 Location of the well 6510/2-1 | 36 |
| Figure 9-7 RHOB vs. NPHI for all wells..... | 37 |
| Figure 9-8 correlating zones in the Skagerrak Formation including CPI from well 6510/7-..... | 39 |
| Figure 10-1 Clay distributions..... | 41 |
| Figure 10-2 T Total porosity vs. Effective porosity [17] | 44 |
| Figure 10-3 Excess conductivity contributed by clay | 47 |
| Figure 10-4 Capillary Pressure vs. Water Saturation | 55 |
| Figure 10-5 Variation of Pc with Sw for the same fluid with different rock systems | 56 |
| Figure 11-1 Log- log plot from DST1, well 15/9-15..... | 61 |
| Figure 12-1 Core porosity properties in well 15/9-9, 15/9-15 and 15/9-17 | 62 |
| Figure 12-2 Histogram of most common grain density in all three wells* | 63 |
| Figure 12-3 Determination of a and m from cores, well 15/9-15 | 65 |
| Figure 12-4 Determination of a and m from cores, well 15/9-17 | 65 |
| Figure 12-5 Cementation exponent m from well 15/9-15 and 15/9-17 vs core permeability, Skagerrak Formation..... | 66 |
| Figure 12-6 Log curve from Indonesia Equation in well 15/9-15, Gungne Field. The red curve represents scenario 1 while the pink represents scenario 2 | 67 |
| Figure 12-7 Saturation exponent vs. porosity, Skagerrak Formation well 15/9-15 and well 15/9-17 .. | 68 |
| Figure 13-1 Porosity distribution in Skagerrak, well 15/9-9 | 71 |
| Figure 13-2 Porosity distribution, Skagerrak, well 15/9-15 | 72 |
| Figure 13-3 Porosity distribution, Skagerrak Formation, well 15/9-17..... | 72 |
| Figure 13-4 Bulk density vs. core shifted porosity of all three wells..... | 74 |
| Figure 13-5 Core permeability vs. core porosity vs. vclay in well 15/9-9 Skagerrak Formation..... | 75 |
| Figure 13-6 Core permeability vs. core porosity for all wells in Skagerrak Formation..... | 77 |
| Figure 13-7 Vertical permeability vs. horizontal permeability, well 15/9-9..... | 77 |
| Figure 13-8 Vertical permeability vs. horizontal permeability, well 15/9-15..... | 78 |
| Figure 13-9 Vertical permeability vs. horizontal permeability, well 15/9-17..... | 78 |
| Figure 14-1 Qv vs porosity from wells 15/9-15 and 15/9-17 | 83 |
| Figure 14-2 Gas/Water Capillary Pressure Curves from well 15/9-15, Skagerrak Formation | 84 |
| Figure 14-3 Gas/Water Capillary Pressure Curves from well 15/9-17, Skagerrak Formation | 85 |
| Figure 14-4 Swirr from cores vs. Klinkenberg corrected perm 15/9-15 and 15/9-17 | 86 |

| | |
|---|-----|
| Figure 14-5 Capillary pressure vs. Normalised Water saturation from well 15/9-15 and 15/9-17 | 87 |
| Figure 14-6 J-function vs. Sw _n for well 15/9-15 and well 15/9-17 | 88 |
| Figure 14-7 The normalised water saturation vs. the J-function | 89 |
| Figure 14-8 Water saturation from Indonesia Equation vs KLOGH, well 15/9-17..... | 92 |
| Figure 14-9 Sw _{irr} from core and log methods well 15/9-15..... | 93 |
| Figure 14-10 J-function vs the normalised water saturation for the Indonesia Equation, well 15/9-17..... | 95 |
| Figure 14-11 J-function vs. Sw _n deduced from log methods..... | 96 |
| Figure 14-12 Sw _r =Sw-Sw _{irr} vs J _{res} | 97 |
| Figure 15-1 CPI from perforated (marked in blue) interval in well 15/9-15 | 98 |
| Figure 15-2 Pressure build-up data, well 15/9-15 | 100 |
| Figure 15-3 History plot..... | 100 |
| Figure 15-4 Log-log plot of the main build-up (red and white lines represents the model) | 102 |
| Figure 15-5 Pressure History plot of the main build-up (Green dots are measured data and red line is modelled) | 102 |
| Figure 15-6 Sketch of the well and distance to barrier, one fault | 103 |
| Figure 15-7 Log-log plot of the main build-up (red and white lines represents the model) | 103 |
| Figure 15-8 Pressure History plot of the main build-up (green dots are measured data and red line is modelled) | 104 |
| Figure 15-9 Sketch of the well and distance to the two parallel faults..... | 104 |
| Figure 15-10 Log-log plot of the main build-up (red and white lines represents the model) | 105 |
| Figure 15-11 Pressure History plot of the main build-up (green dots are measured data and red line is modelled) | 105 |
| Figure 15-12 Sketch of the well and distance to the two intersecting faults..... | 105 |
| Figure 16-1 Histogram of V _{clay} well 15/9-17 | 109 |
| Figure 16-2 Core permeability vs. Effective porosity for all wells..... | 110 |
| Figure 16-3 Average values from well 15/9-9, Cut offs: k=0.05 md and phi=0.1 | 110 |
| Figure 16-4 Average values from well 15/9-15, Cut offs: k=0.05 md and phi=0.1 | 111 |
| Figure 16-5 Average values from well 15/9-17, Cut offs: k=0.05 md and phi=0.1 | 112 |
| Figure 16-6 Comparing the water saturation methods 15/9-15..... | 114 |
| Figure 16-7 Comparing the water saturation methods 15/9-17..... | 114 |
| Figure 16-8 Comparison of water saturation well 15/9-15 | 116 |
| Figure 16-9 Comparison of water saturation well 15/9-17 | 116 |
| Figure 21-1 CPI-plot of well 15/9-9, Skagerrak Formation | 127 |
| Figure 21-2 CPI- Plot, well 15/9-15, Skagerrak Formation..... | 128 |
| Figure 21-3 CPI- Plot, well 15/9-17, Skagerrak | 129 |
| Figure 21-4 Correlation of Zone 1 and 2 in well 15/9-15 and 15/9-17 | 131 |
| Figure 21-5 Core permeability vs. core porosity vs. V _{cl} , well 15/9-15..... | 132 |
| Figure 21-6 Core permeability vs. core porosity vs. V _{cl} , top part of well 15/9-17..... | 132 |
| Figure 21-7 Core Permeability vs. core porosity vs. V _{cl} , middle part of well 15/9-17 | 133 |
| Figure 21-8 Core Permeability vs. core porosity vs V _{cl} , lower part of well 15/9-17 | 133 |
| Figure 21-9 Average values from well 15/9-9, Cut offs: k=0.05 md, phi=0.1, V _{cl} =0.5 | 134 |
| Figure 21-10 Average values from well 15/9-15, Cut offs: k=0.05 md, phi=0.1, V _{cl} =0.5 | 135 |
| Figure 21-11 Average values from well 15/9-17, Cut offs: k=0.05 md, phi=0.1, V _{cl} =0.5 | 135 |
| Figure 21-12 Watersaturation from Indonesia vs KLOGH 15/9-15 | 137 |
| Figure 21-13 Water saturation from Archie vs.KLOGH well 15/9-15..... | 137 |
| Figure 21-14 Water saturation from Waxman Smits vs KLOGH, well 15/9-15 | 138 |
| Figure 21-15 Water saturation from Archie vs. KLOGH, well 15/9-17 | 138 |
| Figure 21-16 Water saturation from Waxman Smits vs. KLOGH well 15/9-17 | 139 |

Figure 21-17 Swn vs J-function from Indonesia Equation, well 15/9-15.....141
Figure 21-18 J-Indo from Indonesia Equation, well 15/9-15141

1 Acknowledgements

The work of this thesis was performed at the University of Stavanger. I would like to thank my Professor Karl and professional supervisor, Karl Audun Lehne, for given me guidance and comments throughout this thesis.

Further, I would also like to thank my father, Geir Byberg, for showing no hesitation in helping me whenever I have needed it.

This has been a good experience, and I am very thankful for that.

Ingrid Byberg

June 2016

2 Abstract

A petrophysical evaluation has been generated for three wells penetrating the Skagerrak Formation in the Sleipner Øst field, the Gungne field, and the Loke field in the Central North Sea,

Figure 5-1. The wells included in this study were 15/9-9, 15/9-15 and 15/9-17.

The porosity was the result of calibrating core porosity with the density log. In addition clay volume was included to create an effective porosity. Pressure data from RFT and logs were utilized to find the fluid contact, and the pressure gradients defined the fluid densities used in the evaluation.

The calculated permeability, KLOGH, was estimated by regression analysis between the overburden corrected core permeability and core porosity. The result was a poorly correlation.

The water saturation modelling has been estimated with three main methods:

- use of logs: Indonesia-, Waxman Smits-, and Archie's method.
- use of cores
- use of a combination of log- and core- evaluated saturations.

A pressure transient analysis was performed from DST1 in well 15/9-15, Gungne Field, where the main objectives were to compare the permeability estimated from the test with the core permeability and look at potential barriers in the reservoir. Three different fault models were estimated in an attempt to match the measured data, one fault, parallel fault, intersecting faults.

A brief sedimentological evaluation of the Skagerrak Formation was implemented in all three wells based on available log data and core data. The well 6510/7-2 from the Norwegian Sea comprising red beds were compared to the Skagerrak Formation to find that the all the wells are comprising fluvial systems in their respectively Skagerrak Formation. The

main difference however was the porosity properties, which implied a much lower porosity in well 6510/7-2.

3 Introduction

A reservoir characterization has been done for three wells in the Sleipner area located in the Central part of the North Sea. (Figure 4-1 Map of Southern North Sea [1]

) The evaluation is covering the Middle to Late Triassic Skagerrak Formation from three exploration wells located in the Sleipner Øst Field, the Gungne field and the Loke Field. (

Figure 5-1) These wells are 15/9-9, 15/9-15, 15/9-17, respectively. Two out of three appeared to be hydrocarbon saturated in the Skagerrak Formation. The available data for this evaluation has been wire line logging data, core data, DST data, and SCAL data.

The thesis is divided into four main sections. The first section include an introduction to the Skagerrak Formation followed by an introduction of the three fields in the Sleipner area and a geological evaluation of the Skagerrak Formation. The second section comprises the general petrophysical log interpretation parameters used in this evaluation, followed petrophysical evaluation. A water saturation model by using capillary pressure from special core analysis (SCAL) to derive water saturation has also been done. In addition water saturation has been estimated from logs by applying three different methods: Archie's equation, the Indonesia equation and the Waxman Smits model. The third section is finally closed up with a DST evaluation of well 15/9-15. The thesis will in the last section finish off with an evaluation of the final results and a conclusion of the reservoir characterization of Skagerrak Formation.

A separate collection of tables and CPI plots are contained in Appendix 21. The petrophysical evaluation is performed by using the Senergy software, Interactive Petrophysics (IP), while the transient pressure analysis by using Saphir which is a part of the Ecrin package delivered by KAPPA. Microsoft Excel has been used to generate several of the plots used in this evaluation.

4 The Skagerrak Formation

The Skagerrak Formation located in the Sleipner Area is frequently recognized for its heterogeneity and often poor reservoir quality. From depositional models of the formation this is clearly observable where it is comprising relatively thin pay interval up to 3 meter thick with low permeability. This has lead to several challenges in attempting to achieve a thorough understanding of the formation, especially involving the modelling of the permeability and the distribution clay content in the formation. [1]

Several undeveloped hydrocarbon accumulations with Skagerrak reservoir are located in within the Central North Sea. Despite of this it has been proven to be a very prolific reservoir in eastern parts of the Central North Sea in a more thicker sandy sequence, and this better reservoir material is often recognisable within channel deposits which can be characterized as important reservoir for gas, condensate and oil production. [2] [3]

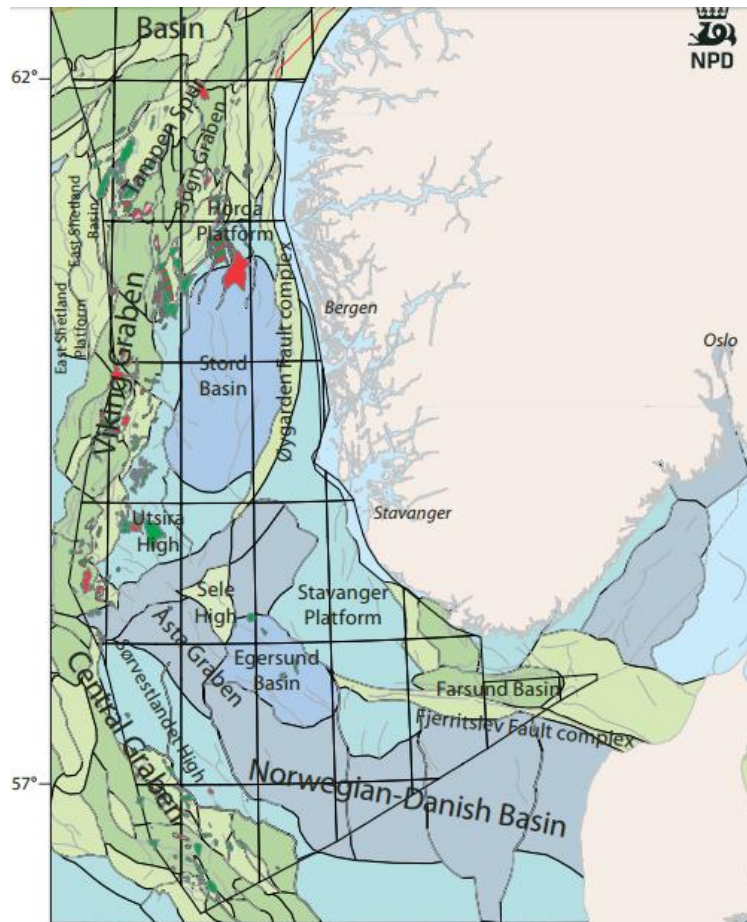


Figure 4-1 Map of Southern North Sea [1]

4.1 General description of the Depositional Environment in the Skagerrak Formation

4.1.1 Alluvial Fan

Alluvial fans are known as fan shaped zones of sedimentation downstream from a sediment source located at higher levels. They are primarily transported by water but also by mass flow deposits like debris flow. The shape of the fan geometry tends to either be wedge shaped or cone shaped bodies comprising silt, gravel and sometimes boulders.[49] They are best developed in arid climates where rain appears rarely but when it occurs it comes down heavily. [7] When the sediments reaches the open plain the water will slow down and spread the alluvium deposits onto the open plain. The slowing down of the water results in that the boulders and gravels are first deposited in the narrow passage known as the apex, the head of the fan in the vicinity of the mountain.[7][50] The deposits here are generally coarse grained and poorly sorted immature material of gravels and sands. [50] Further down the

gravel passes into sand in the middle of the fan and then the lighter sediments, silt and clay, further into the apron, the tail of the fan.

Fluvial fans are built up by successive aggradations and then avulsion of a river. The river channel may be meandering, split- channel or fully braided. Fluvial may be completely terrestrial, or may have a distal portion with standing water known as fan deltas. [51]

Two types of river deposits commonly are excellent reservoirs: braided and meandering rivers. [10] Figure 4-2, Figure 4-3

4.1.1.1 Braided Rivers

Braided rivers are known as complex networks of low-sinuosity multi channels that flow on alluvial plains with slopes greater than 1.5 to 2 degrees. The lateral continuity of the pay is usually good to excellent while the vertical continuity is fair to good. [10] The flooding can be known as sporadic and may therefore carry enormous volumes of water and sediments into the system. Existing channels can be overloaded with deposits during these flooding leading to new channels are cut and quickly filled with coarser sediments. This continuously branching and bar formation develops the braided channels. The water that spills over the channel banks spreads fine silt and clay particles that are then deposited in abandoned.

Figure 4-2 [10] ,

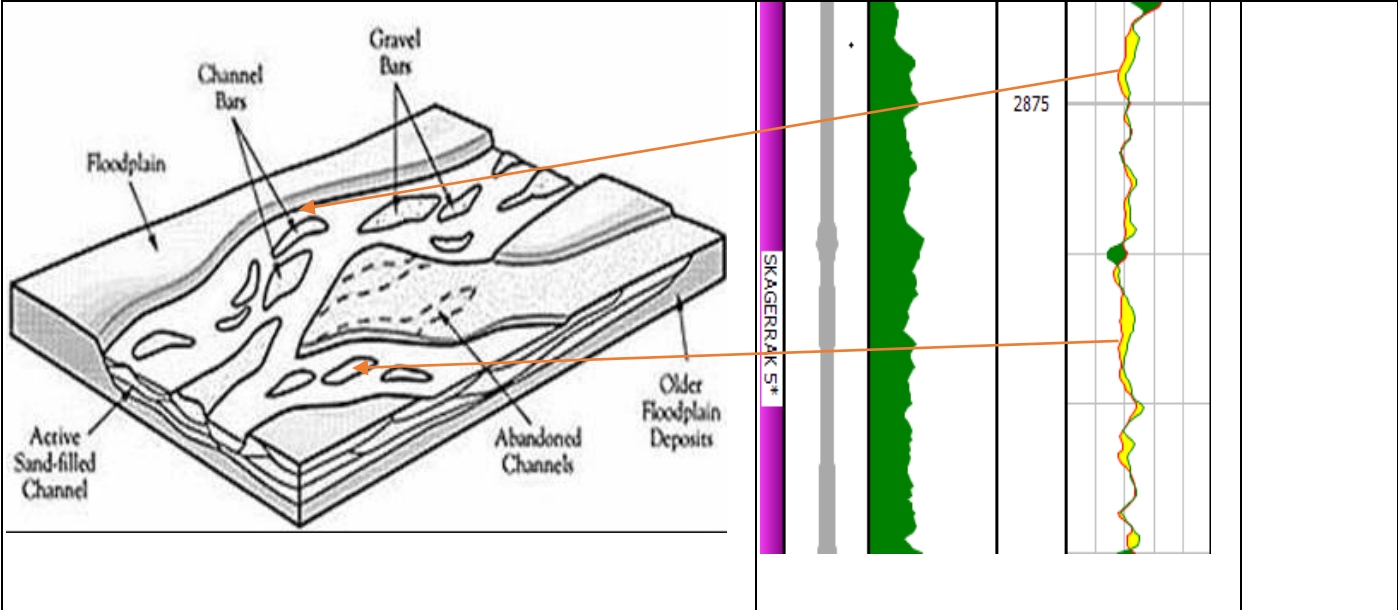


Figure 4-2 Schematic channels and plains of braided river system, CPI from Zone 5 in well 15/9-15, Gungne Field

4.1.1.2 Meandering Rivers

Meandering rivers are characterized by high sinuosity channels located on flat alluvial plains with slopes less than 11 to 12 degrees. Two main processes are responsible for development of sand bodies. These are point bar deposits left by channel migration, and oxbow-lake deposits left abandoned in loops of the river course. Point bars left in abandoned loops forms when the stream cuts a new course during flooding. Extremely high floods will spill sediments over the banks and deposit sheet of very fine sand, silt and clay into the flood plain. Figure 4-3 [11]

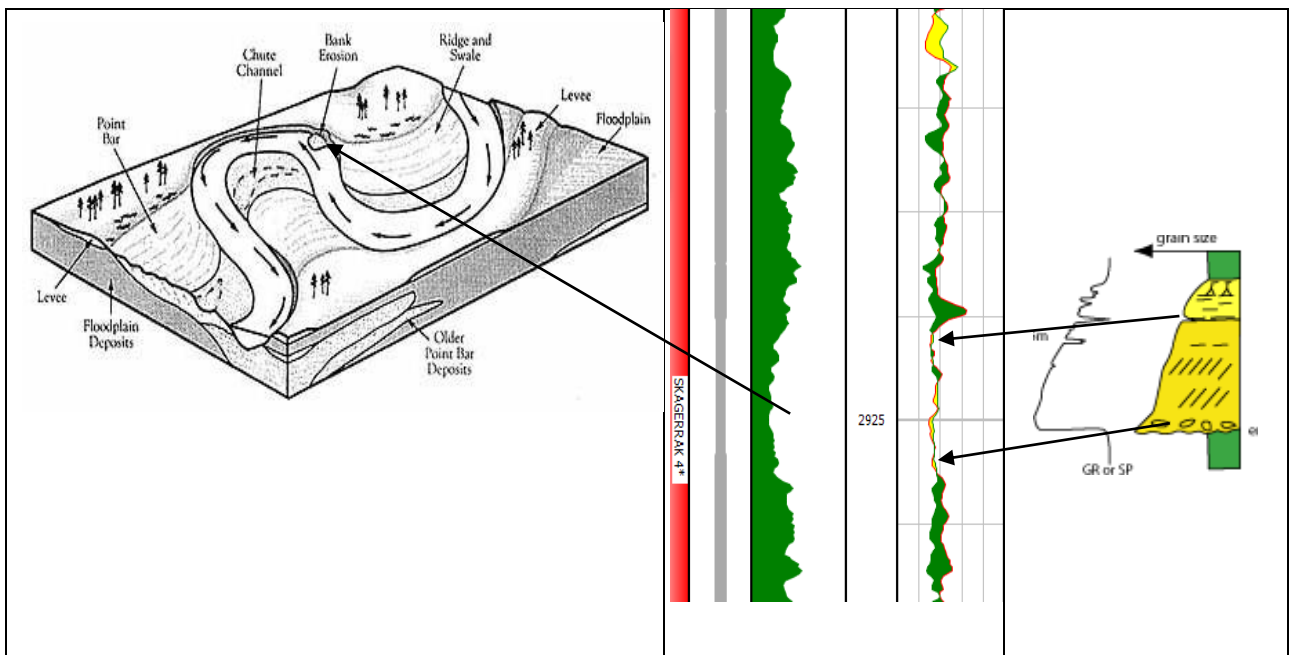


Figure 4-3 Meandering rivers and plain, CPI from Zone 4 in well 15/9-15, Gungne field

In both cases the complex of the rivers may move its location back and forth across the depositional area. The streams move into new areas during a flooding and expand in this way. The porosities and the permeability can comprise a large variation. This variation is especially good reflected with depth due to the rapidly depositional cycles of the flooding. The permeability will comprise the highest values at the base of the channel deposit where the coarser materials are left behind and are decreases further away reflecting the finer particles. If an entire channel sequence is preserved and not eroded away by later channels, very thin shale lamina observed in cores from the top of a channel may drastically reduce these properties. [50] [49]

4.2 Brief geological history and Depositional Environment

During the Early Triassic period rifting activity followed by thermal subsidence of the basin floor characterized the central North Sea. The North - south to northeast - southwest faulting controlled the sedimentation through the Triassic. [1] [4] Successions of continental clastic sediments interbedded with anhydrite and carbonate beds were deposited in a series of rift basins as a result of this activity. These successions represents episodic extensional tectonics, erosion and climate change.[4] The expansion of the fluvial system of the Skagerrak formation took most likely place during pauses from the fault activity. Fluvial expansion occurred during pluvial events which appear to have been driven by the arid climate. [52] The Skagerrak formation was then deposited by braided rivers located on large alluvial plains where the channels changed their course partially or completely during each flood due to large deposition of alluvial sediments. The rivers eventually became meandering. [4]

The deposition occurred mainly under dry conditions with varying levels of a humid climate through the Triassic period. Distribution and thickness patterns, particularly of the coarser grained units indicate major source areas lay to the west and northwest of the northern North Sea and to the east, north east and south of the central North Sea. Local tectonics has a significant influence on the patterns of deposition. The transition between the Triassic and Jurassic is marked by a widespread marine transgression from north and south. [1]

In the Early Triassic period the warm climate lead to a vaporizations of the water and several hundred meters of mud were deposited in the basin recognized as the Smith Bank Formation. These mudstones is deposited below the Skagerrak Formation and the contact between the Skagerrak Formation and Smith Bank Formation show a variation from gradational to sharp. [54] [1]

4.2.1 The Skagerrak Lithology

The Skagerrak Formation has an age of Middle to Late Triassic. In some areas it may extend down to the Early Triassic. [4] The sandstone varying in a thickness of around 500-1000 m comprises fine to medium grained fluvial sandstones.[1] Also coarser materials like conglomerates are present. The sand is interbedded with siltstones and mudstone

successions. From cores it is possible to observe various shades of red and brown coloured shales and mudstones. The colour is due to an oxidized environment.[1] [4] The sandstone sequences show a range in colour from light grey, orange to brick red. The presence of shale, carbonate and anhydrite are suggested by preserved faunal components to be deposited in lakes.[1] The fluvial sandstones may display complex internal geometries and complicated diagenetic histories which have contributed in difficulty for reservoirs to develop in the Skagerrak formation. [1]

4.2.2 The Lithostratigraphy

Poor stratigraphic control in the Skagerrak Formation area creates limitations on the lithostratigraphic correlation between the German Triassic sequence and the Southern North sea. [1][4] This is due to the formations frequently variation- and thin inter beddings in the lithology sequence. In the Central North Sea the Triassic sediments are normally unconformable overlain by Jurassic to lower Cretaceous rocks. (Figure 4-4 Lithostratigraphy of Skagerrak Formation [1]Figure 4-4) [1] [4]

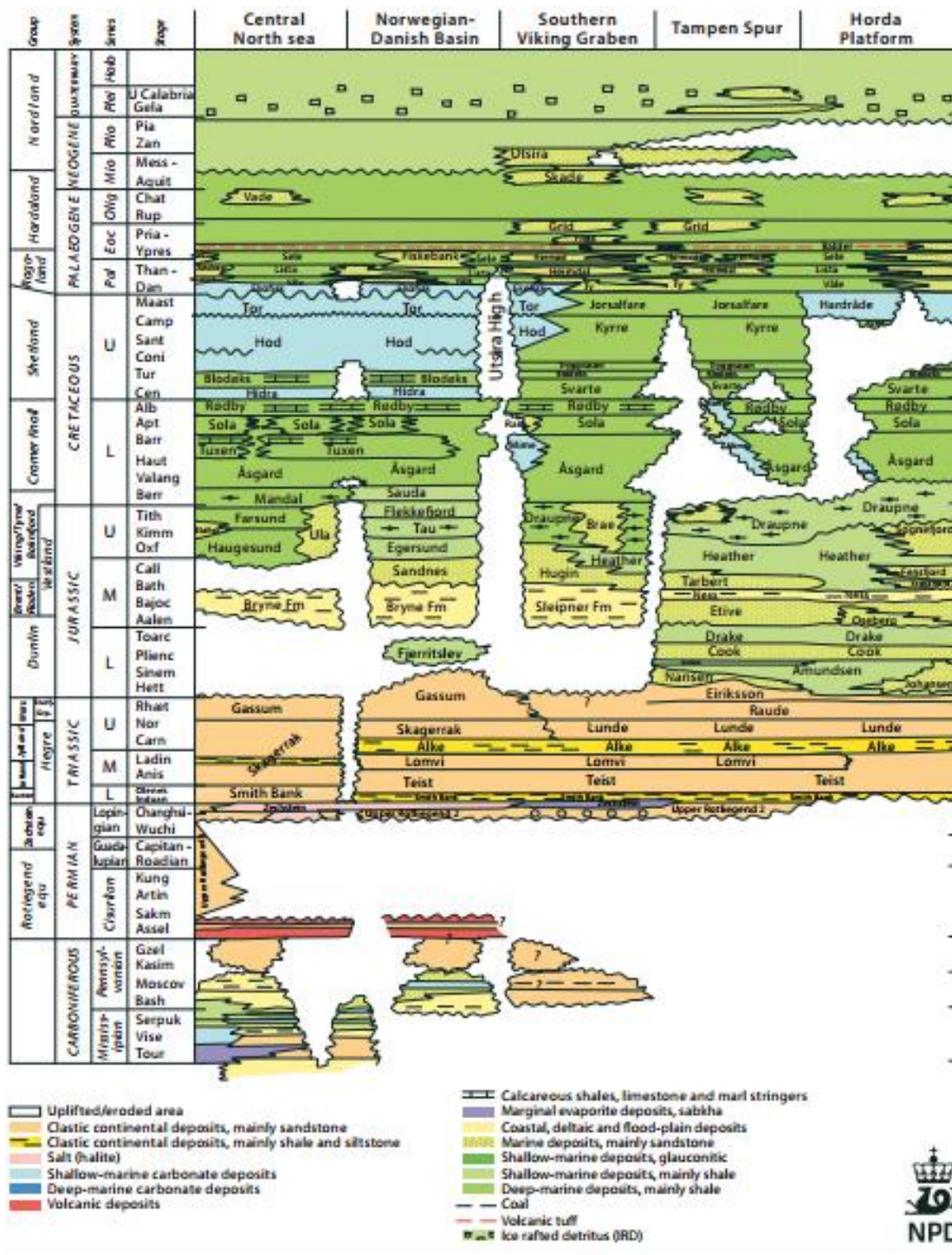


Figure 4-4 Lithostratigraphy of Skagerrak Formation [1]

5 The Sleipner Area

The Sleipner Area is located in the Central North Sea, and includes the gas and condensate fields Sleipner Øst, Gungne and Sleipner Vest. [55] (Figure 5-1) The Sleipner installations is also processing from the surrounding fields, Sigyn, Volve, Gudrun and Loke. In 2017 Gina

Krog Field will also be included for processing hydrocarbons. [12] The area is located in blocks 15/6, 15/8 and 15/9, and is considered as major production areas in the North Sea. The gas pipeline system in the Sleipner Area transport the dry gas to Europe while the condensate is transported to Kårstø for a final processing. [1][12]

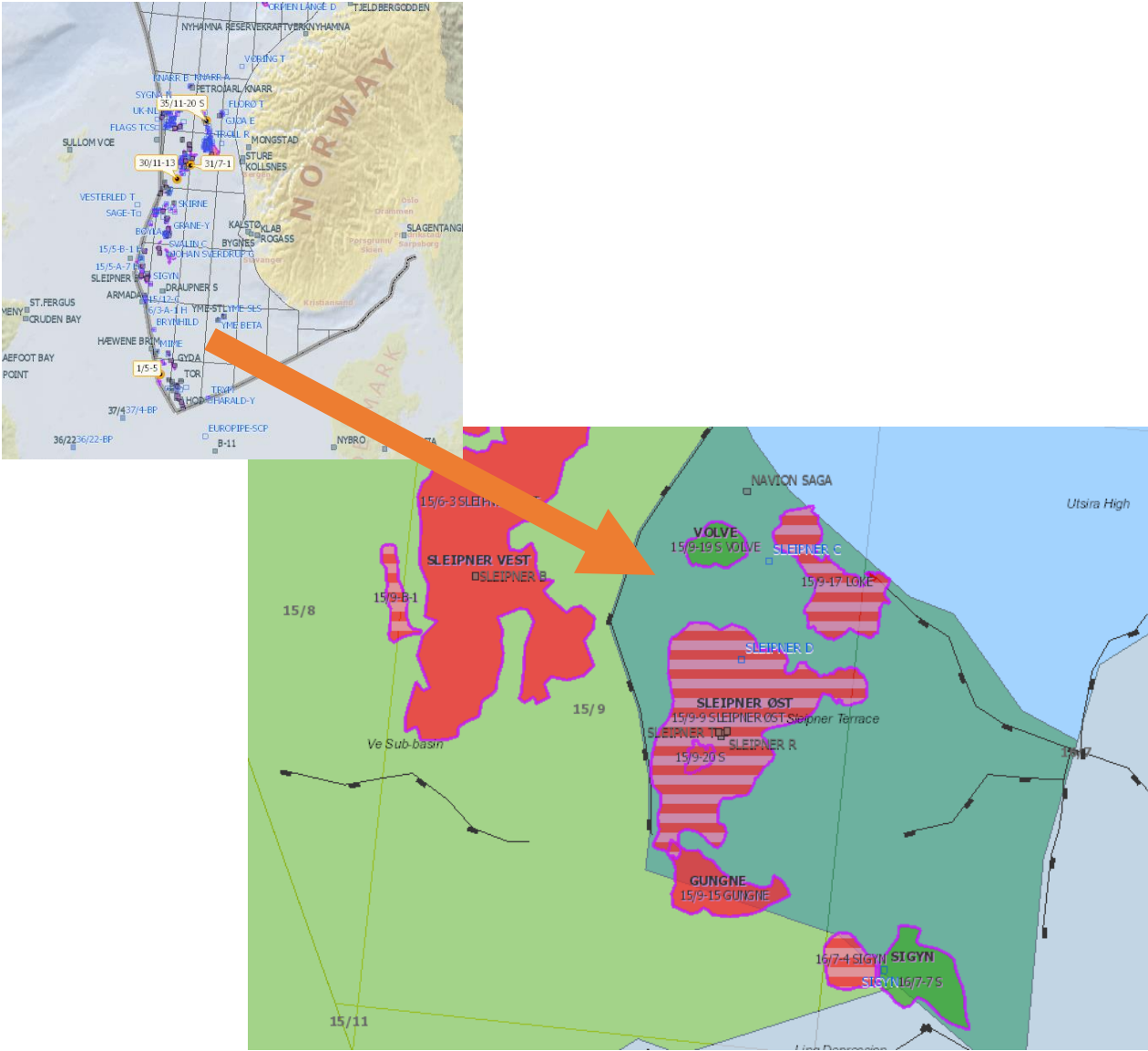


Figure 5-1 Map over the Sleipner Area, Central North Sea [1]

5.1 The Sleipner Øst Field and Well 15/9-9

The Sleipner Øst Field was the first development of the Sleipner Area and was discovered by the exploration well 15/9-9 in 1981. The field is a gas condensate field with a water depth of

82 meter situated in block 15/9, in the Central North Sea. Production start of the field was in August 1993 and operated by Statoil ASA. [1] [12]

The producible gas and condensate reservoirs consists of the Ty Formation of Palaeocene age and the Hugin Formation of Middle Jurassic age. Gas has also been proved in the Heimdal Formation located above the Ty Formation. The formations mainly comprise sand of good reservoir properties interbedded with thin shale beds. [1]

The exploration well 15/9-9 was drilled on the Sleipner Terrace in the North Sea to test possible hydrocarbons in Jurassic sandstones on the 15/9 Gamma structure. (Figure 5-1) It was also to get a better understanding of the sand distribution in the area. The Skagerrak Formation was encountered at 2642 m, but the Skagerrak Formation in this area was water filled. [1]

5.2 The Gungne Field and Well 15/9-15

The Gungne Field is a satellite field connected to Sleipner Øst in block 15/9. The reservoir was discovered in 1982 and was put on production in April in 1996 with a well drilled from the Sleipner A-platform. The water depth is around 83 meters and the field is developed by three wells drilled from Sleipner A. The field is producing gas and condensate which is processed on the Sleipner A platform. The reservoir comprises the sandstone from the Triassic Skagerrak Formation, and the reservoir depth is around 2800 meters. The reservoir quality is in general good but the reservoir is segmented and the lateral shale layer works as internal barriers. [1] [12]

Well 15/9-15 was drilled as an exploration well on the My-structure located in block 15/9 south of the Sleipner Øst Field. (Figure 5-1) The main objective was to prove hydrocarbons in this structure from Palaeocene and Mesozoic age. The content was gas and condensate and the first level was proved in the Triassic Skagerrak Formation. In a depth interval from 2821 m to 2923 m the formation was proved to be gas bearing. The Palaeocene sand from the Heimdal Formation was not encountered in this well.

Four cores were cut across the reservoir from 2805 m in the Heather Formation to 2878.2 m in the Skagerrak Formation.

5.3 The Loke Field and Well 15/9-17

The Loke Field is another satellite field attached to the Sleipner A-platform. The field was discovered in 1983 in the 15/9 block, and was put on production in 1993. The reservoirs are mainly located in sandstones from the Ty Formation of Palaeocene age and from the Middle Jurassic Hugin Formation. The Heimdal Formation has also proven contents of gas. The reservoir depth is approximately 2300 metres.

Exploration well 15/9-17 was drilled in December 1982 as an exploration well on the Theta-structure in block 15/9. (Figure 4-1) The primary objective was to find possible hydrocarbons in the sandstones of Jurassic and Triassic age, and the well proved hydrocarbons in the Heimdal Formation and the Skagerrak Formation. From the log analysis it was suggested that the gas/water contact was located at 2418.5 m, while pressure data could give a contact at 2413 m.

6 Zonation of the wells

The wells were divided into zones based on the lithology and the gamma ray log response. Due to the large variation in the Skagerrak Formation, it is a challenging task to find potential correlating zones between these layers. Only Zone 1 and 2 from well 15/9-15 and 15/9-17 seemed to correlate based on the petrophysical logs. [1]

Table 6-1 Zonation of all three well in the Sleipner Area

| Well 15/9-9 - Sleipner Øst Field | | |
|----------------------------------|---------|----------|
| Zone | Top [m] | Base [m] |
| Skagerrak Upper | 2642 | 2703.17 |

| | | |
|------------------------------------|----------------|-----------------|
| Skagerrak Lower | 2703.17 | 2776 |
| Skagerrak | 2642 | 2776 |
| Formation Thickness | 134 | |
| Well 15/9-15 - Gungne Field | | |
| Zone | Top [m] | Base [m] |
| Skagerrak 5* | 2860 | 2905 |
| Skagerrak 4* | 2905 | 2946 |
| Skagerrak 3* | 2946 | 2977 |
| Skagerrak 2 | 2977 | 3019 |
| Skagerrak 1 | 3019 | 3091 |
| Skagerrak | 2860 | 3091 |
| Formation Thickness | 231 | |
| Well 15/9-17 - Loke Field | | |
| Zone | Top [m] | Base [m] |
| Skagerrak 9 | 2741 | 2750 |
| Skagerrak 8 | 2750 | 2755 |
| Skagerrak 7 | 2755 | 2763 |
| Skagerrak 6 | 2763 | 2779.8 |
| Skagerrak 5 | 2779.8 | 2786.2 |
| Skagerrak 4 | 2786.2 | 2786 |
| Skagerrak 3 | 2786 | 2791 |
| Skagerrak 2 | 2791 | 2808 |
| Skagerrak 1 | 2808 | 2814 |
| Skagerrak | 2741 | 2814 |
| Formation Thickness | 73 | |

7 Fluid Contacts

The fluid contacts in this work is based on logs, pressure data and water saturation modelling produced in the program Senergy software Interactive Petrophysics. Data from all three wells are included. Table 7-1 below summarized the observations in each well and

the estimation of free water level (FWL) for the different areas. In Figure 7-1 all the formation pressure data is plotted from well 15/9-15 and 15/9-17. This plot shows 2 different water gradients. [13]

Table 7-1 Contacts in the wells

| Area | Well | Contact | Pressure data | FWL (m TVDMSL) | Fluid gradient (bar/m) | Comments |
|--------------|---------|---------------|---------------|---|------------------------|--------------|
| Sleipner Øst | 15/9-9 | no contact | - | - | 0.102 | Water filled |
| Gungne Field | 15/9-15 | FWL | RFT | 2927 | 0.032 | Gas filled |
| Loke Field | 15/9-17 | Not specified | RFT | No water gradient available , chosen to 2858 (GDT*) | 0.032 | Gas filled |

* GDT Gas Down To

Well 15/9-9 is water filled implying that no indication of gas water contact would be possible to locate. Well 15/9-15 showed a gas water contact in the zone Skagerrak 4 (2905-2946 m). (Table 7-1). It is believed that the contact can be located further down in the defined transitional zone from Skagerrak Formation to the Smith Bank Formation. Due to lack of information by adjacent wells this would not be possible to give any exact estimation of this contact but from Table 7-1, it has been estimated at a depth of 2858 m.

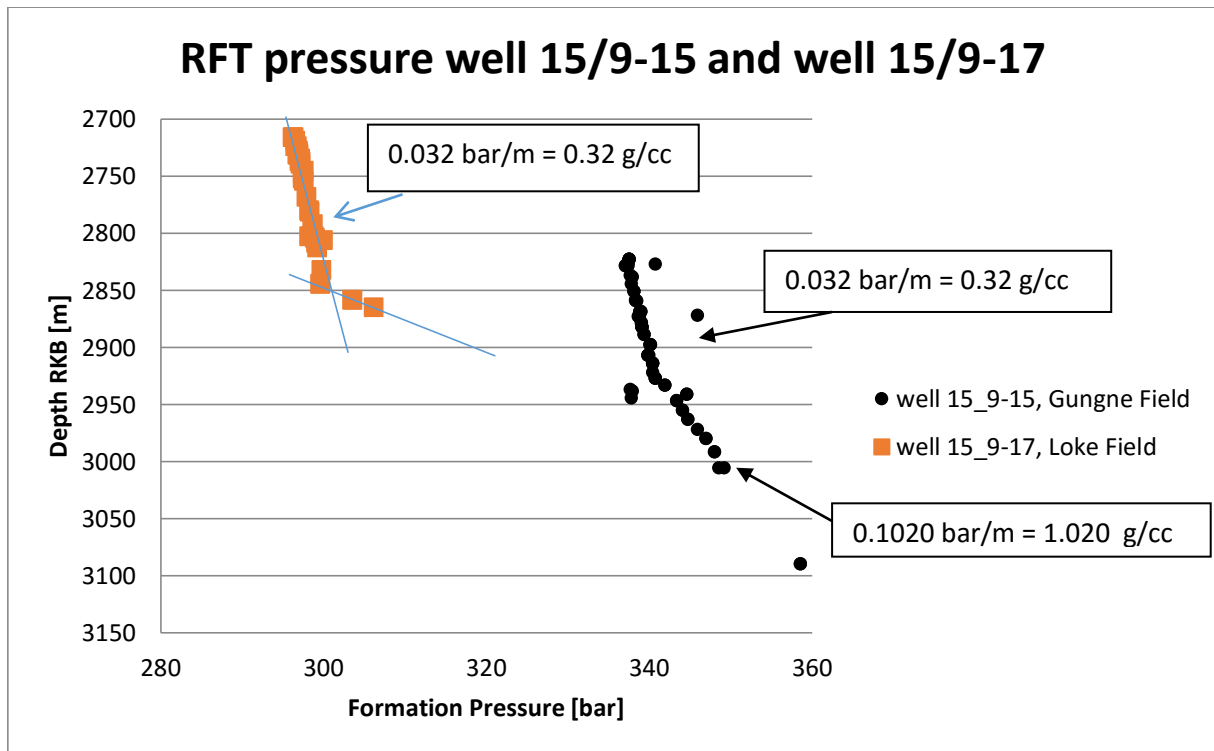


Figure 7-1 RFT pressure data [13] from well 15/9-15 and well 15/9-17

8 Log Quality

The log quality evaluation is based on the CPI plots from well 15/9-9, 15/9-15 and 15/9-17 in appendix 20 and different cross plots.

The caliper log reveals that the log quality from the three wells are generally good within well 15/9-15 and 15/9-17, while well 15/9-9 seems to be more affected by washouts in the lower part. These wash outs are especially affecting logs as density and neutron. The resistivity logs are affected by shale and calcite streaks due to lower resolution. This will cause a smearing effect where the resistivity will show lower values in the hydrocarbon zone near a shale or calcite layer and too high values in the same layers in a water zone. Several areas the bore holes are more or less in gauge and identification of permeable zones from thin mud cake has established in well 15/9-9 at a depth 2730 m where the permeability value showed a value of 134 mD which is a relative high value in the Skagerrak Formation. Table 8-1 shows the bit size used in the three wells in the Skagerrak Formation interval.

Table 8-1 Bit size used in all three wells in the Skagerrak Formation [1]

| Well | Depth [m MDRKB] | Bit size used in the Skagerrak Formation [inches] |
|---------|-----------------|---|
| 15/9-9 | 2527-3044 | 8.5 |
| 15/9-15 | 2478-3200 | 8.5 |
| 15/9-17 | 2616-2950 | 8.5 |
| 15/9-17 | 2950-3120 | 6.0 |

The following Figure 8-1,

Figure 8-2, Figure 8-3, display cross plots of washout affecting density neutron logs in the Skagerrak Formation in well 15/9-9, 15/9-15 and 15/9-17. In well 15/9-9 most of the readings from the caliper log are located within a hole size of 8-9 inches represented by the magenta colour in figure 7-1. There are some points in the range of 9-10 inches represented by green colour and a few in the range of 10-11 represented by the dark red colour. These are mostly readings from the lower part in the Skagerrak Formation in well 15/9-9. The green and dark red colour from the plot will be indicating wash out in this area.

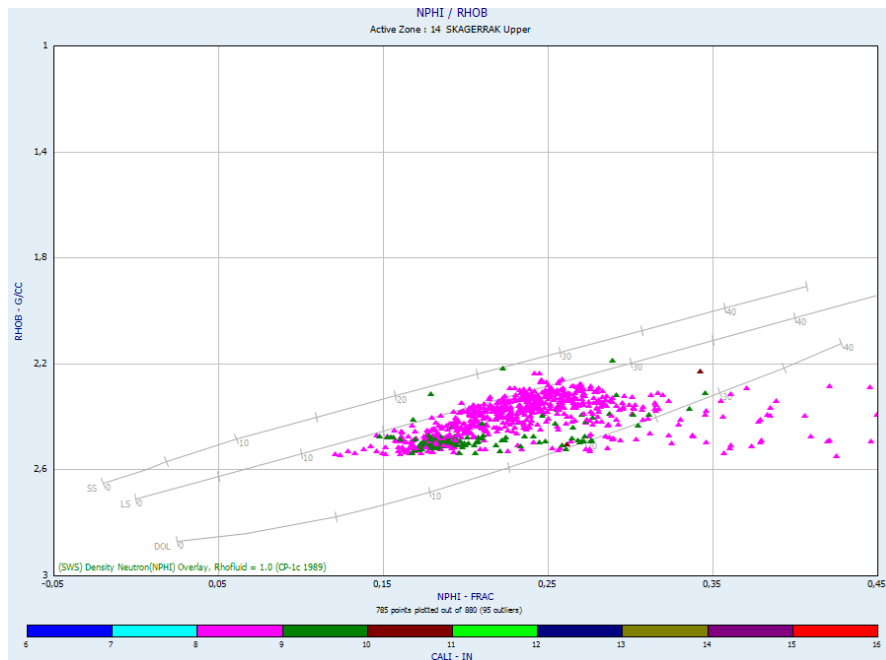


Figure 8-1 Caliper vs. RHOB vs. NPHI, well 15/9-9

In well 15/9-15 most of the measurements from the Caliper log are located in the range of 7-8 inches (aqua blue colour) and in the range of 8-9 inches (magenta colour). The few zones

of wash out mostly located in the top of the Skagerrak Formation due to the presence of finer materials in the formation. In general the log quality in this well is relatively good. (

Figure 8-2)

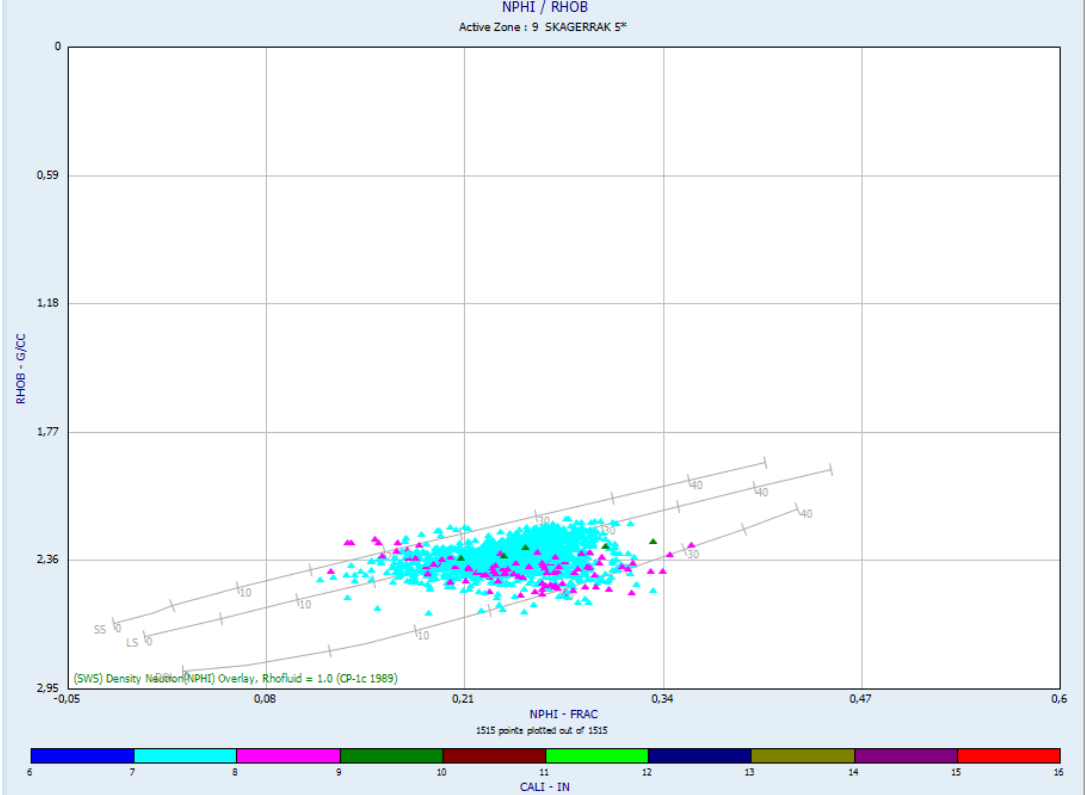


Figure 8-2 Caliper vs. RHOB, vs. NPHI, well 15/9-15

Well 15/9-17 shows similarity in the caliper range found in well 15/9-9. Few wash out zones are detected, only in the range of 9-10 inches from the caliper log represented in green colour in Figure 8-3 .

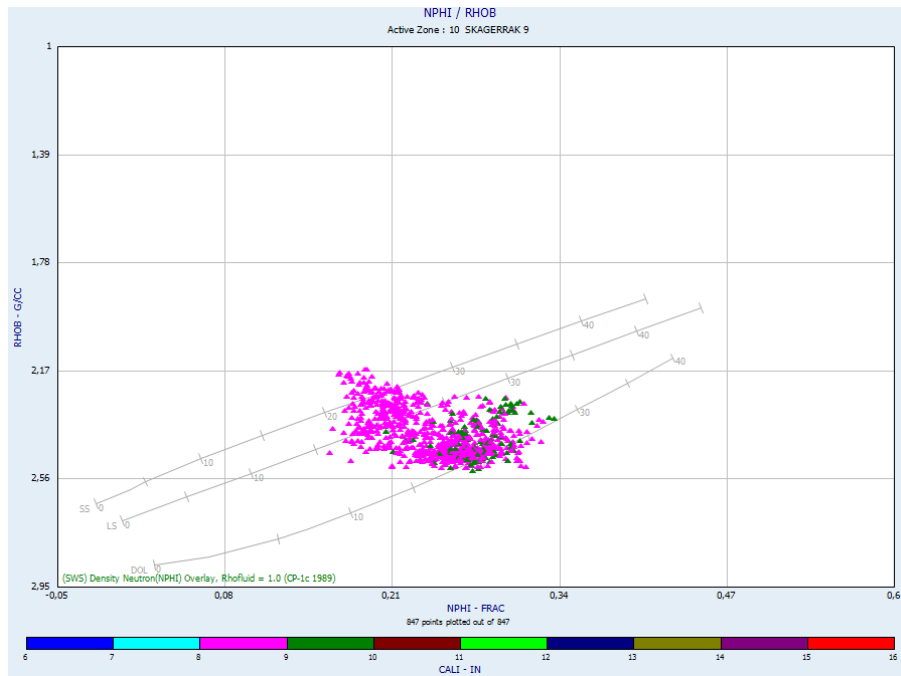


Figure 8-3 Caliper vs. RHOB vs. NPHI, well 15/9-17

9 Geological Evaluation

In this section a geological interpretation is presented of the well 15/9-9, 15/9-15 and 15/9-17 in the Skagerrak Formation. The determination of the facies is mainly based on the Gamma ray log. To look further into the quantities in Skagerrak, density neutron log, caliper, water saturation, permeability, porosity log and vclay log were utilised. Due to its heterogeneity the Skagerrak Formation has been divided into zones based on the changes in gamma ray and indications that is possible to receive from the logs. (Table 6-1) The zones described in section 9.1 is based on coring intervals in the three wells. A correlation plot of the three wells are found in Appendix 20.1.1. The section will be finished off with an evaluation based on the sedimentology of the well 6510/7-2 located in the Norwegian Sea.

9.1 The Depositional Environment in the Skagerrak Formation

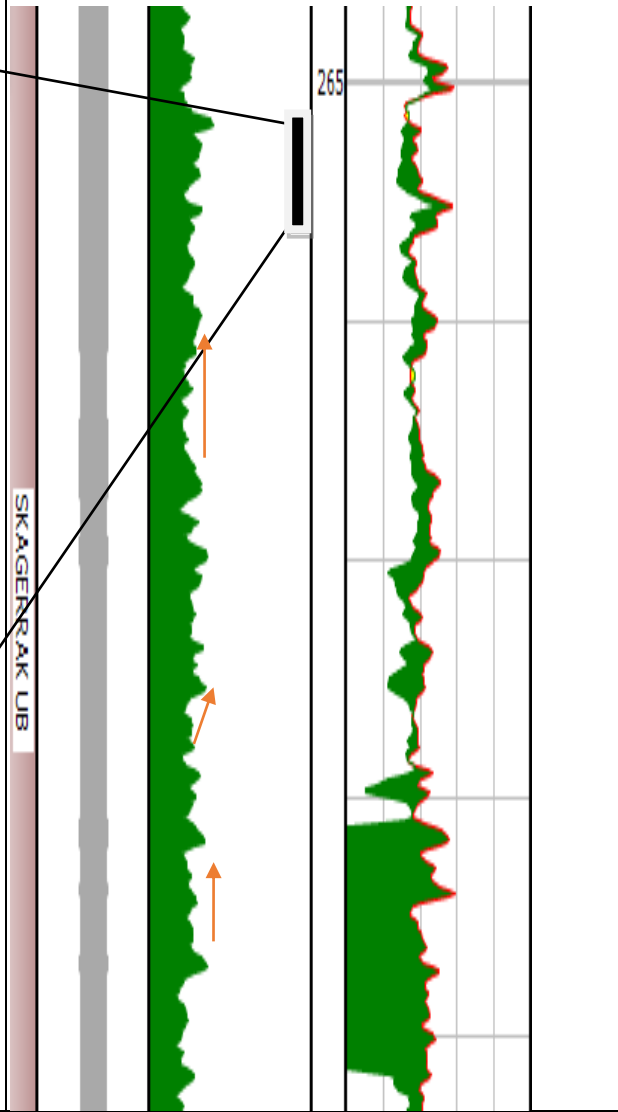
Earlier in section 4.1.1 the depositional environment in the Skagerrak formation was described as alluvial in both terrestrial and marine environment dominated by a braided and meandering system. A general description of these type of depositional environments were explained in the sections 4.1.1.1-4.1.1.2.

9.1.1 Well 15/9-9, The Sleipner Øst Field

Upper Skagerrak, Coring interval: 2654-2657 m

Well 15/9-9 is divided into two following zones in the Skagerrak Formation, Upper and lower Skagerrak. The Upper part of the Skagerrak Formation in well 15/9-9 is proposed to be deposited in a marine environment.[1] From the gamma ray log a combination of serrated cylindrical pattern and some small weak tendencies of up fining sequences corresponds to a heterogeneous sand interbedded with silt and clay formation. (Figure 9-1) The depositional energy can be described by fluctuation. From cores it is interpreted that the sandstone unit is fine to medium grained, and the colour of the rock is brown to grey in colours, figure 11-1. [1] From the cored interval, 2654-2657 meters, the average permeability of the sandstone is ranging from 134-235 md while the average porosity is around 24 %. The clay volume in this thin zones are around 0.15 which is a relatively low V_{clay} value compared to what is normally found in the Skagerrak Formation.

| Coring interval: 2654-2657 m | Gamma Ray response: | Comment: |
|------------------------------|---------------------|----------|
|------------------------------|---------------------|----------|



Serrated cylindrical pattern from the Gamma ray log indicating an environment affected by finer materials like silt, shale and clay. Relatively high permeability values and porosity values from cores compared to the Skagerrak Formation in other areas.

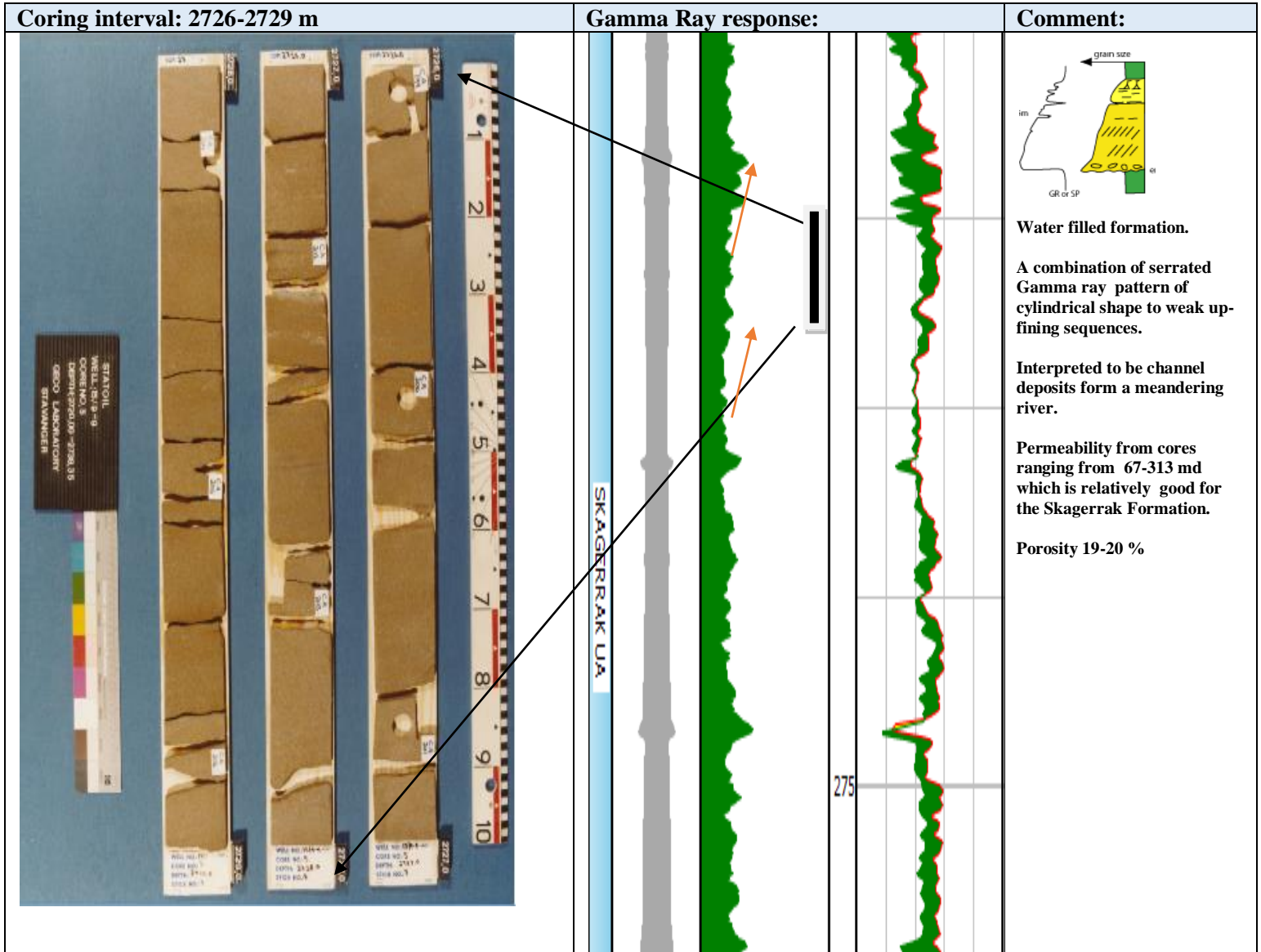
There are possibilities for locating intervals of calcite cementation are present at 2650 m and 2655 m.

Lower Skagerrak Formation, Coring interval 2703-2776 m

The lower part of the formation is corresponding better to the typical description of the Skagerrak Formation described in surrounding wells in the Sleipner Area. From core samples it is observable to see that the sandstone is changing in colour from fine grained brownish and light grey. (Figure 9-2) These changes has been interpreted as a change in the depositional environment from the one described in the upper part of the Skagerrak Formation.

It is interpreted as a alluvial deposit dominated by several up fining sequences involving that the shale content is weakly increasing while the grain size decrease. The depositional energy will also have a decreasing trend towards the top of the unit.

The porosity and permeability values in this area are generally good compared to the rest of this part of the Skagerrak Formation. Ranging from 19-20 % in porosity and 67-313 md in permeability. Suggesting that this must be in a typical point bar from the meandering depositional environment where coarser material like sand and gravel are located. The lower values found in the areas above and below this cored interval can be implying overbank deposition or abandoned meandering river curves.



9.1.2 Well 15/9-15, The Gungne Field

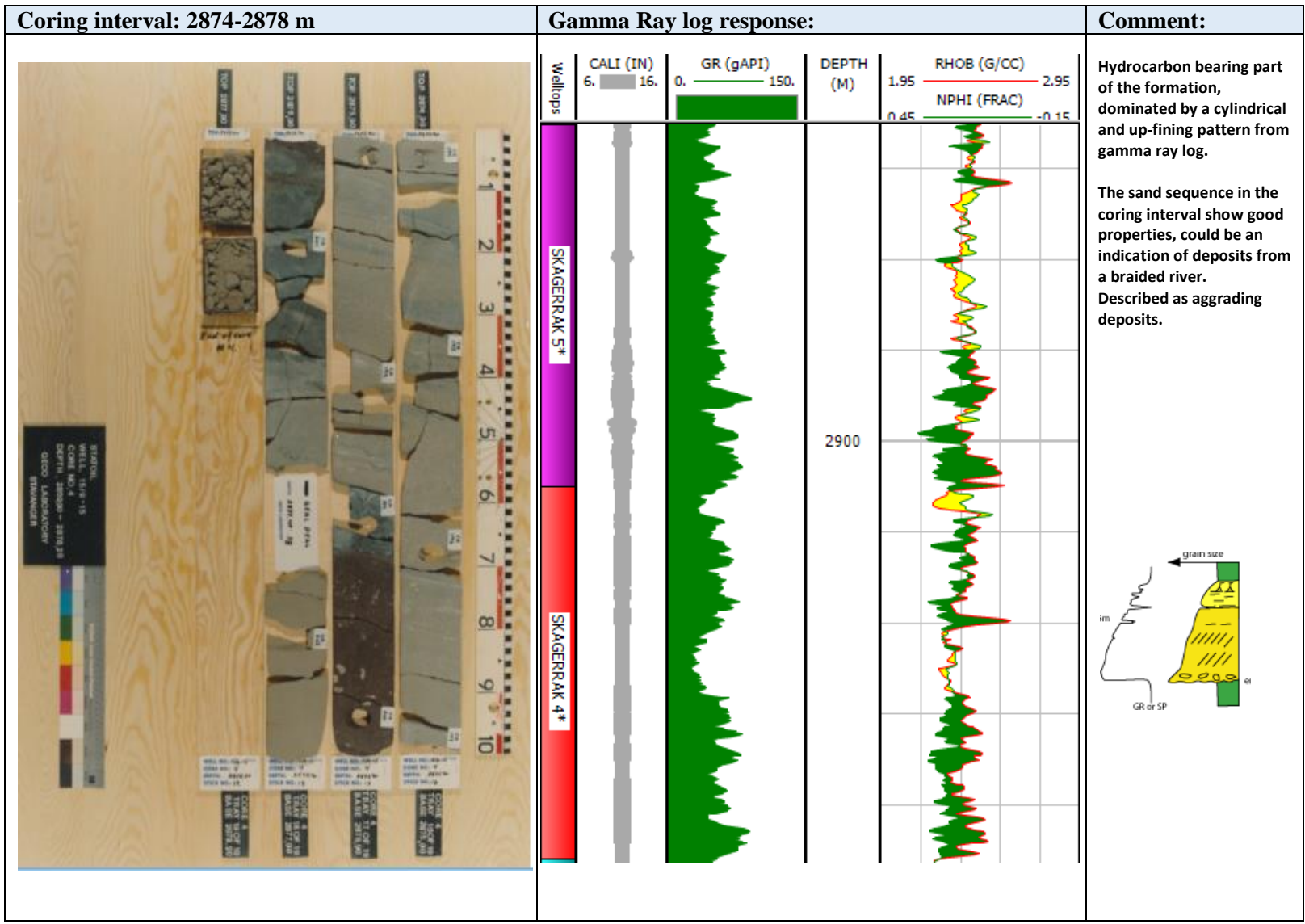
Skagerrak Zone 5, Coring interval 2874-2878 m

The Upper Skagerrak formation is comprising gas in relatively clean and coarse sandstones. The permeability and porosity values from the cored interval (Figure 9-3) is ranging from 0.58-225 md and 13-23 %, respectively.

The depositional environment is interpreted to be in a braided river deposits. The deposits of sand are relatively coarse grained interbedded with thin beds of shale/claystone. These beds tend to be laterally continuous over large areas of the alluvial plain, but shale beds may disrupt the continuity locally. Limestone stringers may occur and could be reflecting a coastal environment.

The gamma ray display a typical cylindrical pattern at the depth range 2875-2890 meters where the sand sequence is located. There is a low vertical variation of the gamma ray pattern in this section. The coarser materials are implying a depositional energy that is higher and more consistent. The fine grained sections located above has a permeability value of 0.173-3.2 md, while the porosity ranges from 3-10 %. This could be indicating splay sands or deposits of the overbank environment. From cores the colour of the sand bodies appear to comprise various shades of grey and brown to red brown. Traces of heavy mineral of pyrite and mica are common and may make disturbance on the gamma ray log.

The Zone 4 in well 15/9-15 comprises weak up fining sequence and cylindrical shape on the gamma ray log, see CPI from Appendix 20. Evident sequences of sandstone is observed which is proposed to be channel deposit sandstone from either a braided or meandering environment formed by point bard on the alluvial plain. They show similarity in the properties with the sand sequences in Zone 5. The thickness of these sandstones are ranging from 5-13 meters.



9.1.3 Well 15/9-17, The Loke Field

Skagerrak Zone 8 and Zone 9, Coring interval 2741-2748

The gamma ray show tendency of several serrated cylindrical shaped patterns. Thick gas bearing sandstones are interbedded with shale/mudstones. The thick mudstone located in the Skagerrak 9 zone could be indicating a marine deposit here due to the presence of the mineral glauconite and chlorite.

The sandstone sequences in the cored interval 2741-2748 m from Zone 9 (Figure 9-4) show a permeability range from 0.4 to 485 md and a porosity range from 11-25 %. This is interpreted to be depositions from a braided river deposits. The coarser materials imply a deposition affected by high energy when deposited. The thickness of the channel sand deposits have a thickness range of 2-5 meter in this specific area.

Skagerrak Zone 7 to Zone 1, coring interval 2764-2771 m

The sandstone sequences of the cored interval in the section 2764-2771 m show a permeability range of 0.31- 150 md while the porosity is ranging from 13 to 20 %. These are values are high over relatively small intervals.

The sands in the cored interval and also the sands below are located in coarsening upward sequences, separated by shale or mudstones of finer materials. The cylindrical shape are still present through the Skagerrak Formation. (Figure 9-5) The properties of permeability and porosity are also in this area within a large range of variation over small intervals. This is typical for braided systems where the deposition happens fast and frequently. The finer content of silt can be from separate channels in this system or from the overbank.

It is interpreted that the Skagerrak Formation below the defined as Skagerrak Zone 1, is gradually transitioning into the Smith Bank Formation in this area. This is based on the gradually higher content of finer particles like silt and mud. The gamma ray pattern are also changed in this area from up fining sequences and coarsening upward sequences to a more blocky appearance

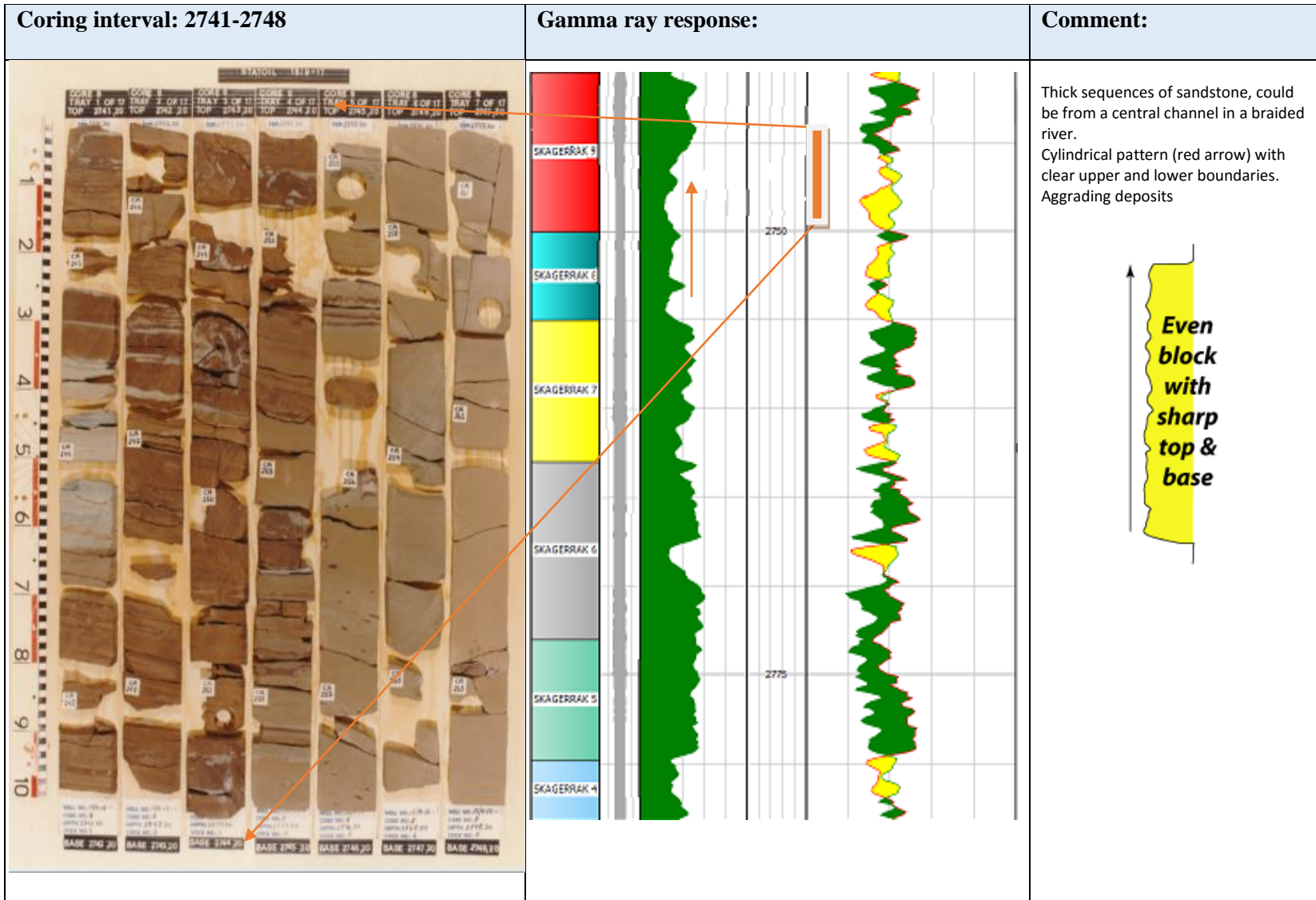


Figure 9-4 core sample and CPI from Top of the Skagerrak Formation, zone 8, well 15/9-17

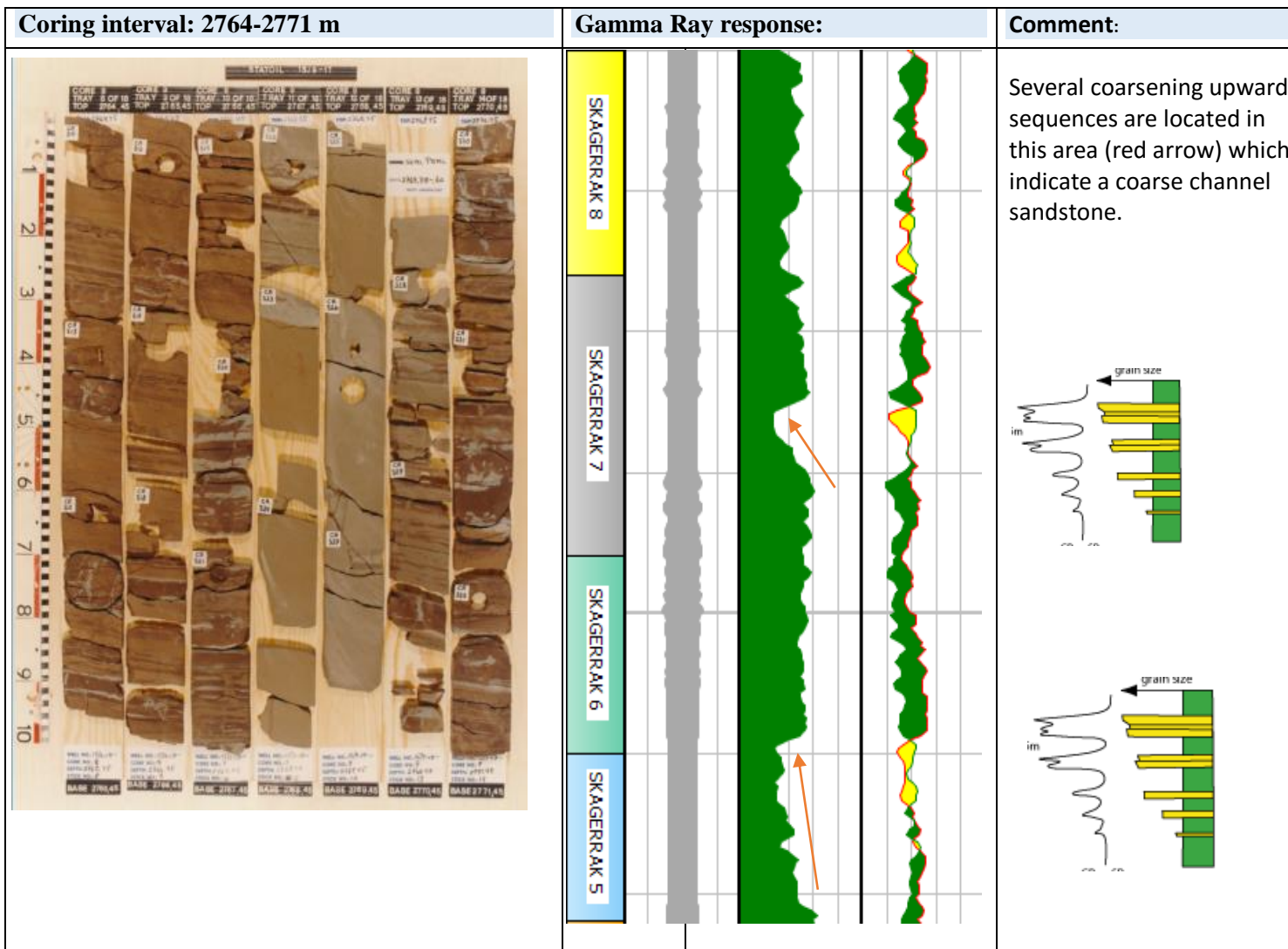


Figure 9-5 Core sample and CPI from 15/9-17

9.2 Well 6510/2-1 from Norwegian Sea, Mid Norway

The exploration well 6510/2-1 was drilled in the Norwegian Sea and reached a total depth of 4700 m in shales of Early Triassic. [1] In this section of the geology evaluation a brief comparison of the facies in Triassic Skagerrak Formation and the Triassic Red beds in the Norwegian Sea was made. Figure 9-6

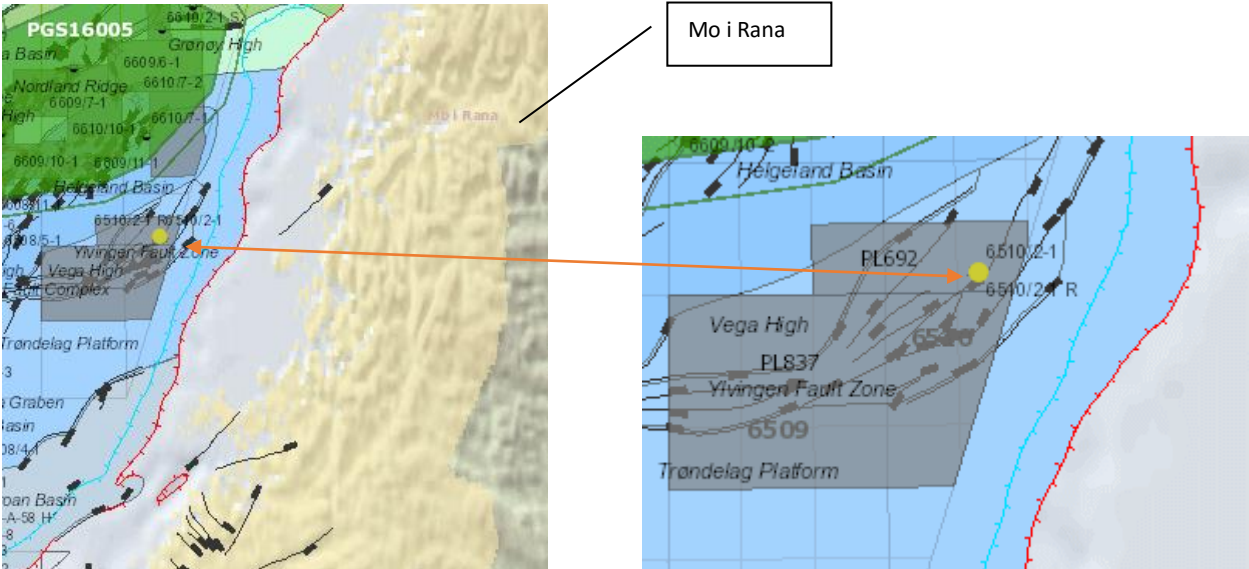


Figure 9-6 Location of the well 6510/2-1

The gamma ray log from well 6510/2-1 in Figure 9-9 shows similar features with 15/9-9, 15/9-15 and 15/9-17 located in the Central North Sea. The cylindrical gamma ray pattern indicates blocky sequences of sand ranging from 1-6 meters in thickness which is separated by thick sequences of shales/mudstones all formed under rapid changes of deposition. These finer deposits are ranging from 3-7 meters.(Figure 9-8) The sandy sequences in this well are found to be fine-grained brownish to red. [1]

The trending from the gamma ray log in well 6510/2-1 are most similar to well 15/9-17, Loke Field, (Figure 9-9), but the gamma ray values are much higher in 6510/2-1, which is indicating a formation dominated by high amount of finer deposits. This is also very clearly from Figure 9-7 where the porosity in well 6510/2-1 (green colour) is evidently lower compared to well 15/9-15 (aqua colour), 15/9-9 (blue colour), and 15/9-17 (pink colour)

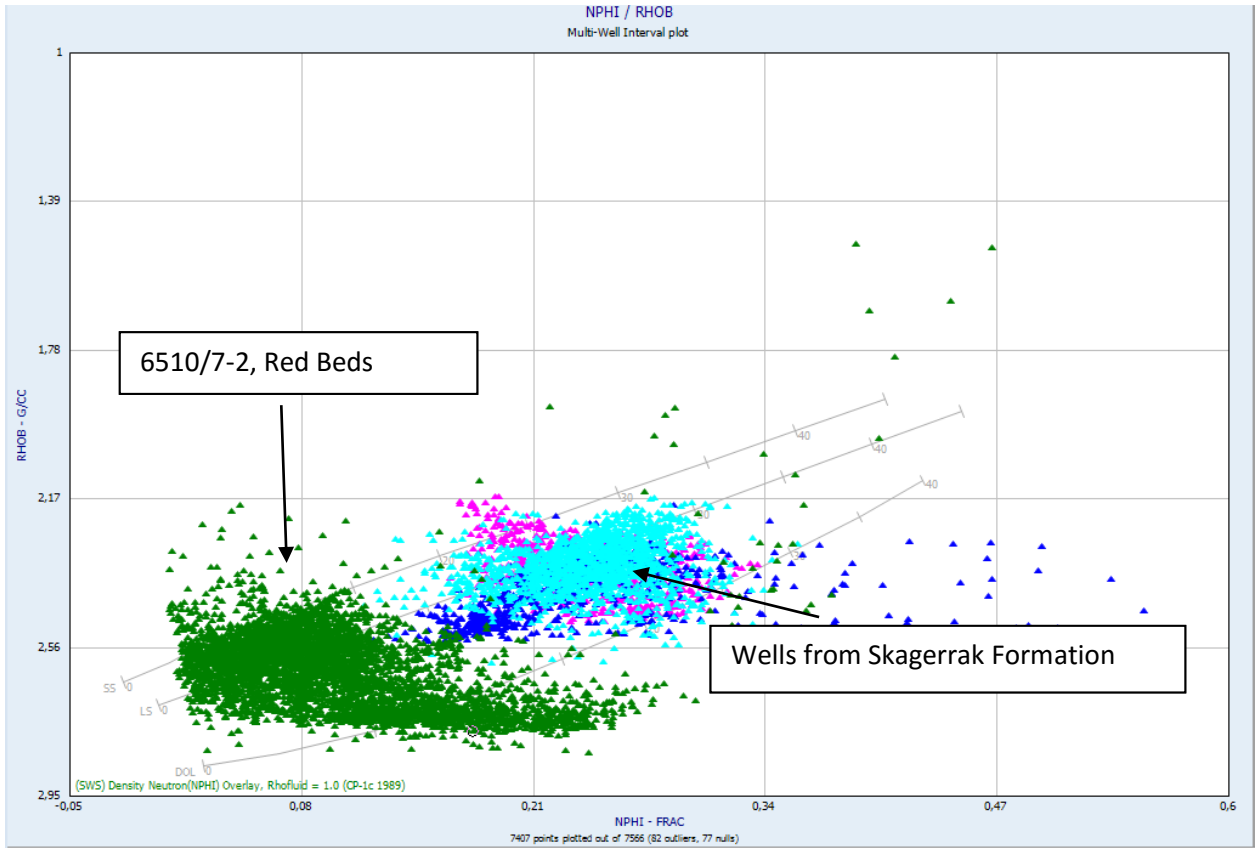


Figure 9-7 RHOB vs. NPHI for all wells

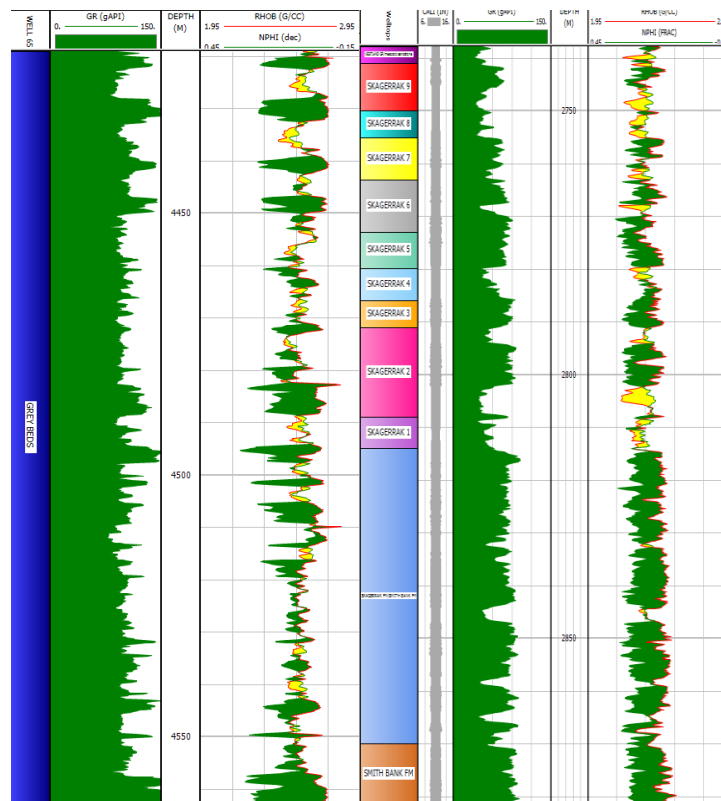


Figure 9-8 well 6510/7-2 to the left showing similar features with well 15/9-17 to the right

9.3 Correlation of Well 15/9-9, 15/9-15 and 15/9-17

The well correlation of the three wells were made by utilising the program Interactive Petrophysics. (Appendix 20.1) This made it possible to see how the wells are ranging in thickness of the Skagerrak in well 15/9-9, 15/9-15 and 15/9-17. Finding correlating layers in these three wells was very difficult due to the highly variation in the gamma ray pattern through the whole Skagerrak Formation in these three wells. It has been interpreted that well 15/9-15 and 15/9-17 show similarities in the gamma ray pattern at the bottom in the wells. (Figure 9-9) The correlating intervals are listed in Table 9-1 below. A thinner Skagerrak Formation is clearly seen in well 15/9-9, and 15/9-17 from Sleipner Øst and Loke Field compared to the thicker Skagerrak Formation from the Gungne Field.

Table 9-1 Correlating zones in well 15/9-15 and 15/9-17

| Well | Zone 1 | Zone 2 |
|-----------------------|---------------|---------------|
| 15/9-15, Gungne Field | 3019-3091 m | 2977-3019 m |
| 15/9-17, Loke Field | 2808-2814 m | 2791-2808 m |

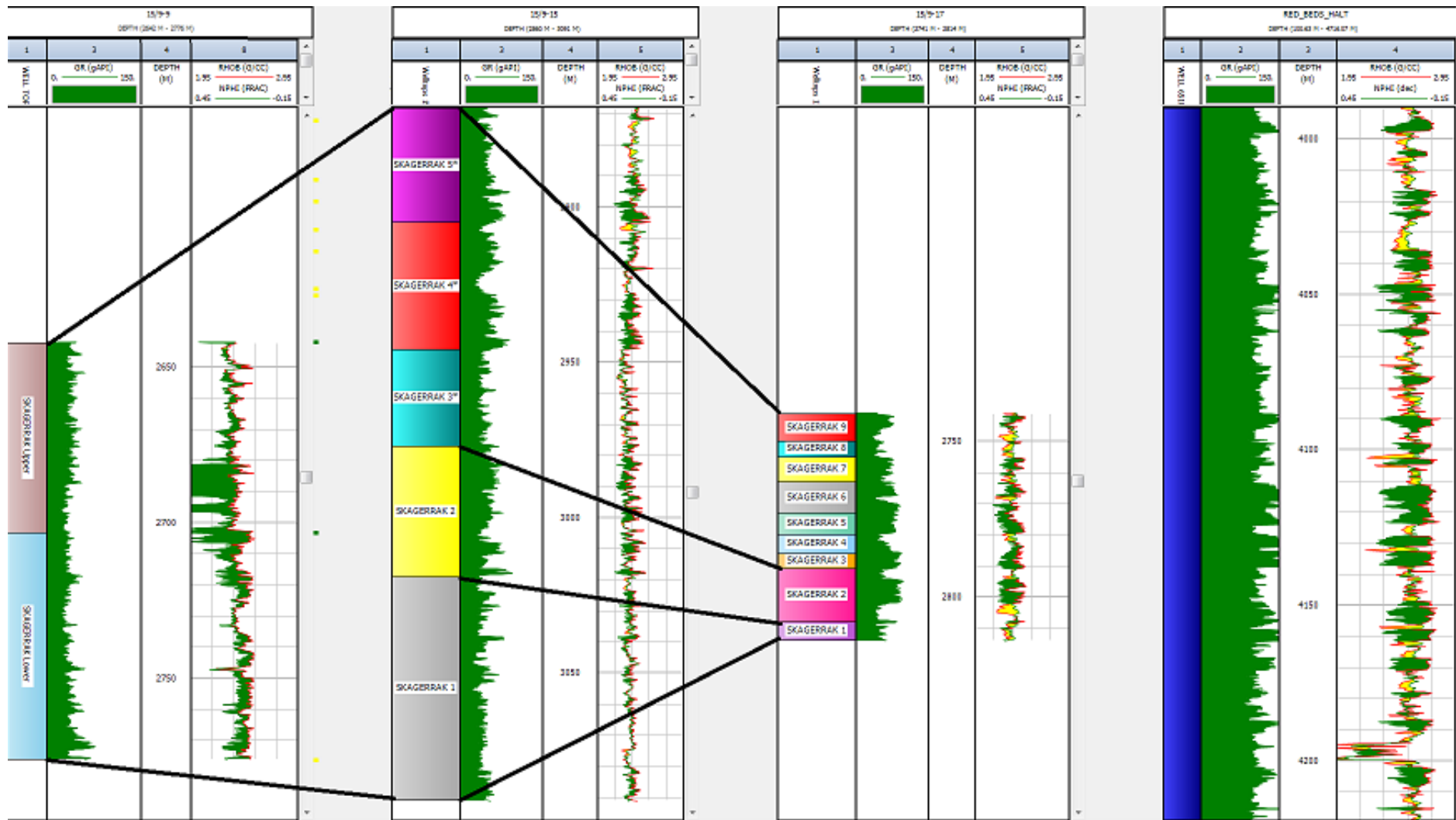


Figure 9-9 correlating zones in the Skagerrak Formation including CPI from well 6510/7-

10 Petrophysical Theory

10.1 Petrophysical Parameters

In a petrophysical study the determination of the quantity, the ability to locate, or to determine whether the hydrocarbons are recoverable are all important factors. In this section a general review of essential properties used in the evaluation of the Skagerrak Formation is given. This is followed by the main of this thesis, interpretation of the Skagerrak Formation.

10.1.1 Clay Rich Formations

Very few clastic reservoir rocks like sandstone or chalks that are hydrocarbon bearing are free of clay minerals. Several geophysical well logs will in some degree be affected in their responses due to its conductivity, and this will be contributing to a possible misinterpretation in the log analysis. [14] High resistivity values that could imply possible hydrocarbons can be reduced. The clay minerals found in formations are composed of small crystalline particles which are classified into groups according to their crystal structure. The fine grain conduce to strong capillary forces that holds the water in place and helps the clay minerals to bound large amounts of water to their structures. The most common clay minerals are Kaolinite, illite, montmorillonite and chlorite. [16]

The clay are known to be conductive, and the contribution of conductivity from clay is depending on the type of clay minerals, the fluid composition and whether we have laminar, dispersed or structured shale. [16] These three clay distributions are presented in Figure 10-1 where they are displaying how they are distributed in three different manners in a formation. [18]

To obtain reliable values of important parameters as the porosity and the water saturation it can be useful to compare the laboratory core derived data with the log derived down hole data information. The higher the amount of clay is present the more reduced will important parameters like the porosity and the permeability be. In cases where the clay content is high, the Archie's equation for clean sand will no longer be sufficient. Due to this it will be preferable to apply saturation models including the clay volume like the Waxman Smits and

the Indonesia Equation for a more accurate water saturation estimation, see sections 10.1.8 and 10.1.9.

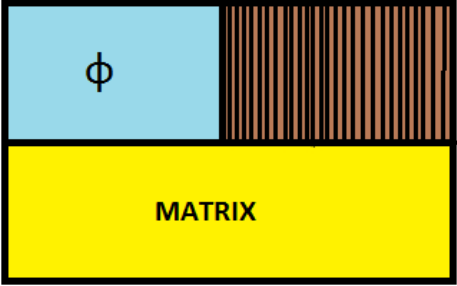
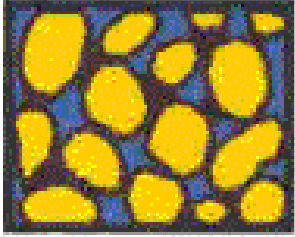

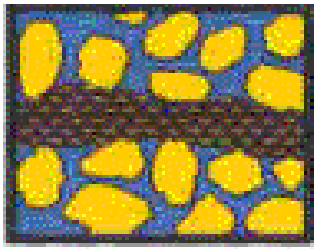
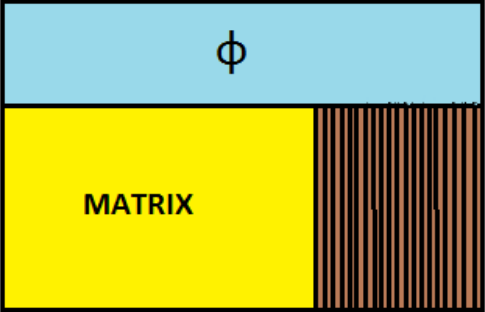
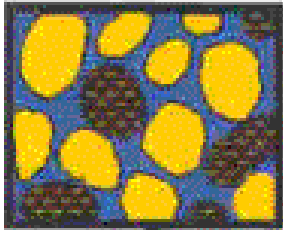
| Distribution | Figure | Comment |
|---|--|---|
|  |  | <p>Dispersed shale prevents the movement of Cl⁻ ions. Clay gets filled into the pores and this contributes to reduce the porosity and permeability. In the North Sea this is the most common clay. Most negative impact on the res properties in a formation. [17]</p> |
|  |  | <p>Laminar shale is laminated between layers with sand. This affects the porosity and the matrix. form tight barriers vertically or horizontally. formed outside the framework of the reservoir rock. [17]</p> |
|  |  | <p>Structural shale appears as separated grains. This affects only the matrix while the porosity is intact. [17]</p> |

Figure 10-1 Clay distributions [17]

10.1.1.1 Determination of Clay Volume (Vcl)

Several methods exist in the determination of the clay volume, Vcl, in a formation. The parameter is presented as a fraction where a clay volume equal to zero is defined as clean sand while a clay volume equal to one indicates shale. In this thesis the method from the gamma ray log method were applied in all three wells. [17] [56]

Gamma Ray Method

The gamma ray method is an uncomplicated method in the determination of the clay volume and it turns out to be the most reliable in general. The calculation of the Vcl from

gamma ray method is expressed in the following $V_{clGR} = \frac{GR_{log} - GR_{min}}{GR_{max} - GR_{min}}$ Equation 10-1: [56]

$$V_{clGR} = \frac{GR_{log} - GR_{min}}{GR_{max} - GR_{min}} \quad \text{Equation 10-1}$$

where

GRlog is actual borehole- corrected GR response in zone of interest

GRmin is minimum borehole- corrected GR response against clean zones

GRmax is maximum borehole- corrected GR response against shale zones

10.1.2 Porosity

The porosity (ϕ) of a rock can be described as the pore volume (V_p) divided on the bulk volume (V_b) of a rock. () The porosity parameter gives a measure of how much fluid the rock can handle to hold in between the matrix grains. Porosity is dimensionless and therefore represented as a fraction between zero and one or in percent. [24]

$$\phi = \frac{V_p}{V_b} \quad \text{Equation 10-1}$$

10.1.2.1 Total Porosity

The total porosity can be defined as the total void space including isolated pores and the space occupied by clay- bound water, figure 8-2. In equation 8-2 the bulk density of sample, bulk density and the density fluid that the sample is saturated with correspond to the porosity that is defined as the total porosity. The theoretical values for bulk density and fluid density for a sedimentary rock ranges from 2.65 g/cc to 2.96 g/cc and from 1.00 g/cc to 1.4 g/cc, respectively. The porosity can be measured by core analysis or by log measurements including density and neutron porosity. [58]

$$\phi = \frac{\rho_b - \rho_{ma}}{\rho_f - \rho_{ma}} \quad \text{Equation 10-2}$$

10.1.2.2 Effective Porosity

Effective porosity can be explained as the interconnected pore volume that contributes to permeability in a reservoir and is mainly less than the total porosity. This type of porosity excludes isolated pores and pore volume that is water. The clay- bound water is subtracted from the total porosity, Figure 10-2. In a core analysis the porosity is measured when the core sample is totally dried out. In this way most of the clay- bound water is removed. The effective porosity on dried core samples is greater than the effective porosity from log analysis and therefore more similar in value to the total porosity from log analysis. [22] The calculation of the effective porosity in the thesis is used in equation 13-1, section 13.2.2.

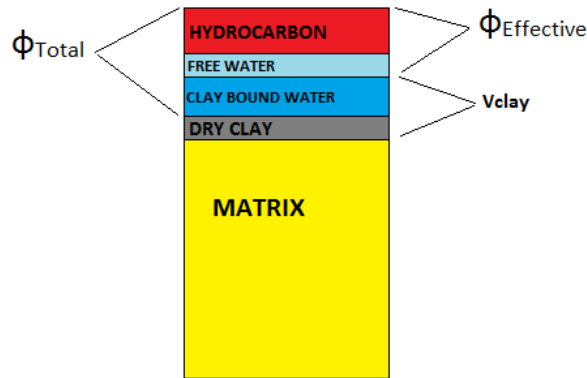


Figure 10-2 T Total porosity vs. Effective porosity [17]

10.1.3 Permeability

Permeability, K , is a measure of the capacity of a porous medium to transmit fluids measured in Darcies or millidarcies. [24] It is one of the most important parameters due to its ability to control the flow rate and direction of the fluid contained in a porous medium. This flow parameter are directional dependent and in general a tensor representation should be applied. [19] Several factors like the rock grain size, grain shape, grain sorting, grain packing and the degree of consolidation and cementation are affecting the permeability. If there are no interconnected pores in the reservoir rock the permeability is equal to zero. Permeability can be obtained from core analysis, well logging and well testing. [19]

10.1.4 Water saturation, S_w

The water saturation can be referred to as the fraction of the total pore volume that is occupied by water. The determination of this parameter in the reservoir formations is an important task in the study of the reservoirs. The calculations of hydrocarbon in place, fluid mechanics and the expected producing performance are all affected by the saturation. [22] The determination of the saturation of a reservoir rock can either be performed by direct measurement of how much fluid in the pore spaces or indirect measurement either performed on core samples or in the borehole. In this evaluation the version of the Indonesia, Archie, and Waxman Smits method and S_w . [21] [22]

10.1.4.1 Saturation Exponent, n

From the saturation exponent we get that the growth in resistivity is proportional to the distribution of non conductive fluids in the pore space. Archie (1942) experienced that a typical n value approximately equal 2.0 for a large number of rocks. [18] Deviations can still occur and this often in shaly sands. Archie proved that the resistivity index (RI) which is the ratio of rock resistivity at any saturation to rock resistivity when 100% water saturation can be related with water saturation (S_w) by the saturation exponent, n. [23]

The relationship between the resistivity index are presented in equation

$$RI = \frac{R_T}{R_o} = S_w^{-n} \quad \text{Equation 10-3}$$

By plotting RI and S_w in a log- log plot will give the saturation exponent n from the slope of the regression line, equation 8-6.

$$\frac{\log R_T}{R_o} = -n \log S_w \quad \text{Equation 10-4}$$

where

RI: resistivity index

R_T: True formation resistivity

R₀: True formation resistivity in water bearing reservoir

[23]

In case of clay content in the formation, the Archie equation should be replaced by equations like the Indonesian, Simandoux, Waxman-Smits. These equations utilises parameters like shale volume, shale resistivity and cation exchange capacity. Due to this there will be additional uncertainty compared to the clean sand model calculation. The saturation exponent is then denoted as n* and will always be larger in value compared to n for a clean formation. In this thesis n* was found by adding a factor of 0.1 to the saturation exponent, n for a clean sand. [59]

10.1.5 Formation Factor F and F*

Archie found out that the resistivity of a water- filled formation, R_o , could be related to the resistivity of the water, R_w , where R_o increased with R_w . This relationship was defined by a constant called the formation resistivity factor, F. [24]

This relationship was defined as the formation factor. The factor is dependent on the geometry of the pores and their connections. When F is small this can indicate the formation comprises a optimal rock texture and the formation will not play a role. A large value of F indicates a large inhibiting effect. [27]

$$F = \frac{R_o}{R_w} \text{ Equation 10-5}$$

From laboratory experiments there has been shown that F is strongly influenced by grain shape. [19] For a given saturation brine water, an increasing porosity will make a lower resistivity R_o of the rock following with a decreasing formation factor, F. The formation factor is inversely related to the porosity of the formation.[27] [25]

$$F = \frac{a}{\phi^m} \text{ Equation 10-6 [27]}$$

where

F: Formation resistivity factor

ϕ : Porosity

m: Cementation factor

a: The tortuosity factor

The formation factor for a clean sand saturated with 100 % water can also be expressed with conductivity as:

$$C_o = \frac{1}{F} * C_w \quad \text{Equation 10-7}$$

When clay is present it will provide an additional excess conductivity, C_e . This excess conductivity will be constant except below a certain value of C_w . A new formation factor, F^* , needs to be represented for rocks containing clay. [24] [33] [34]

The equation will become as follows:

$$C_o = \frac{1}{F^*} (C_w + C_e) \quad \text{Equation 10-8}$$

In Figure 10-3 plot of the two responses, clean formation vs. clay formation indicates the different behaviour by looking at the curves linearity. A linear response will represent the clean core with a slope of the reciprocal of the F while a curved response will represent the shaly sandstone with the slope F^* . The arrow between the two curves in Figure 10-3 represents the excess conductivity due to the role clays have as conductors of current. When the conductivity value of the water is large enough, the response from the shaly formation may be displaced by the Archie relation. [24] [34]

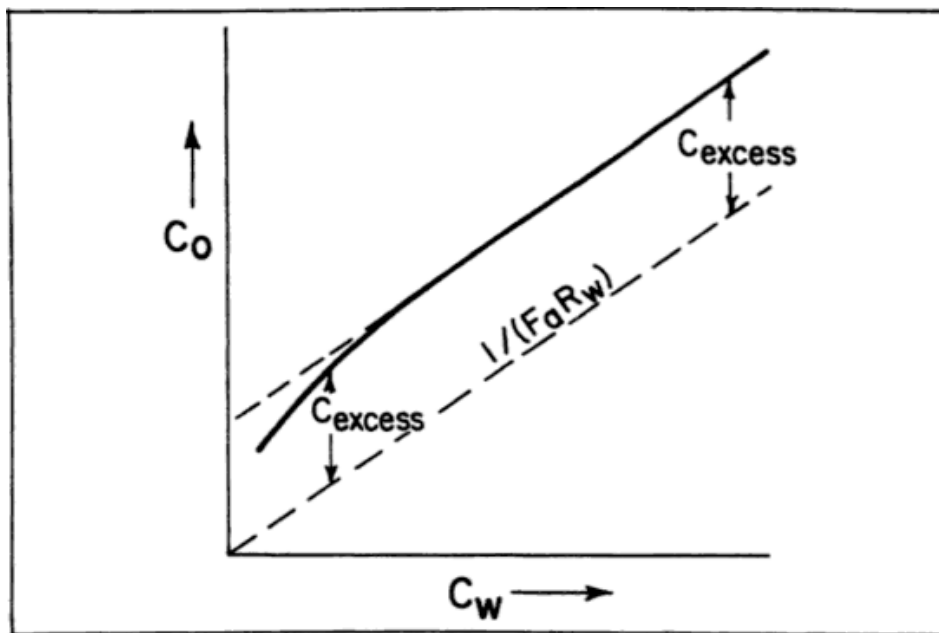


Figure 10-3 Excess conductivity contributed by clay, arrows are indicating the excess conductivity

The excess conductivity, C_e is defined as

$$C_e = B^* Q_v \text{ Equation 10-9}$$

where

B: The counter ion equivalent conductance in s/m per meq/cc.

Qv: The cation exchange capacity per unit pore volume.

10.1.6 Cementation Exponent (m) and Tortuosity Factor (a)

The cementation factor is related to the shape, size and distribution of pores and the tortuosity in a formation.[29] The m will be increasing with the complexity of the currents path. In consolidated sandstones the most common value is 2 while it is 2.15 for unconsolidated sandstones. [27] The tortuosity factor ,a, varies from 0.62 to 1.2 and represents the distance a fluid must travel to pass through the given interval. [28] As for the cementation factor the values of the tortuosity factor are also related to the pore characteristics and may vary in different kinds of reservoir rocks.

The best choices for a and m are determined by laboratory experiments of rock samples. In these experiments also the porosity is measured.[29] The cementation factor can then be derived from using the formula for the formation factor. Equation 8-13 and equation 8-14 and equation shows the relationship between F, a, m and ϕ

$$F = \frac{R_o}{R_w} \quad \text{Equation 10-10}$$

$$F = \frac{a}{\phi^m} \quad \text{Equation 10-11}$$

When the formation factor value and the porosity are known, a log- log plot can be made where the formation factor is plotted against the porosity. A regression line drawn across the values represents the cementation factor m.[17] This is an inverse function of porosity, the greater the porosity the smaller the tortuosity. [28]

10.1.7 The Archie's Equation

The Archie's equation can be described as an equation attempting to describe the saturation in a clean consolidated sandstone. [31]The equation relates the true resistivity of a saturated

rock, to its total porosity resistivity of the formation water, R_w . The determination of the total porosity is defined in section 13.2.3 This method is also referred to as the total water saturation and requires SCAL data to be calculated. [34] [49]

Archie's equation (1942) is given by the following relationships [27]

$$S_w^n = \frac{R_o}{R_T} \rightarrow \left(\frac{R_o}{R_T}\right)^{\frac{1}{n}} \quad \text{Equation 10-12}$$

where

R_o : The resistivity of a rock which is 100% fully water saturated, $S_w=1$

R_T : The resistivity of a rock containing hydrocarbons and water

n : The saturation exponent

By combining equation 8-13 and equation 8-15 give [27]

$$S_w = \left(\frac{F \cdot R_w}{R_t}\right)^{\frac{1}{n}} \quad \text{Equation 10-13}$$

By substituting from equation 8-14, Archie's equation for water saturation, S_w of a reservoirs un invaded zone gives the general form of Archie's equation [27]

$$S_w = \left(\frac{a \cdot R_w}{R_t \cdot \phi^m}\right)^{\frac{1}{n}} \quad \text{Equation 10-14}$$

where

S_w : Water saturation

n : Saturation exponent

R_o : True resistivity in water bearing reservoir

R_t : True formation resistivity

a: Tortuosity factor

ϕ : Total porosity

m: Cementation factor

R_w: Formation water resistivity

10.1.8 The Indonesian Equation

The Indonesian equation is a complex formula, but at the same time a good option to use in the determination the water saturation when the formation is influenced by clay. It is also referred to as the effective water saturation due to its dependency on log data. No special core analysis data are needed in this calculation and due to this it is very applicable for the first drilled wells in a area where there is not possible to obtain SCAL data.[34] The method of determining the water saturation by Indonesia can be divided into two main groups; either treating the shale as a volume of conductive material or analyzing the effects of clay counter ions. In the interpretation performed in this thesis the version of the Indonesia Equation where the shale is treated as a volume has been used. The Indonesia equation is very applicable in calculations where the shale content is higher than 30% and the ratio of shale resistivity to formation water resistivity is lower than 10%. [17] [32]

The Indonesia equation is given below

$$\frac{1}{\sqrt{R_T}} = \left[\frac{V_{cl}^{1-\frac{m}{2}}}{\sqrt{R_{cl}}} + \frac{\phi^{\frac{m}{2}}}{\sqrt{a \cdot R_w}} \right] * S_w^{\frac{n}{2}} \text{Equation 10-15}$$

where

R_t: True formation resistivity

V_{cl}: Clay volume

R_{cl}: Clay resistivity

R_w: Water resistivity

a: Tortuosity factor

m: Cementation factor

ϕ : Porosity

n: Saturation exponent

S_w: Water saturation

10.1.9 The Waxman Smits Equation

The Waxman Smits equation is a saturation model that to deals with the excess conductivity introduced by clays in a total porosity model. It can be thought of as an extension of the

Archie's equations for clean sands into shaly sands where the Waxman Smit account for the presence of the clay counter ions. The model is based on the laboratory observations on nearly 200 samples of shale sandstones and it provides the link between CEC and excess conductivity mentioned in section 10.1.5 [33] [34] [35] The saturation equation may be formulated as:

$$S_w^{-n^*} = \left[\left(\frac{R_t}{R_w} \right) * \phi^{m^*} * \left(\frac{1 + R_w * B * Q_v}{S_w} B Q_v \right) \right] \quad \text{Equation 10-16}$$

where

B: Constant related to the temperature.

Qv: Cation exchange capacity per unit pore volume (meq/cc)*

m* and n*: cementation exponent and saturation exponent for shaly formations

φ: Total porosity

Rw: Formation water resistivity

Sw: Water saturation

RT: Resistivity from logs

A computational complication from the equation is that Sw appears on both side of the equation. Due to this it is necessary to initially assume the saturation value on the right hand side of the equation is equal to 1. By rounds of iterations it will be possible to find a sufficient answer when the Sw on the left hand side ceases to change beyond 0.001. [36]

*The Qv are derived from the cation exchange capacity, CEC, of the clays measured in the laboratory.

$$Q_v = \frac{CEC * \rho}{100 * \phi} \quad \text{Equation 10-17}$$

10.2 The Saturation Modelling

10.2.1 The Capillary Pressure

The capillary pressure phenomenon has several important tasks in the petroleum industry. It can for instance be used to evaluate reservoir rock quality, pay vs. non pay, expected reservoir fluid saturations, depth of the reservoir fluid contacts and also the seal capacity. [37] The capillary pressure controls the static distribution of fluids in the reservoir at initial state and distribution of the remaining hydrocarbons after primary production [30]

The capillary pressure occurs in a porous medium when two or more immiscible fluids are present in the pore space at the same time. Factors like the surface, interfacial tension, pore size and shape and wetting properties affect the capillary forces. [37] [38] [39]

The most common definition for the capillary pressure is described as the pressure difference between the non- wetting and wetting phase across an interface that is curves

$$P_c = P_{nw} - P_w \quad \text{Equation 10-18}$$

where

P_c : capillary pressure

$P_{nonwetting}$ phase: Pressure of the non wetting phase

$P_{wetting}$ phase: Pressure of the wetting phase (often water)

When a non- wetting fluid is displacing a wetting fluid in a porous rock, a curved interface is formed in the pores.[38] From this we can observe that the capillary pressure is dependent on the interfacial tension of the system together with the curvature of the interface. The following formula is often used to express the relation between the two phases by capillary pressure for a tube of radius, r :

$$P_c = \left(\frac{2 * \sigma * \cos\theta}{r} \right) \quad \text{Equation 10-19}$$

where

σ : Interfacial tension

θ : Contact angle

r: radius of the cylindrical capillary

The gravity forces are balanced by the capillary forces and for this reason it can also be possible to determine the capillary pressure at a point in the reservoir from the product of the height above the free water level and the difference in fluid densities.

$$P_c = \Delta\rho * g * h \text{ Equation 10-20}$$

where

ρ_w : Specific gravity of the wetting phase

ρ_{nw} : Specific gravity of the non wetting phase

g: Gravitational constant

h: Hydrocarbon height

σ : Interfacial tension

θ : Contact angle between fluid and capillary tube

10.2.2 Interfacial Tension and Surface Tension

The interfacial tension and surface tension, σ , can be defined as the force F per unit length, also known as the work, that must be applied to a fine element in contact with a liquid or gas surface to maintain it in equilibrium. The two expressions may be separated into each more specific definitions. The surface tension is a tension that arises over the boundary between a liquid and a gas in equilibrium. [41] [42] This can either be an interface of a liquid/ gas or liquid/vapour. The interfacial tension on the other hand is a tension when the interface is between two different liquids in equilibrium. [40] The tension in these two parameters is in the first place a result of unbalanced forces at the boundary between liquid/liquid or liquid/gas, which develops in order to balance the forces out. Interfacial tension and surface tension are often expressed in dynes per centimetre or in N/m.

During the production of natural gas the gas phase are generally in the presence of a liquid hydrocarbon phase or in the presence of an aqueous liquid phase. Due to this it will be

necessary to determine the surface tension of the liquid phases together with their interfacial tension.

Interfacial tension and contact angle will vary as a function of temperature, pressure and wettability conditions, and should be measured and evaluated for each relevant fluid system both laboratory and reservoir conditions. Values of $\sigma\cos(\theta)$ for oil- brine at reservoir conditions vary significantly but are generally in the range of 10-30 while for gas- brine 30-50. [42]

Table 10-1 Contact angles and Interfacial tension

| Fluids | σ | θ | $\sigma*\cos(\theta)$ |
|--------------|----------|----------|-----------------------|
| Air- Mercury | 480 | 140 | 368 |
| Air- Brine | 72 | 0 | 72 |

10.2.3 The Capillary Pressure Curve and Irreducible Water Saturation (Swirr)

The capillary pressure curve gives the relation between the saturation and the capillary pressure. These capillary pressure curves are deduced from the routine core analysis in the laboratory. The capillary pressure curve for a porous medium is a function of many different parameters like the pore size, pore size distribution, pore geometry, fluid saturation, fluid saturation hysteresis, wettability and interfacial tension have all impact on the capillary pressure curve. [44] [37] [35]

The curve can be divided into the drainage capillary pressure curve and the imbibition capillary pressure curve. The drainage capillary pressure curve defines the displacement of the wetting phase, like water, from the porous medium by a non- wetting phase, hydrocarbons. The imbibition curve describes the displacement of the non- wetting phase by the wetting phase. For both drainage and imbibition, the capillary pressure is given as the difference between non-wetting phase pressures subtracting the wetting phase pressure.

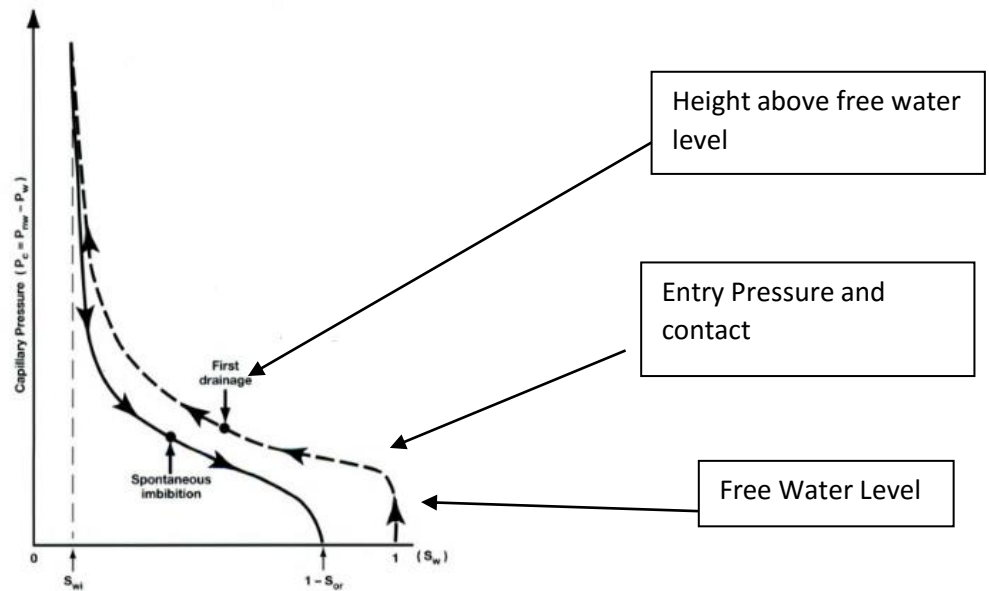


Figure 10-4 Capillary Pressure vs. Water Saturation

The irreducible water saturation, S_{wir} , is located where the capillary pressure curve is nearly vertical, see Figure 10-4. If the capillary pressure is increased, there will be no effect on the water saturation. S_{wir} is commonly estimated as log derived saturation measured a certain height above the free water level. It can also be defined from the core capillary pressure data, often at the endpoints of a porous plate experiment or a centrifuge drainage experiments.

The increase of the pressure of the non-wetting phase results in several smaller pores becomes invaded.

The capillary pressure from Figure 10-4 has a value of zero when the system is fully saturated by the non-wetting phase. In order to displace the non-wetting phase from the largest pores in the porous medium, the displacement pressure, P_D , is introduced. The term can due to this be defined as the lowest capillary pressure that is required to introduce the non-wetting phase in the largest pores present in a rock sample. A displacement pressure that is defined by a low value is indicating larger pores and due to this relatively higher permeability. When the capillary pressure increases will this result in that several smaller pores also becomes invaded.

In Figure 10-5 of the capillary pressure curve this is represented in the middle section of the curve, the transition area. How low the middle section of the curve is located will give an indication of increase in pore size and a resulting higher permeability. The larger the slope of this middle section is, the poorer sorting and pore size distributions resulting in low porosity and permeability in the current rock. The vertical section is where the irreducible water saturation, S_{wirr} , has been reached. The reservoir rocks will in this part of the curve represent very fine grained, low porosity and permeability rocks. The pore size will therefore be an important factor to determine the value of the capillary pressure and the irreducible water saturation.

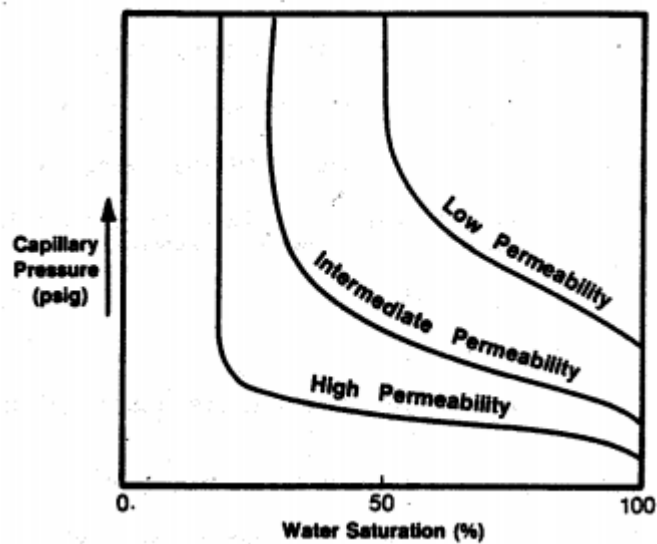


Figure 10-5 Variation of P_c with S_w for the same fluid with different rock systems

10.2.4 The Free Water Level (FWL) and the Gas Water Contact (GWC)

From section 10.2.1, it was defined that the capillary pressure is referred to as the height located above the free water level. The free water level can from this be defined as the elevation point where the capillary pressure is equal to zero and are increasing upwardly in the hydrocarbon column. Capillary pressure can be converted to height, h , and plotted against water saturation, S_w as a capillary pressure curve. [46] [47]

The transition zone is often referred to the zone where saturation changes with height. The transition zone goes from 100% water saturation to the irreducible water saturation, S_{wirr} . [24]The gas water contact appears at a shallower depth compared to the FWL where the

capillary entry is reached. The contact can be defined anywhere on the gradual transition from 100% water to maximum gas saturation.

10.2.5 The Leverett J-function

Leverett (1941) defined the J-function as a way to average all capillary pressure curves into a universal curve through normalizing the capillary pressure for a reservoir. [41] This is based on parameters like the core permeability and porosity and the interfacial tension. The permeability and porosity has high impacts on the capillary pressure data and must always be considered with respect to the permeability and porosity of the cores they are measured from. The capillary pressure measurements are obtained from SCAL data from core samples measured on the laboratory. These core samples will only indicate the properties of the reservoir in small portions and this is the reason for gathering all the capillary data to obtain the best characterization of the reservoir in the most optimal way. [41]

The normalization approach will in theory only function as intended when the pore size to the pore throat ratio is similar. This means that for the function to work in the most optimal way it is necessary that the normalization is completed on similar rock types.

The Leverett J- function is a dimensionless function and is defined as

$$J = \left(\frac{P_c}{\sigma^* \frac{\cos\theta}{3.141}} \right) lab * \left(\sqrt{\frac{k}{\phi}} \right) lab \text{ Equation 10-21}$$

where:

Pc: Capillary pressure

σ : Interfacial tension

K: Permeability

ϕ : Porosity

11 Well testing

A well test functions as a reliable provider of important information that is related to the reservoir pressure, reservoir size, the distance from well to possible boundary systems, type of boundaries (permeable/impermeable), the heterogeneity in the reservoir (geology), flow rates and identifying skin. From this information a well test will have the ability to improve, look for consistency with data already known, and forecast the reservoir performance. [43], [48], [22]

11.1 Pressure Transient Test and Pressure Transient Analysis

Pressure transient test are designed to create pressure disturbance generated in reservoir by drawdown and build up tests. these are controlled flow periods where draw down means that the well is opened at constant rate giving. This will lead to a decrease in bottom hole pressure, while a build up is when the well is shut in which will give an increase in the bottom hole pressure. A standard pressure transient well test consists of a cleanup, initial build up, main flow and a final build up. The term clean up is described as first a draw down with the purpose to make the well clean of any drilling or completion fluids present in the wellbore and clean the perforations. [22] [48]

Build up tests are the best method to determine near well boundaries, skin and flow capacity due to the constant rate. By including the derivatives in addition to the pressure plot it will be easier to identify the different flow regimes. The presence of wellbore storage, skin effects, production history and rate changes will contribute in a distortion of important features in pressure and rate responses.

The collected data from the pressure transient test is applied to a mathematical model together with basic reservoir data to analyse the pressure changes generated in the reservoir over a period. The shape of the derivative of early, middle and late time in a flow period is therefore helpful in the interpretation.

11.1.1 Wellbore Storage (WBS)

The wellbore storage are recognized as the after- flow of fluid into the wellbore after the wellbore is shut. The ability to identify and recognize this effect is important. To reduce the wellbore storage effect as much as possible (from hours to minutes) is important to install the down hole gauges close to perforations. The wellbore storage will lasts until the pressure between the wellbore and formation are equalized. The longer a wellbore storage lasts, the longer unit slope extends before breaking over to radial flow. [48]

11.1.2 Skin

The skin effect describes the condition of the well, whether it is damage of stimulated. It is normally seen on pressure response and described as an additional pressure drop near the well. The skin factor is described by the equation. [48]

$$S = \left(\frac{k}{k_s} - 1 \right) * \ln \left(\frac{r_s}{r_w} \right) \quad \text{Equation 11-1}$$

where

S: Skin factor

ks: Permeability of damaged formation

rs: Radius of damaged formation

k: Permeability

r: Radius of the well bore

A positive skin value indicates damaged well near the wellbore which will slow down pressure recorded. A negative skin value indicates higher permeability near wellbore and intersecting fractures can be one of the reasons for this. [48]

11.1.3 Identification of the Infinite Acting Radial flow and kh

The identification of the infinite acting radial flow is a important factor. This is when the flow in the reservoir is radial and not influenced by any outer boundaries so the reservoir is looking infinite in size due to the no outer boundary effects are located. Reaching a radial flow during the well test will contribute in simplifying the mathematical solution of diffusivity equation. The interpretation will then become less complicated. [48]

The important parameter permeability-thickness, kh, is identified in this period. this is a key factor in the flow potential for a well. It can be used for a large number of reservoir calculations like future well performance, recovery potential (secondary and tertiary) and different well stimulation processes. It is possible to obtain the Kh value by calculating the slope from the semi- log plot vs. time vs. pressure by the following equation:

$$m = 162.6 * \frac{q * B * \mu}{KH} \text{Equation 11-2}$$

where

m: Slope from the semi- log plot

C= 162.5 for oilfield units

q: Rate

B: Formation factor

my: Viscosity

Kh: Permeability thickness

11.1.4 The Radius of Investigation

The radius of investigation gives an indication of how far into the formation a pressure transient signal has travelled from the well as a two-way event, for instance to a sealing fault and back. The distance depends on rock and fluid properties present in the formation. For pressure transient analysis test the radius of investigation can be used to estimate the distance from the wellbore to specific effects present in the formation.

On a log- log plot it is possible to recognize wellbore storage effects, skin/transition zone, radial flow period and boundary effects. (Figure 11-1) [48]

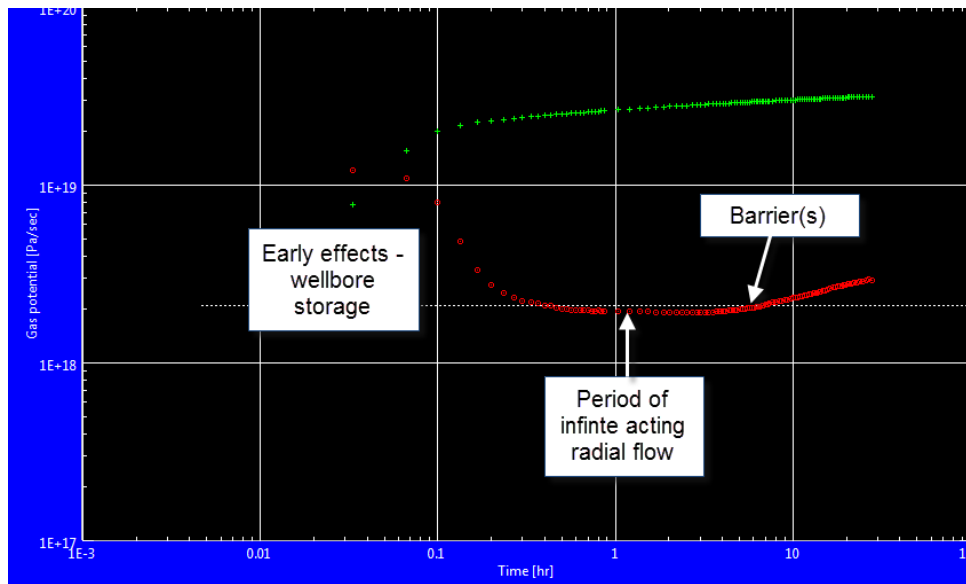


Figure 11-1 Log- log plot from DST1, well 15/9-15

11.2 Permeability in Well Tests

Most of the petrophysical interpretation techniques provides an estimation of absolute permeability. The well tests on the other hand measures the effective permeability to the hydrocarbons at the saturation, pressure and temperature conditions prevailing in the reservoir.

At the condition when the reservoir is at irreducible water saturation, S_{wirr} , the effective permeability to the hydrocarbons (oil or gas) are a fraction of the absolute permeability. In many cases this value, which correspond to the maximum relative permeability of the oil/gas can be close to 1 and due to this it is possible to achieve a direct comparison of absolute and effective well test permeability. However when the relative permeability is lower than 1 the well test permeability can result in significantly lower values compared to the core permeability. This can be even (worse) more reduced when water saturation in the reservoir is higher than the s_{wi} or in the presence of gas. [22]

12 Core Data Evaluation

The coverage of the core data in the Skagerrak formation is variable in amounts but were available in all three wells. The Table 12-3 and Table 12-4 shows the available special core analysis data from the three mentioned areas. The evaluation of the saturation and cementation exponent are presented in section 10.1.4.1 and 10.1.6.

Well 15/9-9 possess no special core analysis data. Due to this the properties from well 15/9-15 and 15/9-17 were compared with 15/9-9 to obtain the most similar properties. From Figure 12-1 it is observable to see from the histogram comparing core porosity that well 15/9-15 and 15/9-9 share more similar trends compared to well 15/9-17. Based on this the SCAL data from well 15/5-15 were used to calculate the parameter the water saturation in well 15/9-9.

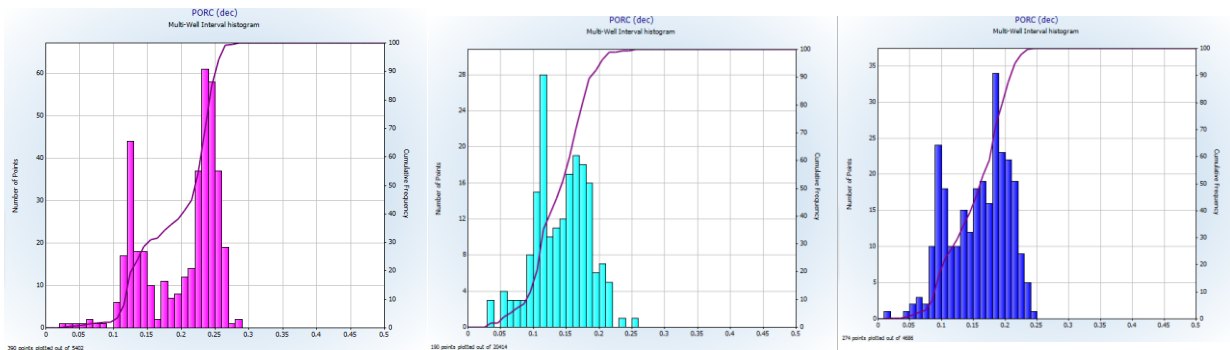


Figure 12-1 Core porosity properties in well 15/9-9, 15/9-15 and 15/9-17

12.1 Depth shift of core data

The core data from porosity and permeability had to be depth-shifted in order to reach a better match with the logs. Table 12-1 Depth shift of core data, well 15/9-15 and well 15/9-17 below shows the result for the depth shifts in well 15/9-15 and 15/9-17.

Table 12-1 Depth shift of core data, well 15/9-15 and well 15/9-17

| Well | Depth shifted [m] |
|---------|-------------------|
| 15/9-15 | 2.8 |
| 15/9-17 | 1.0 |

12.2 Grain density from cores

The density of the matrix, ρ_{ma} , is determined from the average core grain density value in each reservoir zone represented in the histogram, Figure 12-2. This is displaying the grain density vs. the number of values from conventional core analysis. The peak values from the histogram were almost the same in all three wells, 2.67 g/cc and 2.68 g/cc. The 2.68 g/cc value were therefore used for the whole interval in well 15/9-9 and 15/9-17, while 2.67 g/cc was used for well 15/9-15.

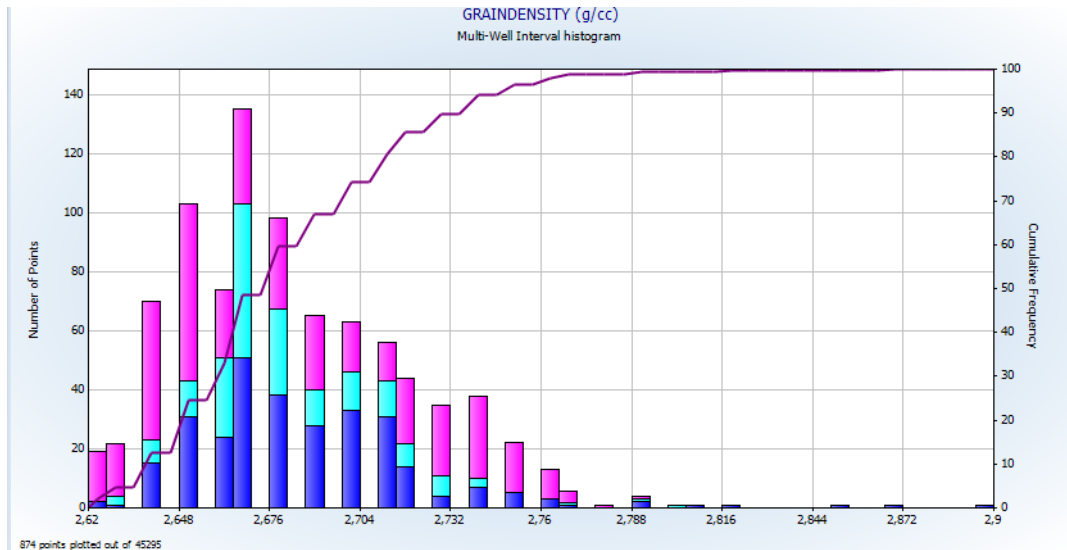


Figure 12-2 Histogram of most common grain density in all three wells*

*From Figure 12-2: Dark blue is representing well 15/9-9, aqua blue is representing well 15/9-15 and purple is representing well 15/9-17

The values are also listed below in Table 12-2.

Table 12-2 Grain density values from Well 15/9-9, 15/9-15 and 15/9-17

| Skagerrak Formation | | | |
|---------------------|---------|---------------|---|
| Area | Well | Grain density | Comment |
| Sleipner Øst | 15/9-9 | 2.68 | The high values of grain density may be due to the content of heavy minerals in the formation |
| Gungne | 15/9-15 | 2.67 | |
| Loke | 15/9-17 | 2.68 | |

12.3 Overburden correction

In order to correlate core values of porosity and permeability with the log values, the core data has been corrected to reservoir conditions. The core porosity and core permeability is therefore higher than the log derived porosity and permeability. This was done by the following equations for the Skagerrak Formation:

$$\Phi_{\text{res}} = 0.94 * \Phi_{\text{lab}} \quad [59]$$

$$K_{\text{res}} = K_{\text{lab}} < 10\text{mD} \Rightarrow 0.5 * K_{\text{lab}} \quad [59]$$

$$K_{\text{lab}} > 10\text{mD} \Rightarrow 0.65 * K_{\text{lab}}$$

12.4 Cementation exponent, m

The cementation exponent, m, has been described earlier in section 10.1.6. The m exponent was established with plotting the formation factor, Figure 12-3 and Figure 12-4, against core porosity but also by a regression analysis between the cementation factor from each core sample vs. the permeability, Figure 12-5.

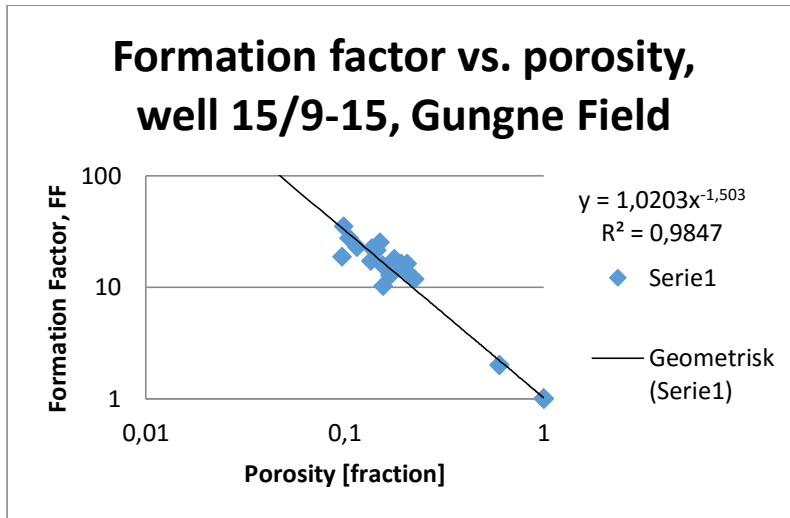


Figure 12-3 Determination of a and m from cores, well 15/9-15

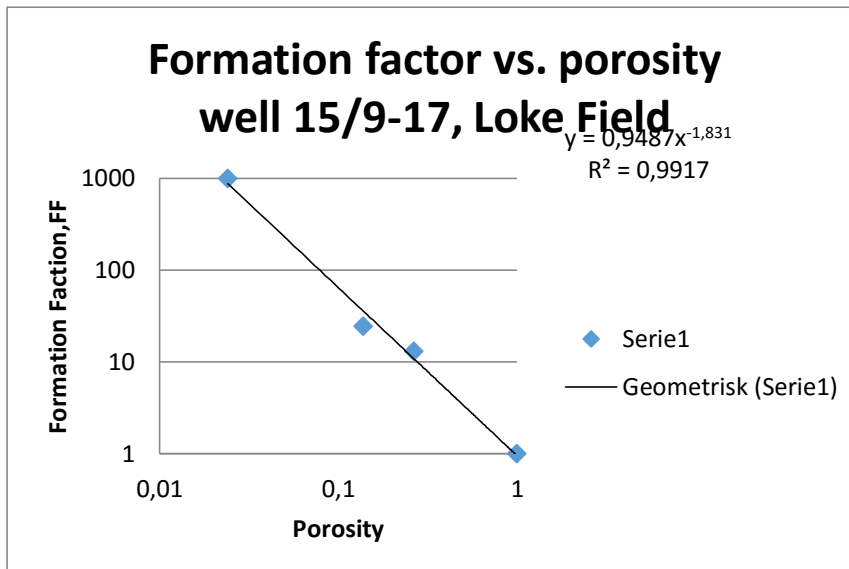


Figure 12-4 Determination of a and m from cores, well 15/9-17

In Figure 12-3 and Figure 12-4 the cementation exponent m , have been calculated and plotted against permeability for the Skagerrak Formation. The data from the special core analysis report showed for well 15/9-15 that the cementation exponent value of 1.55 gave a water saturation that were too low. A cementation factor equal to 2 which is a typical value for consolidated sand gave a more realistic water saturation. Figure 12-3 and Figure 12-4 shows the different scenarios of m values that were used in the evaluation of the water saturation. Scenario 2 seemed to obtain the most realistic S_w , especially in the water zone, and was therefore used further in the evaluation of the water saturation.

High m means high water saturation and lower hydrocarbon volume due to high water saturation.

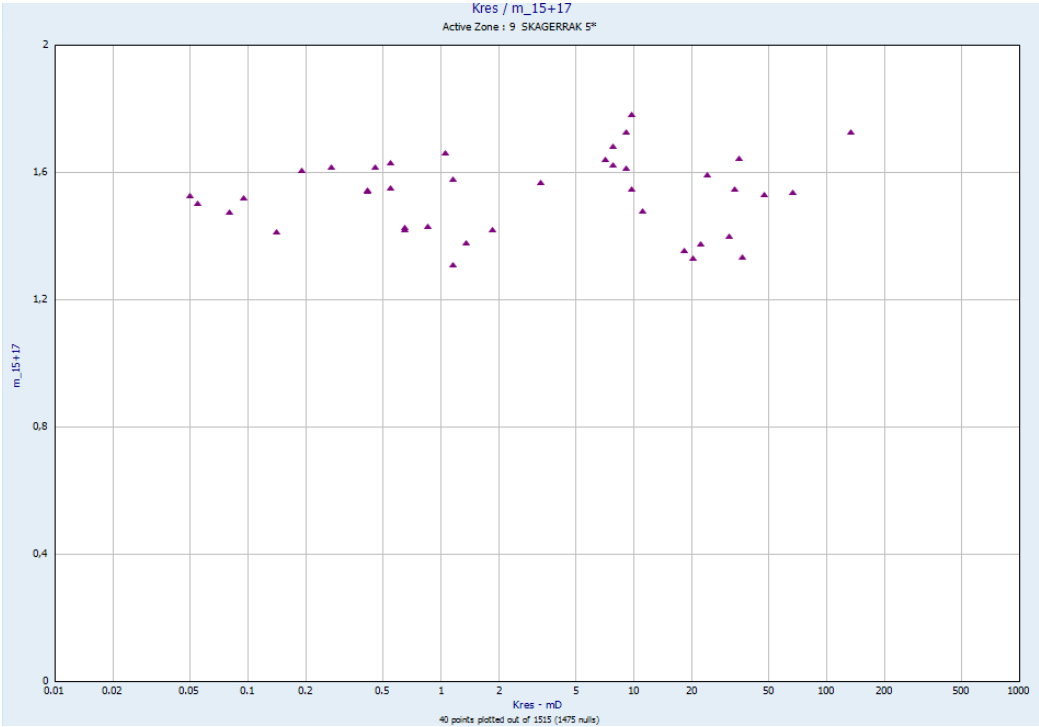


Figure 12-5 Cementation exponent m from well 15/9-15 and 15/9-17 vs core permeability, Skagerrak Formation

From Figure 12-6 water saturation from Indonesia Equation is plotted in the same track in Interactive Petrophysics to compare the two scenarios with different values of cementation exponent, m and saturation exponent, n .

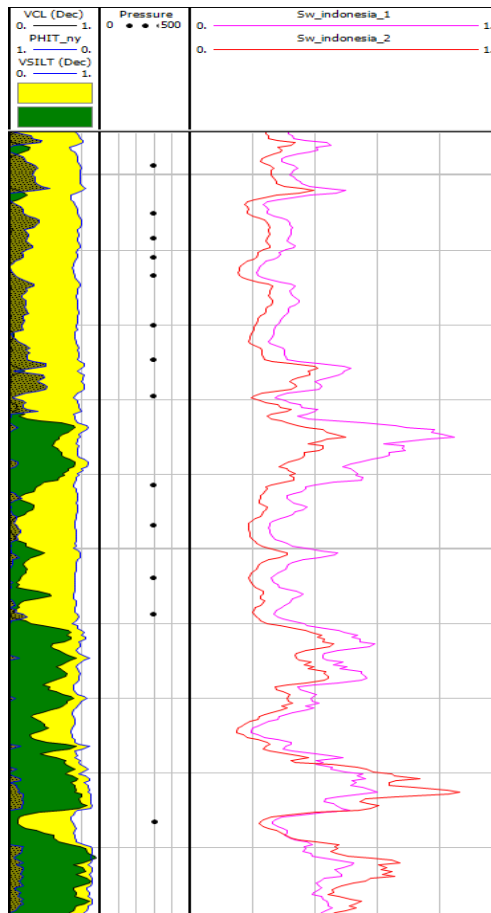


Figure 12-6 Log curve from Indonesia Equation in well 15/9-15, Gungne Field. The red curve represents scenario 1 while the pink represents scenario 2

12.5 Saturation exponent, n

The saturation exponent n has been described in section 10.1.4.1. The n exponents values was found from regression analysis of the resistivity index, RI, against water saturation, SW and listed below for the Skagerrak formation. Also for this parameter it was necessary to look at different scenarios of the water saturation by changing the n . The data from the core report show lower values than what was used in this evaluation. The n values below a value of 2 gave not the best result. In Figure 12-7, the n exponents from conventional core report are plotted against core porosity in the Skagerrak formation for well 15/9-15 and 15/9-17.

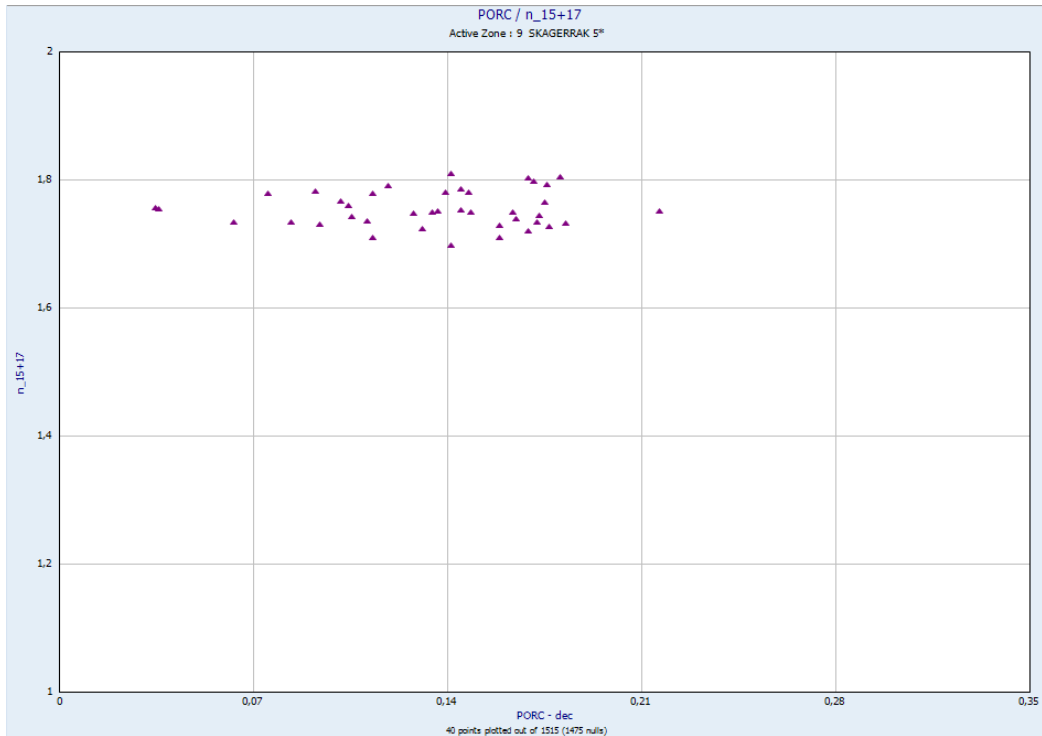


Figure 12-7 Saturation exponent vs. porosity, Skagerrak Formation well 15/9-15 and well 15/9-17

The displays the values used in the Indonesia equation and Archie's equation. These are marked in blue, scenario 2, Table 12-3.

Table 12-3 a, m and n values used in Skagerrak evaluation

| Well/area | Scenario | a | m | n |
|---------------------|----------|---|------|------|
| 15/9-9 Sleipner Øst | 1 | 1 | 1,55 | 1,79 |
| | 2 | 1 | 2 | 2 |
| 15/9-15 Gungne Area | 1 | 1 | 1,55 | 1,79 |
| | 2 | 1 | 2 | 2 |
| 15/9-17 Loke Area | 1 | 1 | 1,83 | 1,9 |
| | 2 | 1 | 2 | 2 |

For the Waxman Smits model the values listed in Table 12-4 were evaluated. The areas marked in blue turned out to be best in this case. The m^* and n^* were given by adding a factor of 0,1 to the m and n value from the SCAL report. [34]

Table 12-4 a, m* and n* determination in all wells

| Well/area | Scenario | a | m* | n* |
|---------------------|----------|---|------|------|
| 15/9-9 Sleipner Øst | 1 | 1 | 1.65 | 1.89 |
| | 2 | 1 | 2.1 | 2.1 |
| 15/9-15 Gungne Area | 1 | 1 | 1.65 | 1.89 |
| | 2 | 1 | 2.1 | 2.1 |
| 15/9-17 Loke Area | 1 | 1 | 1.93 | 2 |
| | 2 | 1 | 2.1 | 2.1 |

13 Petrophysical Model

A petrophysical evaluation has been done in the Skagerrak formation from the wells 15/9-9, 15/9-15 and 15/9-17, located on Sleipner Øst, Gungne and Loke, respectively. The software program Interactive Petrophysics by Senergy has been used to visualize the logs and to show how the modelled continuous KLOGH and PHIF from the best correlations fits the core data. A separate collection of tables and CPI plots are contained in Appendix 20.

The petrophysical model is based on total porosity from density and neutron log with water saturation from the Indonesia equation, the Waxman Smit Method and the Archie equation. Shale volume has proven to be useful in the evaluation of the continuous permeability and porosity and also as an additional cut off when determining the net sand.

13.1 Clay Volume

The clay volume is derived from the gamma ray log by using a linear relationship as shown in the equation below. It was also derived by cross plot, but this was not the representative method in this analysis and therefore the Vclay curve was based on the gamma ray for all wells. To estimate the gamma ray clean and shale parameters the gamma ray curve has been examined and also the gamma ray log vs. depth. Gamma ray parameters are summarized in

Table 13-1. The silt and clay content is high, probably higher than what the clay indicator was able to indicate.

Table 13-1 used Gamma ray values in Vclay determination

| Well | Area | Formation | |
|---------|--------------|-----------|--------|
| | | Skagerrak | |
| | | GR min | GR max |
| 15/9-9 | Sleipner Øst | 28 | 88 |
| 15/9-15 | Gungne | 29 | 87 |
| 15/9-17 | Loke | 35 | 94 |

13.2 Porosity

The total porosity is derived from the density log calibrated to overburden corrected core porosity and by cross plot derived from the density -and neutron log. The following section will show results by applying these two methods. The effective porosity method is described in section 10.1.2.2.

13.2.1 Cross plot derived from density- neutron logs

These cross plots were made in the Interactive Petrophysics software from Senenergy. From this method it is possible to get an good overview of how the measurements are affected by porosity, hydrocarbon density and lithology which include both clay and non clay minerals.

The wells shows an overall heterogeneous sand. Due to the clay content, the porosity points will be located below the sandstone line Figure 13-1, Figure 13-2 and Figure 13-3. Clean water bearing sandstones in these wells, will fall on the straight line of equal density and neutron porosity estimates. The points located above the sandstone line in well 15/9-15 and 15/9-17 are due to the hydrocarbon effect. Well 15/9-9 is water filled and shows therefore no indication to gas in the cross plot. Heavy minerals can also be affecting the points to be located below the sandstone line.

The porosity in all three well are fairly good with an average ranging from 13- 16 %. Well 15/9-9 shows very high neutron values due to the disturbance from the neutron log readings in the intervals around 2682- 2697 m. This is contributing to give a

misinterpretation of the effective porosity in these intervals. Due to this it is important to exclude these intervals from the log curve and instead use the total porosity.

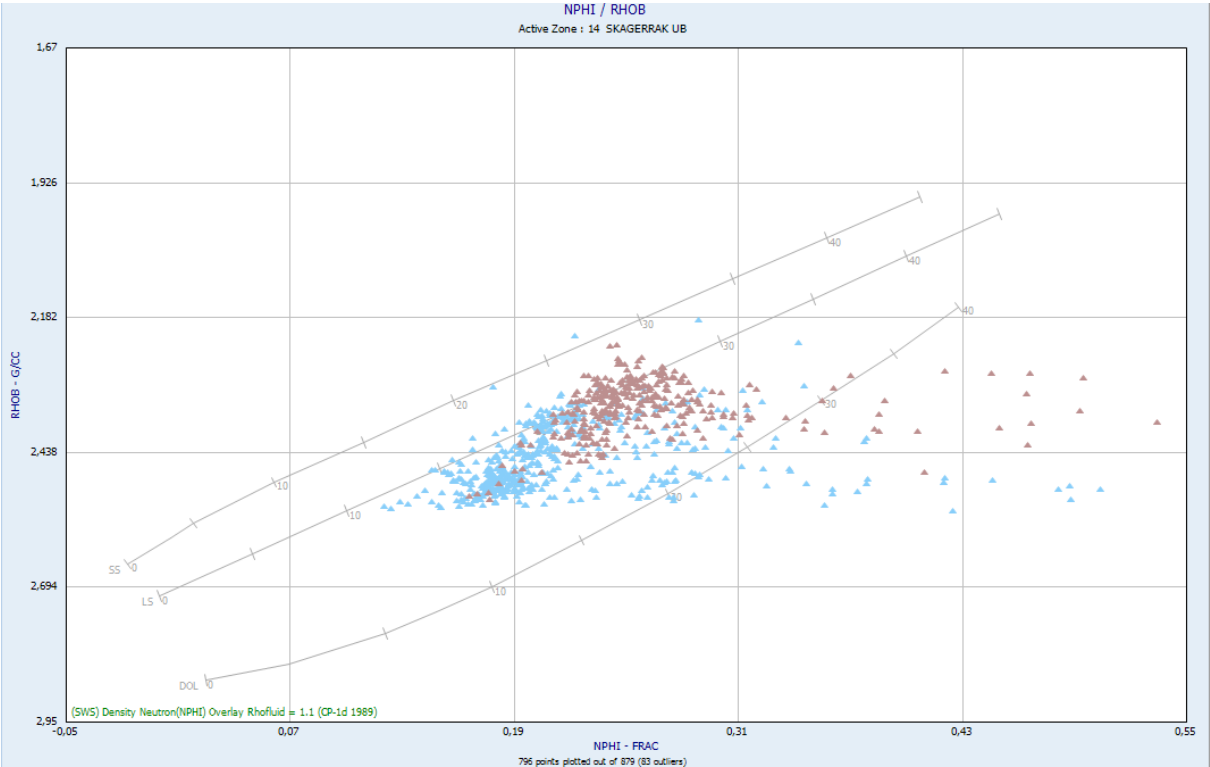


Figure 13-1 Porosity distribution in Skagerrak, well 15/9-9

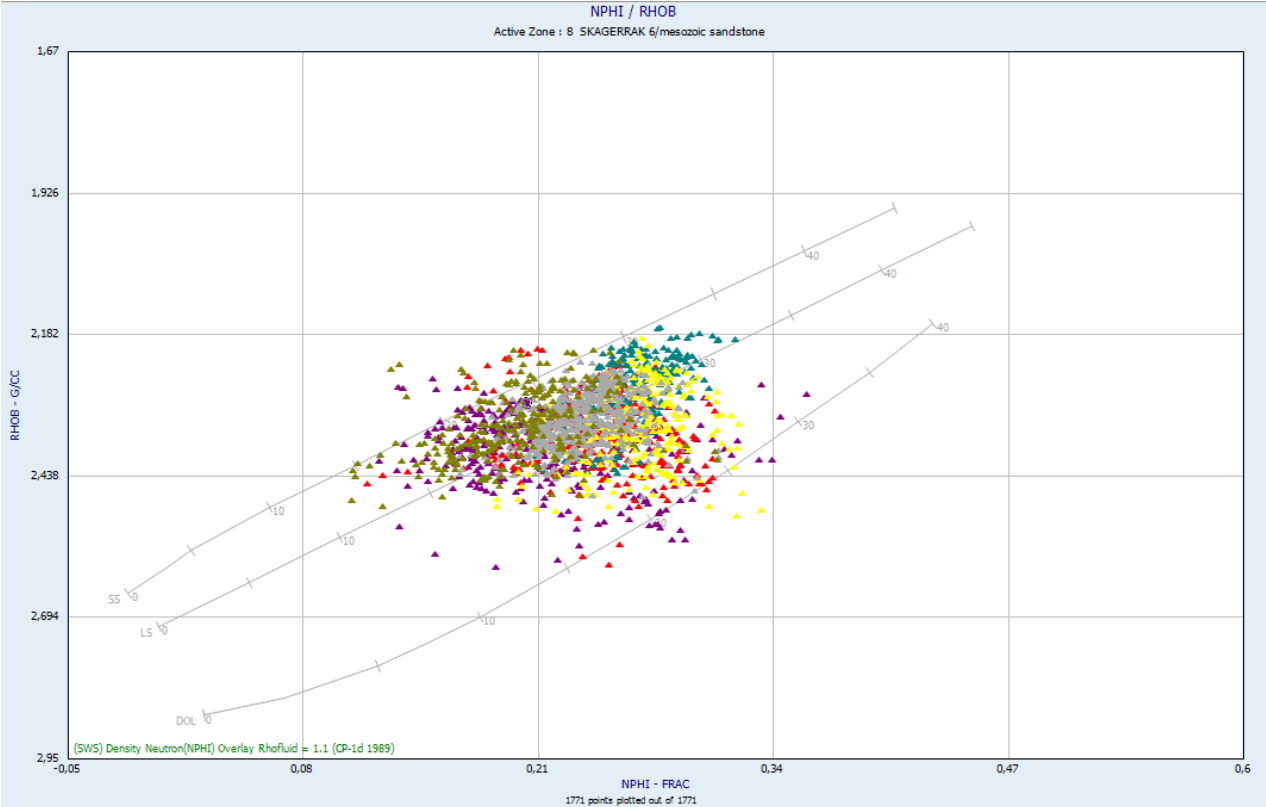


Figure 13-2 Porosity distribution, Skagerrak, well 15/9-15

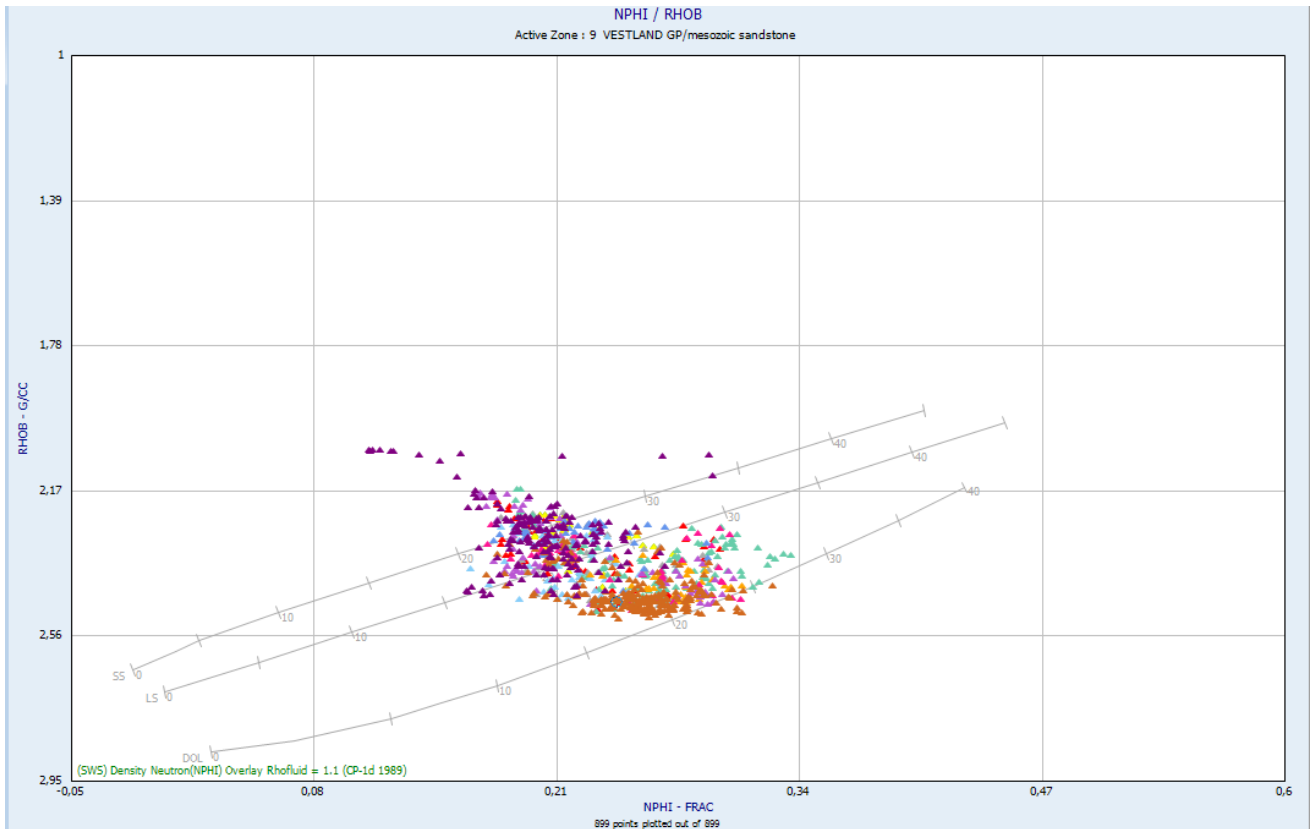


Figure 13-3 Porosity distribution, Skagerrak Formation, well 15/9-17

13.2.2 Effective Porosity Determination

The effective porosity has been established by applying Vclay correction and using the weighted formula shown in equation 13-1

$$\phi_E = \frac{7*\phi_{DC} + 2*\phi_{NC}}{9} \quad \text{Equation 13-1}$$

where

ϕ_{DC} : the porosity from the shale corrected density,

ϕ_{NC} : the porosity from the shale corrected neutron log

Both equations are given in equation 13-2 and 13-3:

$$\phi_{DC} = \frac{\rho_{ma} - \rho_b}{\rho_{ma} - \rho_f} - V_{cl} * \frac{\rho_{ma} - \rho_{cl}}{\rho_{ma} - \rho_f} \quad \text{Equation 13-2}$$

$$\phi_{NC} = (\phi_N + 0.04) - V_{cl} * (\phi_{Ncl} + 0.04) \text{Equation 13-3}$$

where

ρ_{ma} : Matrix density, g/cc

ρ_{fl} : Fluid density, g/cc

The value 0.04 is used as a correction for sandstone

13.2.3 Total Porosity Determination

The density porosity is based on the linear relationship between the bulk density and overburden corrected porosity from the cores. The core porosity is helium porosity measured under laboratory conditions and representing the total porosity that exceeds the effective porosity, ϕ_E .

The fluid density, ρ_{fl} , and ρ_{ma} is estimated from correlation of depth shifted and overburden corrected core porosity vs. the density log in the water zones. The parameters are summarized in Table 13-2. The regression lines determining the fluid density from the cross plots are shown in

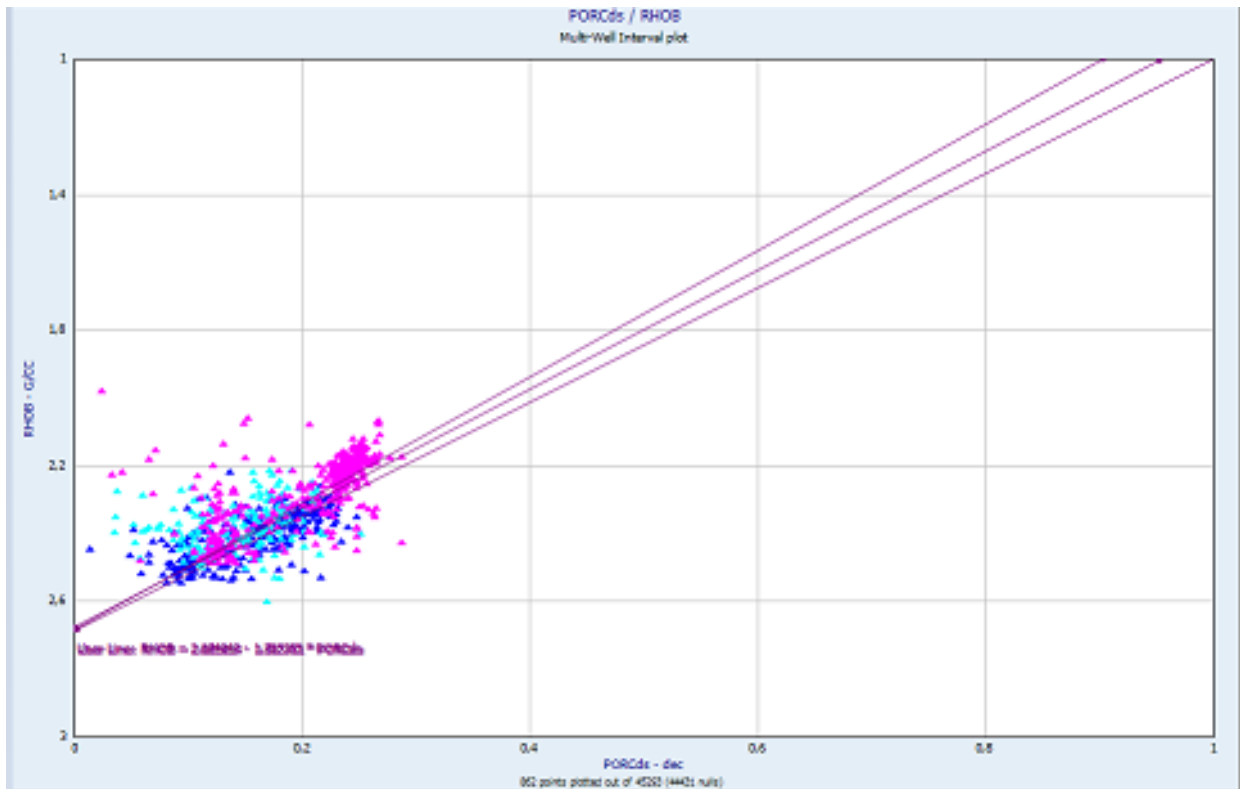


Figure 13-4 Bulk density vs. core shifted porosity of all three wells. Core data from water zones for the core porosity are available in all three wells.

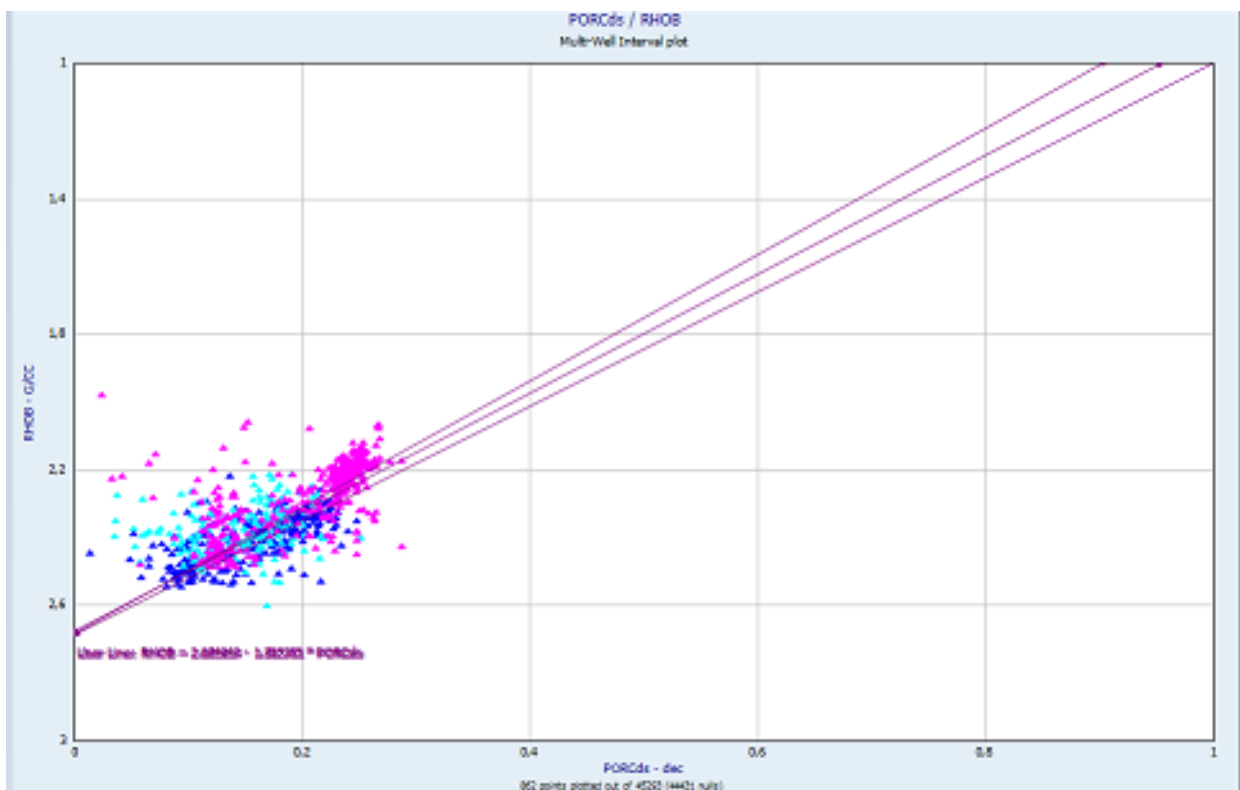


Figure 13-4 Bulk density vs. core shifted porosity of all three wells

The parameters for the clay density values and the shale neutron values are summarized in Table 13-2. The effective porosity and total porosity is represented in the CPI plot together with the depth shifted core porosity, Figure 20-1, Figure 20-2, Figure 20-3, Appendix 20.

Table 13-2 Input for the total porosity calculations

| Depth [m] | Well TVDSS, 100 % water zone | ρ_{ma} [g/cc] | ρ_{fl} [g/cc] | ρ_{cl} | NPhiclay | Mud | Formation |
|-----------|------------------------------|--------------------|--------------------|-------------|----------|-----|-----------|
| 2769.3 | 15/9-9 | 2.6878 | 1 | 2.481 | 0.224 | WBM | Skagerrak |
| 2903.3 | 15/9-15 | 2.6719 | 1 | 2.537 | 0.289 | WBM | Skagerrak |
| 2838.3 | 15/9-17 | 2.6824 | 1 | 2.502 | 0.256 | WBM | Skagerrak |

13.3 The Permeability determination

The continuous log permeability, KLOGH, is based on the widely used regression analysis between log porosity vs. overburden corrected core permeability applied for all three wells. The following general equation was used:

$$KLOGH = 10^{(-b+a*\phi_E)} \text{ Equation 13-4}$$

This is based on porosity and core permeability from special core analysis of well 15/-9-15 and well 15/9-17. Figure 13-5 shows the plot from well 15/9-9 while the other plots from well 15/9-15 and 15/9-17 are found in Appendix 20.2.1. The results of the continuous permeability curve, KLOGH are presented in Table 13-3.

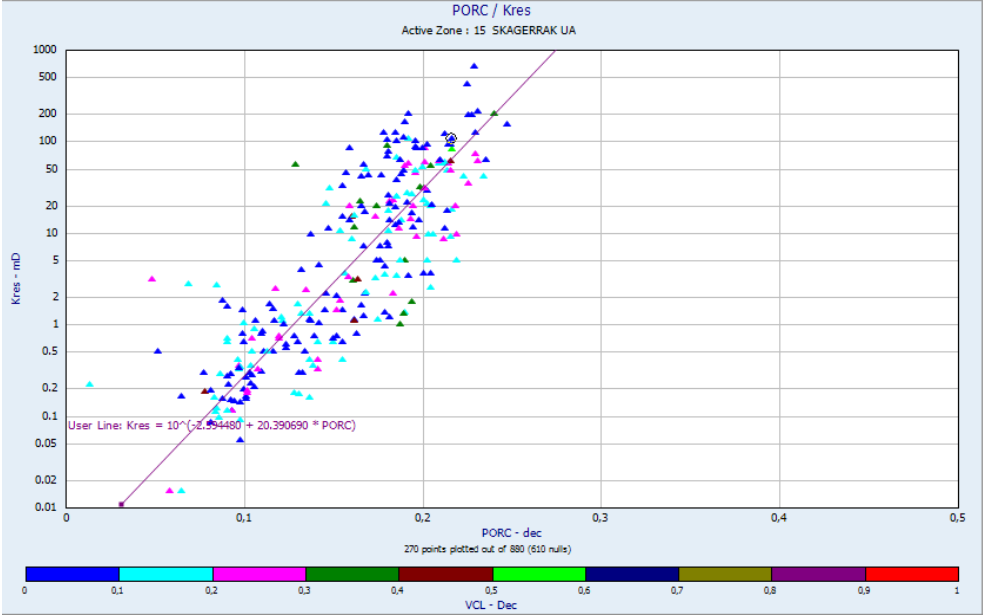


Figure 13-5 Core permeability vs. core porosity vs. vclay in well 15/9-9 Skagerrak Formation.

From (Figure 13-5) there is a trend of high Vclay values with lower permeability values in these plots, suggesting that Vclay is controlling the permeability.

An attempt to make a mutual regression line for the wells did not give satisfying result of the calculated permeability in this evaluation. There is a too large variation in Skagerrak for each well to be correlated together. Figure 13-6 shows the plotted core permeability vs. core porosity for all wells. The well 15/9-17 represents a correlation that is trending differently compared to the more similar trends in the wells 15/9-9 and 15/9-15. The high variation of the permeability in well 15/9-17, made it necessary to utilise more than one regression line for the permeability to achieve the best correlation between the log data and core data, Table 13-3 and figures listed in Appendix 20.2. Due to the similar trending in the permeability in Well 15/9-9 and 15/9-15, it would be possible to make a mutual correlation

between them for the field modelling of the Skagerrak formation when utilising several wells. Despite of this, there were done regression analysis separately for these two wells as well to avoid the possibility of too high and not realistic permeability values in the calculated permeability, appendix 20.2.1.

Table 13-3 Correlations from core permeability vs. core porosity used in the KLOGH evaluation

| Well | Area | Zone | Depth | | KLOGH | |
|---------|--------------|----------------|-------|------|---------|----------|
| | | | Top | Base | a | b |
| 15/9-9 | Sleipner Øst | Upper+Lower | 2821 | 2869 | 13.4379 | -1.79029 |
| 15/9-15 | Gungne | Skagerrak 5* | 2860 | 2905 | 19.6839 | -2.00813 |
| 15/9-15 | Gungne | Skagerrak 4*-1 | 2905 | 3091 | 15.9672 | -1.99053 |
| 15/9-17 | Loke | Skagerrak 9-7 | 2741 | 2763 | 16.0993 | -2.03189 |
| 15/9-17 | Loke | Skagerrak 6-2 | 2763 | 2808 | 15.1211 | -2.32792 |
| 15/9-17 | Loke | Skagerrak 1 | 2808 | 2814 | 19.3603 | -2.88363 |

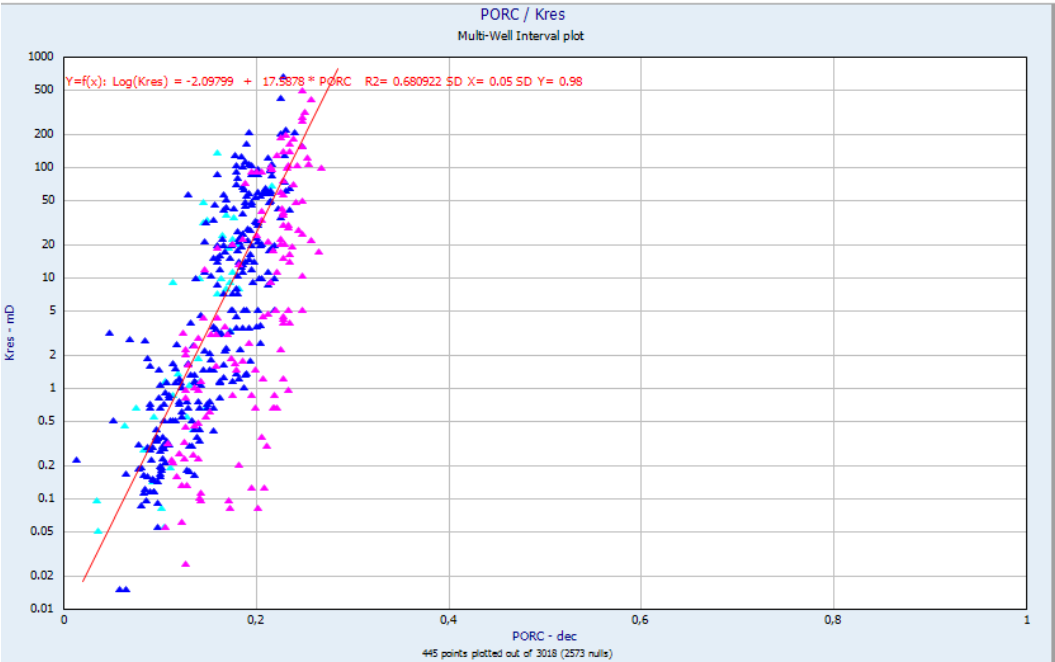


Figure 13-6 Core permeability vs. core porosity for all wells in Skagerrak Formation

13.4 Ratio of Vertical to Horizontal Permeability

The vertical permeability was plotted vs. the horizontal permeability in all three wells. The results are illustrated in Figure 13-7, Figure 13-8 and Figure 13-9:

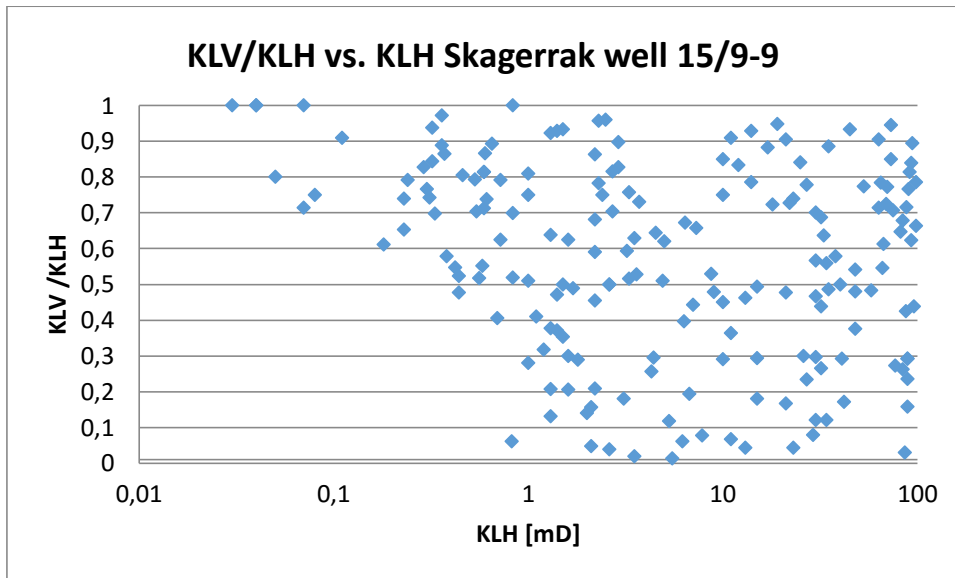


Figure 13-7 Vertical permeability vs. horizontal permeability, well 15/9-9

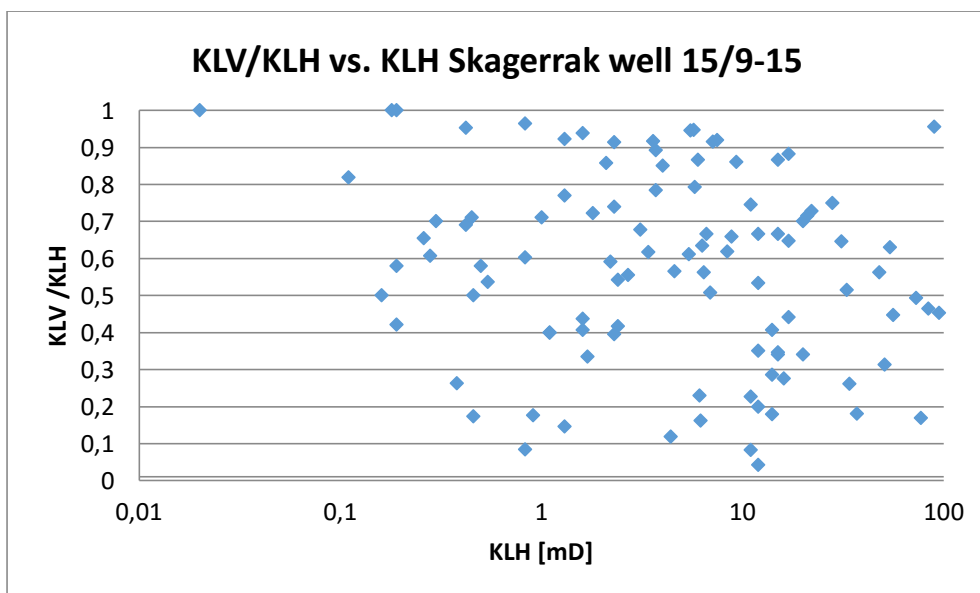


Figure 13-8 Vertical permeability vs. horizontal permeability, well 15/9-15

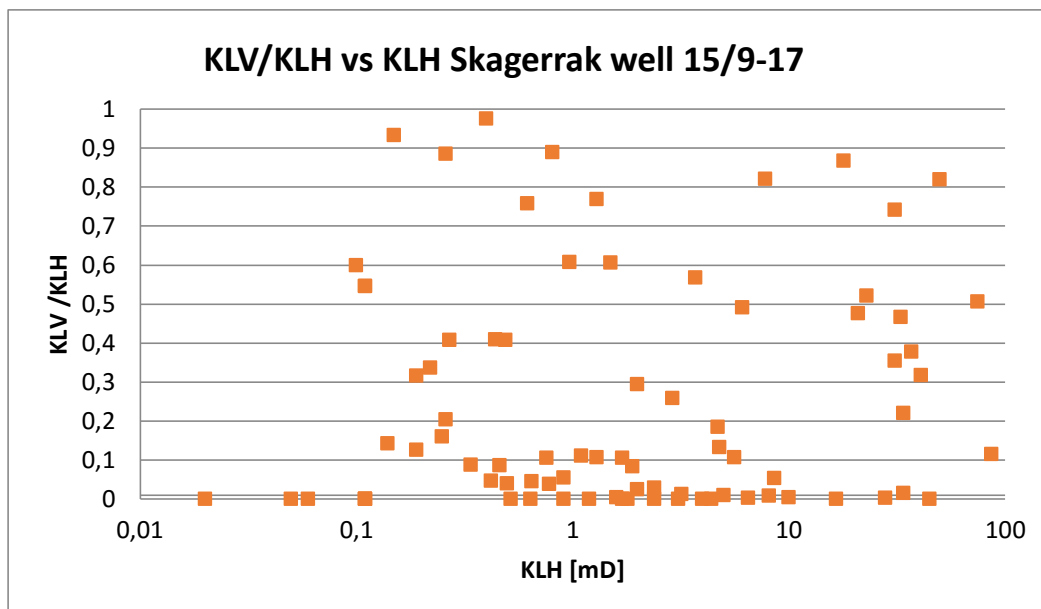


Figure 13-9 Vertical permeability vs. horizontal permeability, well 15/9-17

13.5 Formation Temperature

The formation temperature used in this evaluation is based on DST data and RFT data. The values are summarized in Table 13-4 below.

Table 13-4 Formation temperatures in Skagerrak Formation

| Well | Area | Test | Temperature [C [®]] |
|---------|--------------|------------------|-------------------------------|
| 15/9-9 | Sleipner Øst | Max RFT pre test | 97.7 |
| 15/9-15 | Gungne Field | Drill stem test | 103.7 |
| 15/9-17 | Loke Field | Drill stem test | 100.2 |

13.6 Formation Water resistivity, R_w , determination

Evaluation of the resistivity of the formation water has been found in all three wells for the Skagerrak Formation. The average value in this evaluation based on the given temperatures in the Table 13-4, is found to be 0.0234 ohm.m.

The formation water resistivity in laboratory/standard conditions used in this evaluation is $R_w = 0.07$ ohm.m at $T = 20$ degrees which is equivalent to a 130 000 ppm NaCl concentration. The resistivity of the formation water was corrected into reservoir conditions using 13-6, Arp's formula [57] and the formation temperature:

$$R_w = R_{w1} * \left(\frac{T_1 + 21.5}{T + 21.5} \right) \text{Equation 13-5}$$

where

R_w : Formation water resistivity at reservoir conditions ohmm

R_{w1} : Formation water resistivity at surface conditions ohmm

T_1 : Surface Temperature (=20degrees)

T : Formation temperature (degrees)

R_w was also determined by reading rock resistivity value, R_o , from the resistivity log in a clean zone which were 100% water saturated. This was calculated by the following formula given in section 10.1.7.

The values are summarized in Table 13-5. The rock resistivity, R_o , in well 15/9-17 was affected by shoulder effects in the reading interval from the resistivity log, R_T . This was due to lack of clean zones below the contact in this well. These calculated measurements from equation were therefore not used.

Table 13-5 R_w determination

| Nacl ppm | Well | Depth TVDSS, 100 % water zone | R_w (Arps formula) | R_{cl} [ohm m] | R_o [ohm m] | T [C°] | PHIF [fraction] | $F = (a/\phi^m)$ | $R_w = (R_o/F)$ [ohm m] |
|----------|---------|-------------------------------|----------------------|------------------|---------------|----------|-----------------|------------------|-------------------------|
| 120 000 | 15/9-9 | 2734.1 | 0.0244 | 1.7 | 0.896 | 97.4 | 0.16 | 39.0625 | 0.02294 |
| 120 000 | 15/9-15 | 3075 | 0.0232 | 2.5 | 0.401 | 103.7 | 0.24 | 17.3611 | 0.02309 |
| 120 000 | 15/9-17 | 2858.3 | 0.02387 | 2.48 | 1.32 | 100.2 | 0.149 | 45.0430 | 0.02930 |

14 Water saturation model

14.1 Water saturation modelling from core and log data

The water saturation modelling has been estimated with the following methods:

- With use of logs: Indonesia-, Waxman Smits- and Archie-method
- With use of core- evaluated (Capillary pressure)
- A combination of log- and core-evaluated water saturation.

The clay parameter is a vital parameter in the Indonesia and Waxman Smits method, either expressed in fraction of total volume or as clay exchange cations. Archie and Waxman are calculated by the use of the total porosity from logs while the Indonesia uses the effective porosity. The saturation from cores is solely related to capillary pressures and wettabilities.

The software Interactive Petrophysics, IP, has been utilised in the water saturation modelling when using Indonesia, Archie and Waxman Smits while Microsoft Excel has been used to establish the water saturation method from cores.

14.2 Water saturation from log data

The Archie equation (1942) mainly used to evaluate hydrocarbon content from a clean reservoir. It is therefore without shale correction and has been taken into this evaluation to compare the effect of the clay content in the Skagerrak Formation.

$$S_w = \left(\frac{a \cdot R_w}{R_T \cdot \phi^m} \right)^{\frac{1}{n}} \quad \text{Equation 14-1}$$

The resistivity of the formation water, R_w , are presented in Table 13-5, section 13.6. The parameters a , m and n are given in Table 12-3.

The Indonesia Equation and the Waxman Smits Method

The log derived water saturation from the Indonesia equation include the content of clay in the Skagerrak Formation.

$$\frac{1}{\sqrt{R_T}} = \left[\frac{V_{cl}^{1-\frac{m}{2}}}{\sqrt{R_{cl}}} + \frac{\phi e^{\frac{m}{2}}}{\sqrt{a \cdot R_w}} \right] * S_w^{\frac{n}{2}} \quad \text{Equation 14-2}$$

The amount of clay volume in the Skagerrak Formation especially in wells 15/9-15 and 15/9-17 make it difficult to find clean zones and due to this the Archie's equation will not be representative in this formation. To take into account the clay volume the Indonesia and Waxman Smits equation are utilized. From the $1/R_t = \phi_t^{m^*} * S_{wt}^{n^*} \left(\frac{1}{R_w} + \frac{BQ_v}{S_{wt}} \right)$

Equation 14-4 for Waxman Smits method, it is necessary to determine the B and the Qv (section 10.1.9). In this evaluation the specific cation conductance B were determined by plot in Appendix 20.3.3 and the cation exchange capacity, Qv, were determined by plotting the Qv determined from SCAL data vs. the porosity. (Figure 14-1) The results are listed in Table 14-1.

$$Q_v = \frac{CEC * (1-\phi) * GD}{100 * \phi} \quad \text{Equation 14-3}$$

where

CEC: cation exchange capacity (meq/gm)

GD: Grain density

Qv concentration of clay exchange cations

ρ_{ma} : matrix density (g/cc or kg/m³)

ϕ : porosity

[34]

Waxman Smits water saturation is determined by

$$\frac{1}{R_t} = \phi_t^{m^*} * S_{wt}^{n^*} \left(\frac{1}{R_w} + \frac{BQ_v}{S_{wt}} \right) \quad \text{Equation 14-4}$$

where

Sw: Water saturation of the total porosity

B: Specific cation conductance in (1/ohm*m)/(meq/mL)

Qv: CEC in meq/mL of total PV

Rw: Resistivity of the Formation Water

Rt: Resistivity from log

m*: Cementation exponent for clay formations

n*: Saturation exponent for clay formations

φt: Total porosity

Table 14-1 Waxman Smits Qv, B, T

| Well | Qv | B from Figure 20-21 | T |
|---------|--------------------|---------------------|-------|
| 15/9-15 | 0.0011* φt ^-3.391 | 18 | 103.7 |
| 15/9-17 | | 17.5 | 100.2 |
| 15/9-9 | | 17 | 97.4 |

The relation between Qv and porosity is not clear, and this is probably one of the largest deficiency of this method in this environment.

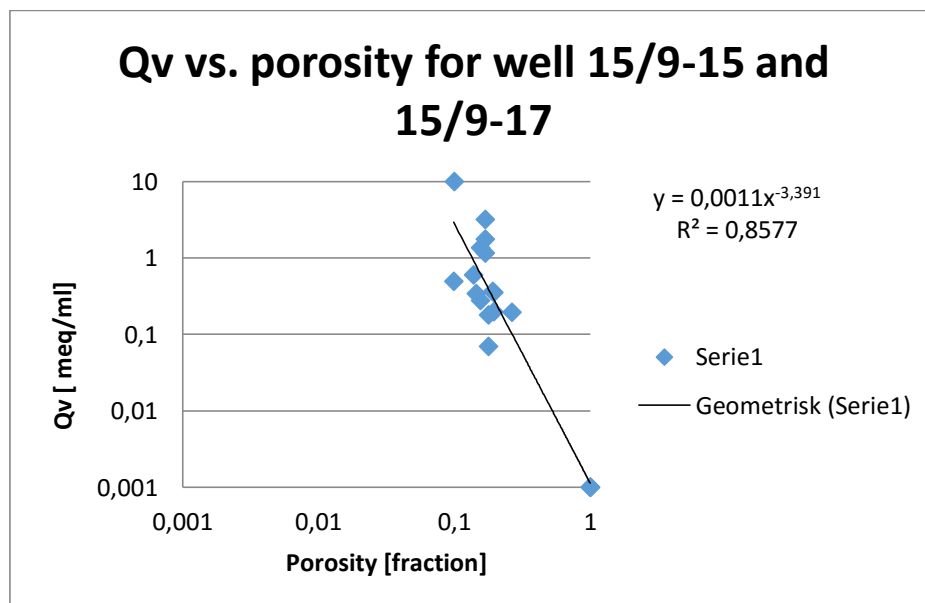


Figure 14-1 Qv vs porosity from wells 15/9-15 and 15/9-17

The Indonesia equation

$$\frac{1}{\sqrt{R_T}} = \left[\frac{V_{cl}^{1-\frac{V_{cl}}{2}}}{\sqrt{R_{cl}}} + \frac{\phi^{\frac{m}{2}}}{\sqrt{a \cdot R_w}} \right] * S_w^{\frac{n}{2}} \quad \text{Equation 14-5}$$

14.3 Water Saturation from core data

The program Microsoft Excel has been used as the tool to do all the curve fitting and plotting of capillary pressure from core data.

14.3.1 Capillary Pressure Curves

Capillary pressure measurements from the wells 15/9-15 and 15/9-17 were done by the porous plate method at eight different pressure levels up to 12 Bar. Gas/water measurements were available on 18 plugs in well 15/9-15 and 2 plugs from well 15/9-17 from the Skagerrak Formation, Figure 14-2 and Figure 14-3. The figures illustrate that the magnitude and shape of the curves are varying with permeability, and the intention is to create a unique curve for the Skagerrak Formation by introducing J-Function section 14.3.4

The procedure to convert capillary pressure to J-functions as a function of normalised water saturation is as follow:

- Plot all the capillary pressure versus water saturation, P_c vs. S_w , Figure 14-2 and Figure 14-3
- Normalise S_w between irreducible saturation and 100%, Figure 14-5
- Calculate J from core plugs $J = \left(\frac{P_c}{\sigma^* \frac{\cos\theta}{3.141}} \right) lab * \left(\sqrt{\frac{k}{\phi}} \right) lab$ Equation 14-10
- Plot J vs. S_{wn} and define $J = a * S_w^{-b}$ $S_{wn} = a * J^{-b} = \frac{S_w - S_{wirr}}{1 - S_{wirr}}$ Equation 14-11
- Convert to $S_{wn} = a * J^{-b}$ Equation 14-6
- This core established J is will be linked to J_{res} established in the from the reservoir (Section 14.3.5)

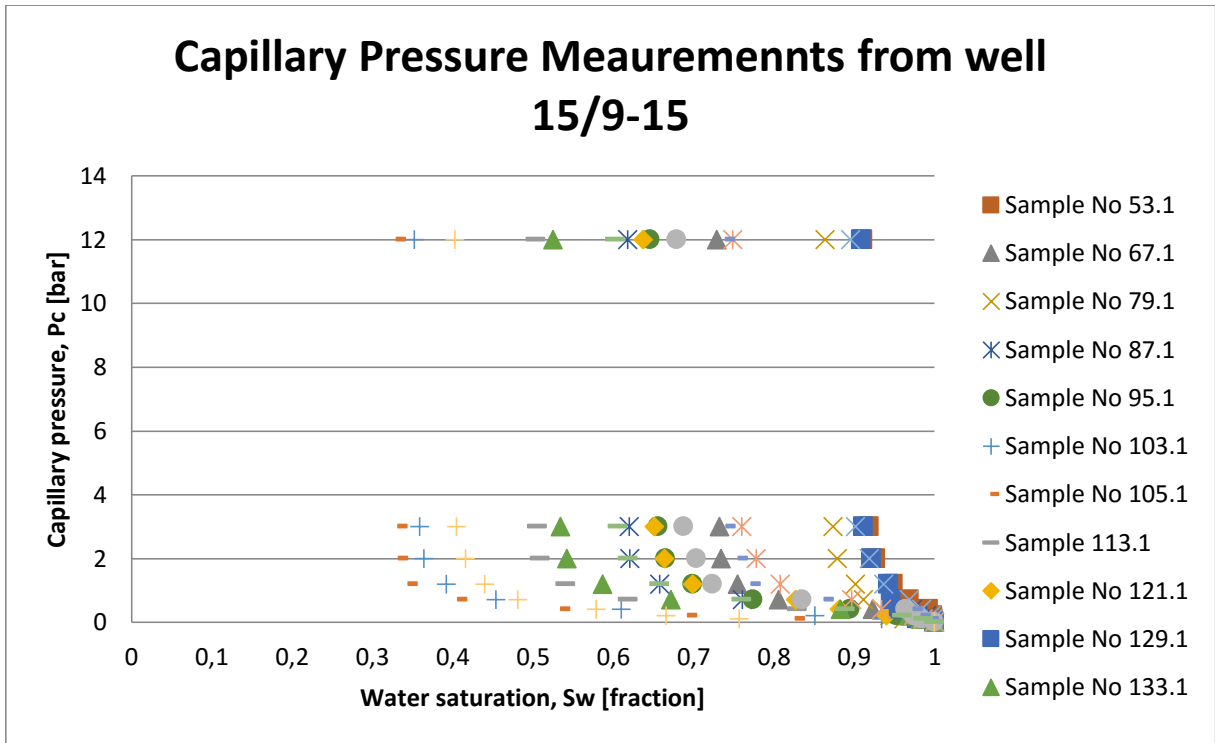


Figure 14-2 Gas/Water Capillary Pressure Curves from well 15/9-15, Skagerrak Formation

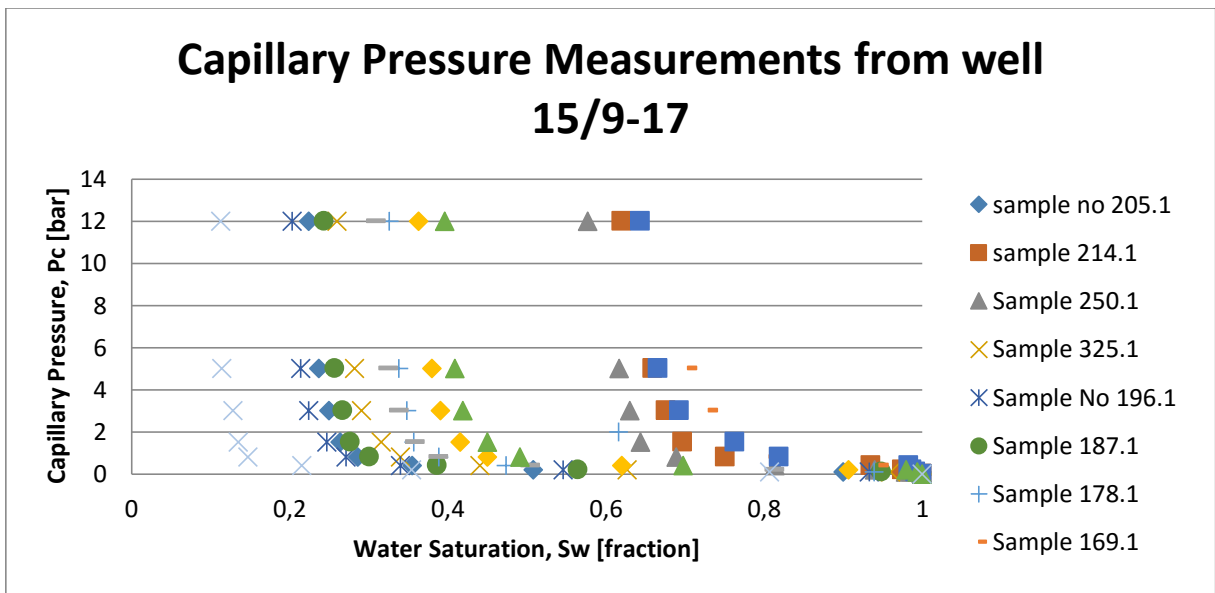


Figure 14-3 Gas/Water Capillary Pressure Curves from well 15/9-17, Skagerrak Formation

14.3.2 Irreducible water saturation, S_{wirr}

The water saturation in the reservoir can be written as a function of the normalized water saturation

$$S_w = S_{wn} * (1 - S_{wirr}) + S_{wirr} \quad \text{Equation 14-7}$$

$$S_{wirr} = a \cdot K_{core}^{-b} \quad \text{Equation 14-8}$$

The irreducible water saturation, S_{wirr} , is determined at 12 bars and utilised when normalising the saturation between S_{wirr} and 1.0. The Figure 14-4 show a correlation

b
e
t
w
e
e
n

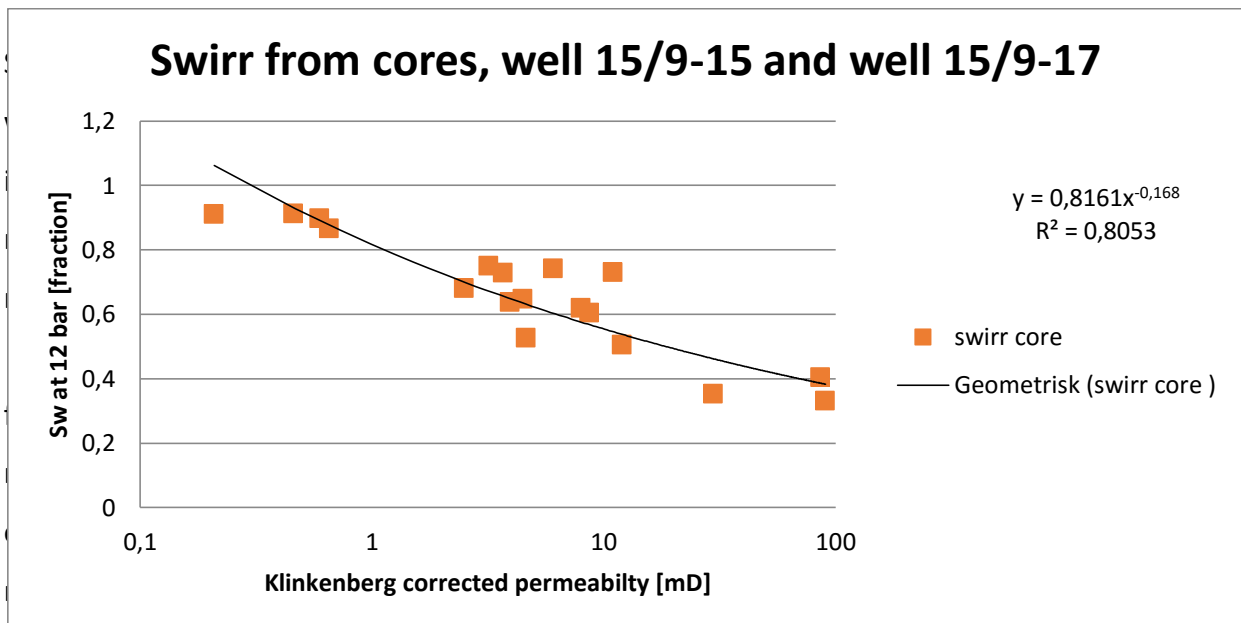


Figure 14-4 Swirr from cores vs. Klinkenberg corrected perm 15/9-15 and 15/9-17

c
o

14.3.3 Normalisation of the Water Saturation

r

The following equation was used to find the normalised water saturation, S_{wn} , for each core sample. This involves excluding the irreducible water saturation.

s

p

l

o

$$S_{wn} = \frac{S_w - S_{wirr}}{1 - S_{wirr}} \text{ Equation 14-9}$$

where

S_{wn} : Normalised water saturation

S_w : Water saturation

S_{wirr} : Irreducible water saturation at 12 bars

As mention in section 14.3.2, this is determined to be the absolute minimum water saturation in each of the plugs and assumed to be the S_{wirr} . In Figure 14-5 the capillary pressure is plotted against the normalised water saturation.

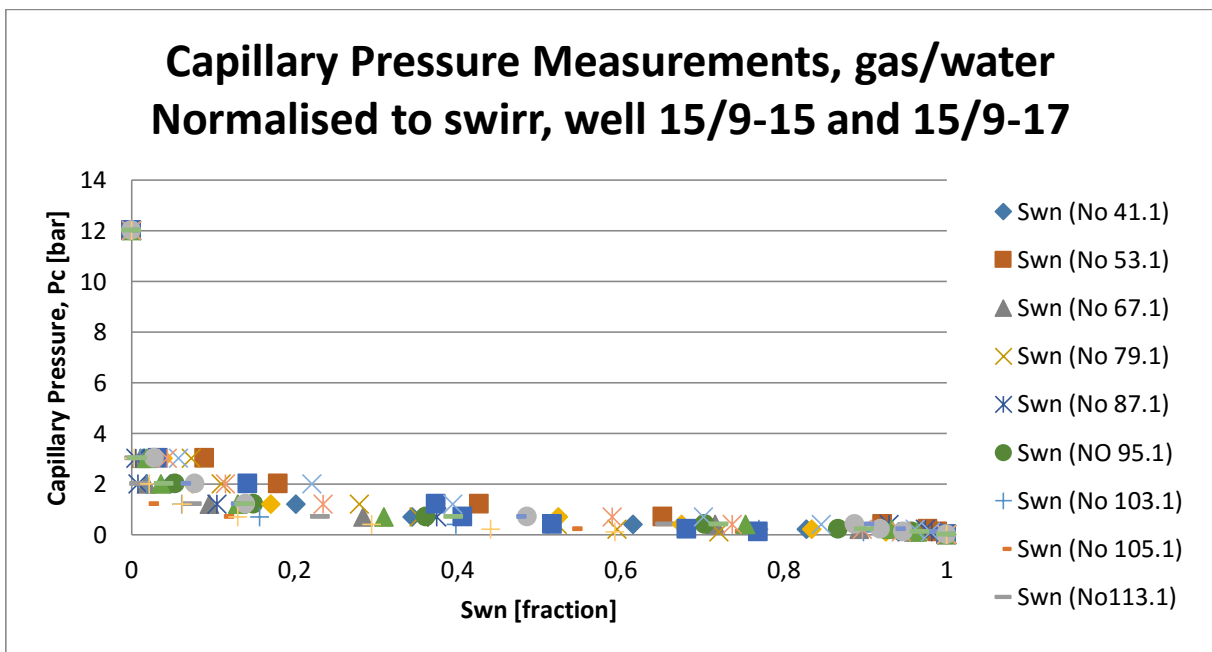


Figure 14-5 Capillary pressure vs. Normalised Water saturation from well 15/9-15 and 15/9-17

14.3.4 J-function and Water Saturation (S_w) from cores

The shape of the capillary pressure curve is dependent on surface tension, porosity and permeability. This has been done by the Leverett J-function Equation 15-10. No information of the surface tension and the contact angle in the laboratory is given in any of the older core report so the standard values for air/brine system were utilised: 72 mN/m and 0 degrees.

$$J = \left(\frac{P_c}{\sigma^* \frac{\cos\theta}{3.141}} \right) lab * \left(\sqrt{\frac{k}{\phi}} \right) lab \text{ Equation 14-10}$$

Where

- Pc: Capillary pressure [bar]
- σ : Surface tension (lab conditions)
- θ : Contact angle against the rock
- k: Permeability of the plug (mD)
- ϕ : Porosity of the plug (fraction)

J has been calculated and plotted against the normalised water saturation, S_{wn} for each plug, given by the following relationship.

$$S_{wn} = a * J^{-b} = \frac{S_w - S_{wirr}}{1 - S_{wirr}} \text{ Equation 14-11}$$

where

- S_{wn} : Normalised water saturation (fraction)
- S_w : Water saturation in the reservoir (fraction)
- S_{wirr} : Irreducible water saturation (fraction)
- k: Permeability (mD)
- a, b: Regression constants determined from cross plot

The constants a and b are determined by the inverse regression curve given in Figure 14-7 for the Skagerrak Formation. Conversion of these equations gives the following expressions of normalized water saturation the J-function.

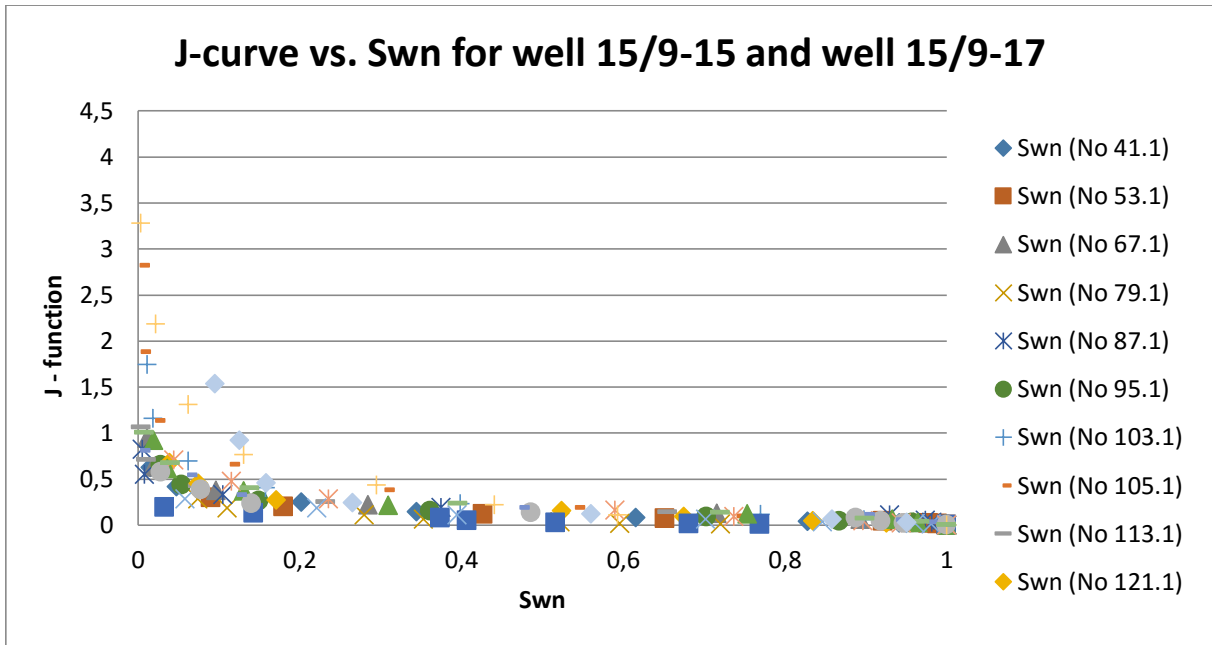


Figure 14-6 J-function vs. Sw_n for well 15/9-15 and well 15/9-17

In Figure 14-6 the J-function is plotted against normalised water saturation for both wells. A power function through the points make a fairly good correlation between the data and generate a representative J-function. The normalised water saturation from the two wells together with the J-function were plotted together due to few core data measurements from 15/9-17.

In Figure 14-7 the inverse of the graph in Figure 14-6 is plotted. The reason for illustrating this inverse function is to show the equation of normalised water saturation with respect to the J-function. From this equation the constants a and b can be determined.

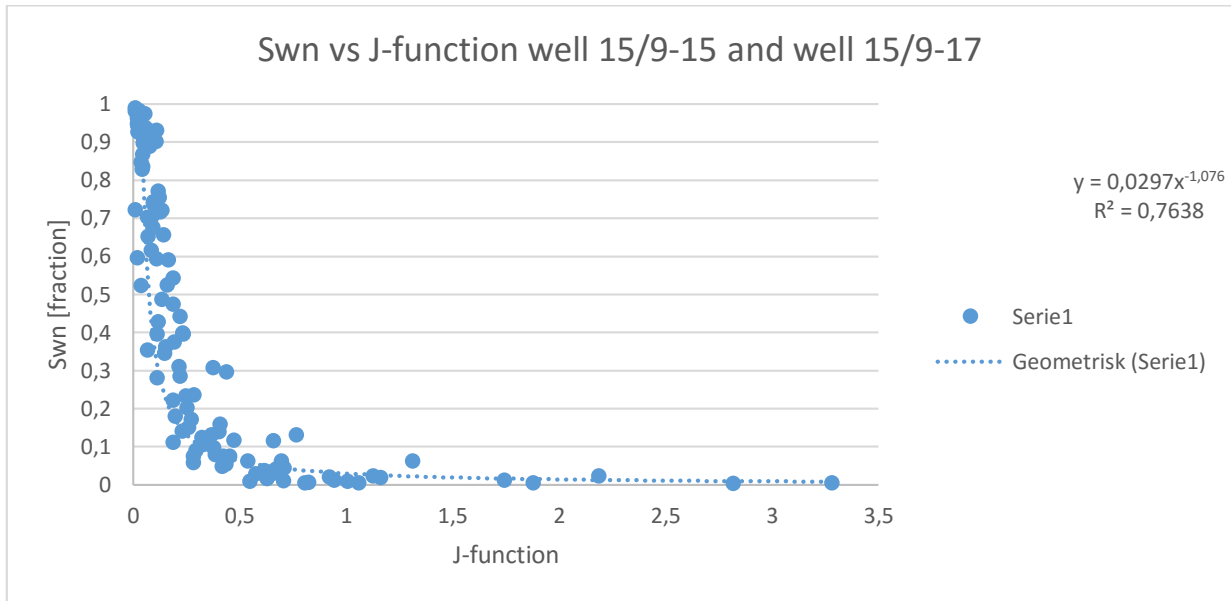


Figure 14-7 The normalised water saturation vs. the J-function

The equation for normalised water saturation from cores for both wells can be summarised in Table 14-2 below.

Table 14-2 Regression constants from the Swn core equation in well 15/9-15 and 15/9-17

| Well | Swn=a*J ^{-b} | |
|-----------------------|--|--------|
| | a | b |
| 15/9-17 Loke Field | 0.0297 | -1.076 |
| 15/9-15, Gungne Field | 0.0297 | -1.076 |
| 15/9-9 Sleipner Øst | Not determined due to water filled Skagerrak Formation | |

These measurements and equations have been further used to calculate the water saturation as a function of height above free water level in section 14.3.5 , modelling of water saturation.

14.3.5 Water saturation from cores in the reservoir

The procedure to connect the core data J with J calculated from the reservoir is as follows

$$\text{Establish } Sw_{irr} = a * KLOGH^{-b} \quad \text{Equation 14-12}$$

$$J_{res} = \left(\frac{\Delta\rho g H}{\frac{\sigma \cos\theta}{3.141} 10^5 \sqrt{\frac{k}{\phi}}} \right)_{res} \quad \text{Equation 14-13}$$

Establish $S_{wn} = a * J_{res}^{-b}$ Equation 14-14

$S_{wcore} = S_{wn}(1 - S_{wirr}) + S_{wirr}$ Equation 14-15

This resulting water saturation from J-function core, S_w (core), was compared to the water saturation from Archie's equation, Indonesia equation and the Waxman Smits method. This S_w (core) was then adjusted by the product of $\sigma c \cos \theta$ to achieve the best correlation between the S_w from log and the S_w (core), Figure16-8 and Figure16-9.

14.4 Water Saturation from combined method

Capillary pressure established from pressure gradients from section 7. using **Feil! Fant ikke referanse**

kilden.. The capillary pressure is converted to J_{res} using $J_{res} = \left(\frac{\Delta \rho g H}{\frac{\sigma c \cos \theta}{3.141} 10^5 \sqrt{\frac{k}{\phi}}} \right)_{res}$

Equation 14-16.

The purpose of this approach is to establish a J function calculated from water saturation the Archie, Indonesia and Waxman-Smits equations. As a result of these equations, J functions versus normalized water saturations are constructed and compared with the results derived from the cores.

The procedure

- Plot S_w (*) from logs vs $KLOGH$
- Establish $S_{wirr} = a * KLOGH^{-b}$
- Calculate $S_{wn} = \frac{S_w - S_{wirr}}{1 - S_{wirr}}$
- Plot J_{res} vs S_{wn} and define $J_{res} = a * S_{wn}^{-b}$
- Convert to $S_{wn} = a * J^{-b}$
- Check this approach with S_w (*)

* Indonesia equation, Waxman-Smits equation, Archie equation

$$J_{res} = \left(\frac{\Delta \rho g H}{\frac{\sigma \cos \theta}{3.141} 10^5} \sqrt{\frac{k}{\phi}} \right)_{res} \quad \text{Equation 14-16}$$

The fluid density is taken from the pressure data, section 7, and listed in Table 14-3.

Table 14-3 Parameters in J- res Equation

| Fluid | Parameter |
|----------------------------|-------------------------------------|
| Gas Density (kg/m3) | 320 |
| Water Density (kg/m3) | 1020 |
| | |
| $\sigma_{res} \cos \theta$ | Ref; 72 dynes/cm, alternative 50 82 |

14.5 The Swirr Equation determined from logs

To be able to find the Swirr from logs in well 15/9-15 and 15/9-17, water saturation from the given log-method (Indonesia, Archie and Waxman Smits) was plotted against the continuous permeability curve, KLOGH. The results of the equation are given in Table 14-4 and Table 14-5 for well 15/9-15 and 15/9-17 respectively, and the plot for the Indonesia water saturation vs. KLOGH from well 15/9-15 is given in Figure 14-8. The Swirr equation from the two other methods are found in Appendix 20.3.1. The Waxman Smits gave a poor correlation in well 15/9-17 and was therefore decided not to use further in the evaluation. The result of the Swirr determination is shown in Table 14-4. The correlation shows a decreasing feature from core derived Swirr to Indonesia derived Swirr with a lowest for Waxman Smits method that is the worst fit.

Table 14-4 a and b for the SWIRRR equation for logs, well 15/9-15, Gungne Field

| Well 15/9-15 | $Swirr = b - a * \log(KLOGH)$ | |
|---------------------------|-------------------------------|----------|
| Water saturation equation | a | b |
| Indonesia | -0.223533 | 0.666589 |
| Waxman Smits | -0.170020 | 0.397812 |
| Archie | -0.220413 | 0.660863 |

Table 14-5 a and b for the SWIRR equation for logs, well 15/9-17, Loke Field

| Well 15/9-17 | $Swirr = b - a * \log(KLOGH)$ | |
|---------------------------|-------------------------------|----------|
| Water saturation equation | a | b |
| Indonesia | -0.143018 | 0.481363 |
| Waxman Smits | -0.097107 | 0.290844 |

| | | |
|--------|-----------|----------|
| Archie | -0.205775 | 0.585860 |
|--------|-----------|----------|

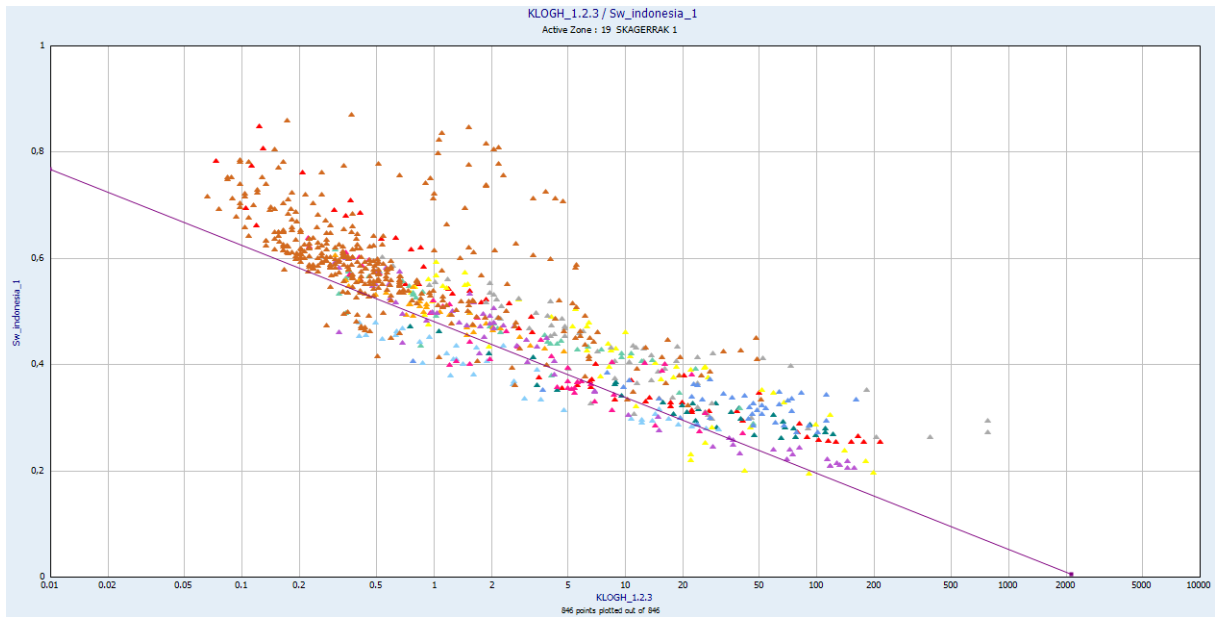


Figure 14-8 Water saturation from Indonesia Equation vs KLOGH, well 15/9-17

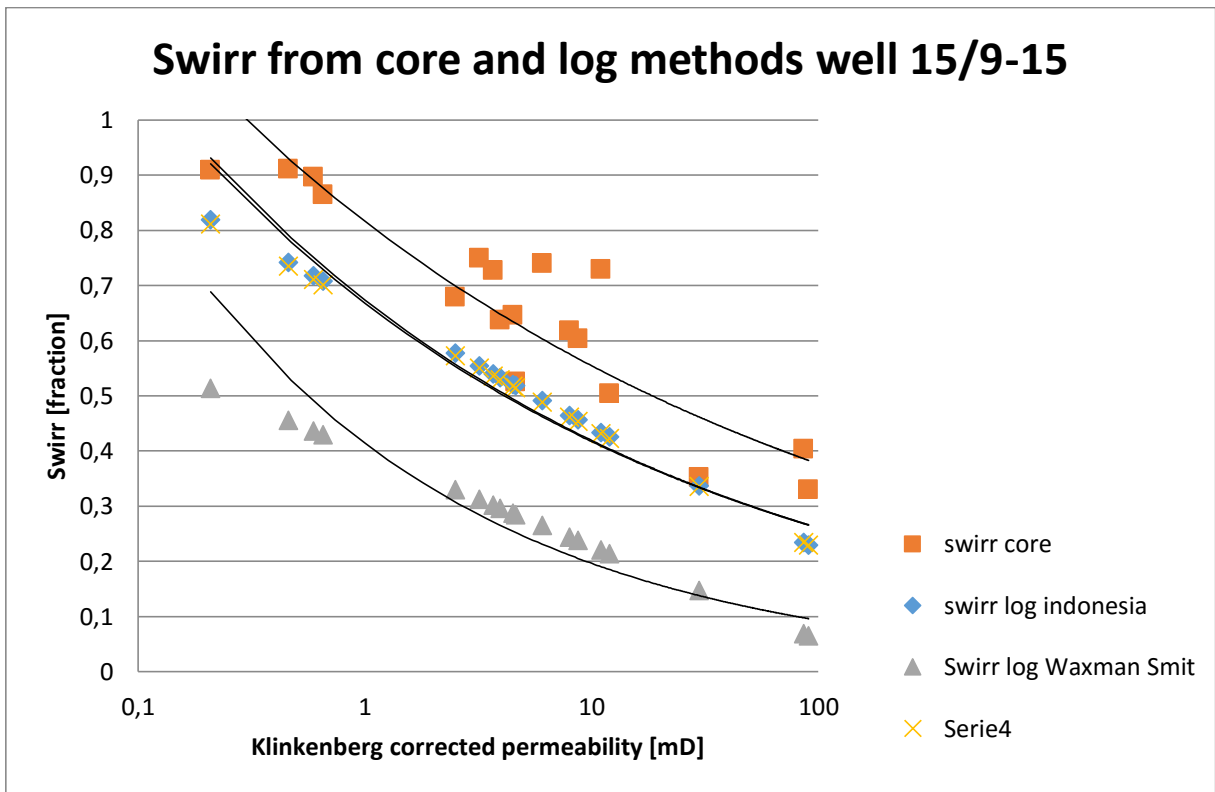


Figure 14-9 Swirr from core and log methods well 15/9-15

Table 14-6 Swirr a and b

| Well 15/9-15 | Swirr = a*permeability ^b | |
|--------------|-------------------------------------|--------|
| Method | a | b |
| Cores | 0.8161 | -0.168 |
| Indonesia | 0.6738 | -0.206 |
| Archie | 0.6679 | -0.204 |
| Waxman Smit | 0.4141 | -0.324 |

14.6 Water Saturation from core method with adjusted Swirr from logs

The procedure is as follows

- Establish $Swirr = a * KLOGH^{-b}$ from Indonesia Equation 14-17
- Convert to $Swn(core) = a * J^{-b}$ Equation 14-18
- $J_{res} = \left(\frac{\Delta\rho gH}{\frac{\sigma c \cos\theta}{3.141} 10^5} \sqrt{\frac{k}{\phi}} \right)_{res}$ Equation 14-19
- Establish $Swn = a * J_{res}^{-b}$ Equation 14-20
- $Swcore = Swn(1 - Swirr) + Swirr$ Equation 14-21

This measure is matching best the use of core data compared with fex. Indonesia method created from logs.

14.7 Water Saturation where J-function and normalised Sw created from logs

The normalised water saturation were calculated by the $S_{wn} = \frac{S_w - S_{wirr}}{1 - S_{wirr}}$ Equation 14-22.

The S_{wn} for each method (Indonesia, Waxman Smits, Archie) was then plotted against the

$J_{res} = \left(\frac{\Delta \rho g H}{\frac{\sigma c \cos \theta}{3.141} 10^5 \sqrt{\frac{k}{\phi}}} \right)_{res}$ Equation 14-23. The results from well 15/9-17 are shown in *Figure*

14-10. It is very challenging to define a S_{wn} curve in the cloud of points, but the regression line is aiming towards the zero water saturation. This is expected since the irreducible water saturation is already been excluded and normalised between 0.0 and 1.0. The spread in the data is also the case for well 15/9-15 and is probably due to shoulder effects on the resistivity log, the goodness correlation of permeability and porosity and also the quality of the porosity logs.

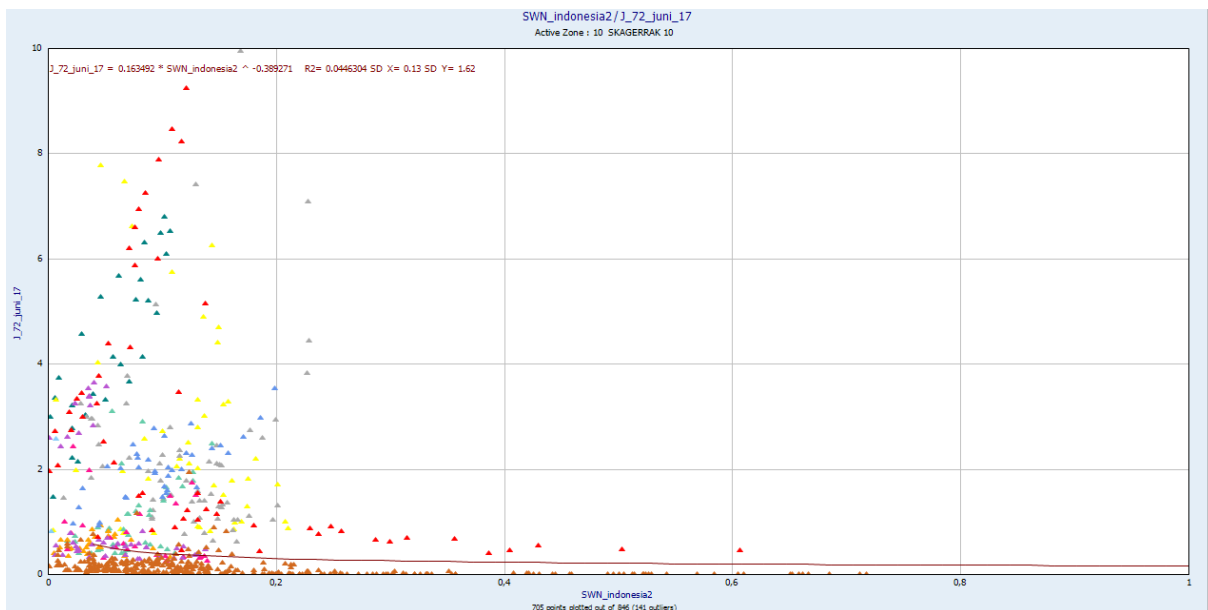


Figure 14-10 J-function vs the normalised water saturation for the Indonesia Equation, well 15/9-17

The established normalised water saturation from this method for well 15/9-17 is given in Table 14-7 together with the corresponding value from the core method. In addition this is shown in Figure 14-11.

Table 14-7 a and b determined from log methods, well 15/9-17

| Well 15/9-17 | $S_{wn} = a * J^{-b}$ | |
|---------------------------|-----------------------|--------|
| Water saturation equation | a | b |
| Indonesia | 0.1126 | -0.741 |
| Waxman Smits | 0.1069 | -1.552 |
| Archie | 0.1278 | -1.157 |
| Core | 0.0297 | -1.076 |

The resulting S_w curves from Indonesia-, Archie- and Waxman Smits method based on a $\sigma \cos \theta$ of 72 were compared in IP with the water saturation derived from log methods. The Indonesia in both well 15/9-15 and 15/9-17 for this method was adjusted to find the best fit to the water saturation calculated from the Indonesia Equation. Results given in.

The plot shows that all the watersaturation methods except Archie are similar, being aware of the relatively large uncertainty shown in section 16.4, Figure16-8 and Figure16-9.

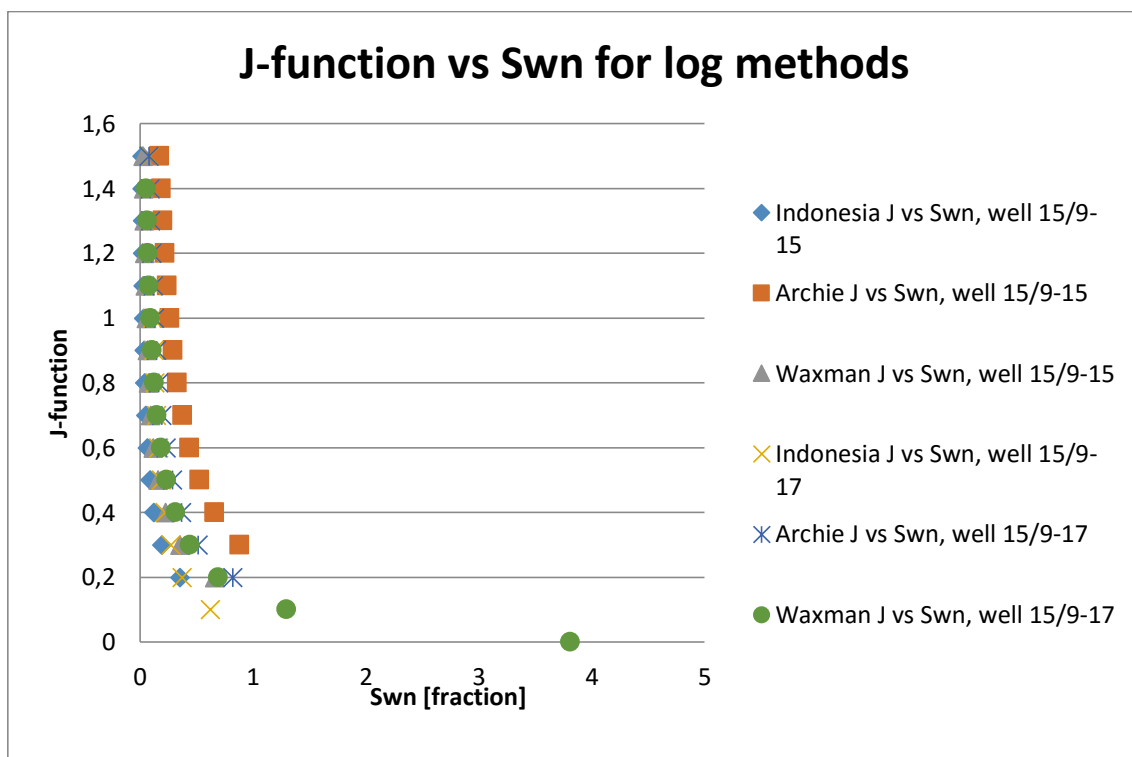


Figure 14-11 J-function vs. Swn deduced from log methods

14.8 Method with Swr

An alternative method is according to Feil! Fant ikke referansekinden. 35 to calculate a $S_{wr} = S_w - S_{wirr}$ that is not normalised. The J-function is calculated as before by

$$J_{res} = \left(\frac{\Delta \rho g H}{\frac{\sigma \cos \theta}{3.141} 10^5} \sqrt{\frac{k}{\phi}} \right)_{res} \quad \text{Equation 14-16.}$$

Reference 35 is suggesting to plot a log log plot of J_{res} vs. Sw_r within an yellow shaded area shown in Figure 14-12. All the other points show no convincing correlation, and the method is therefore not followed up.

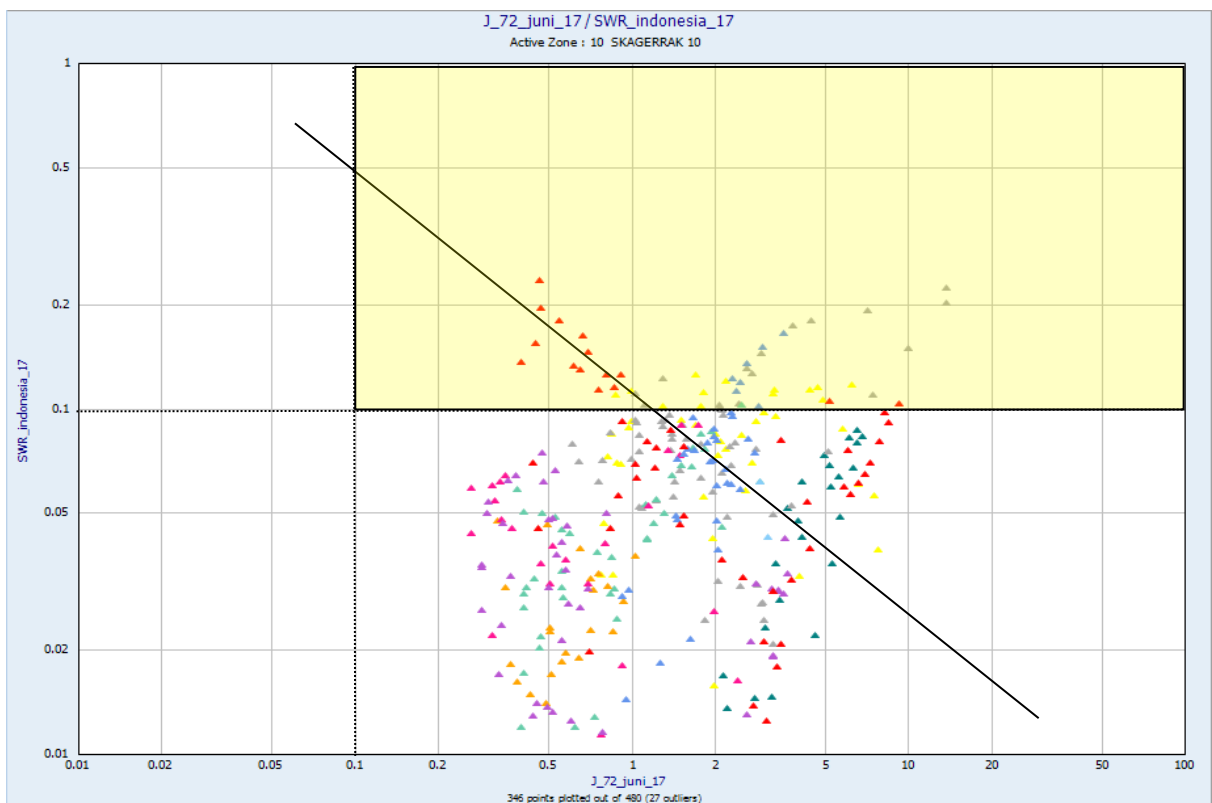


Figure 14-12 $Sw_r = Sw - Sw_{irr}$ vs J_{res}

15 Evaluation of DST from well 15/-9-15,Gungne Field

15.1 Introduction

In July 1982 there were performed two drill stems tests (DST) in well 15/9 on the Gungne field. DST 1 was performed in the interval 2880-2890 m RKB and DST 2 in the interval 2830-2850 m RKB (Table 15-1). Both test intervals are from the Skagerrak Formation (Figure 15-1). Pressure and rate data from DST 1 was used to perform a conventional transient pressure analysis in order to:

1. Compare permeability from DST 1 with corresponding core data
2. Interpret the geological setting and potential barriers to fluid flow

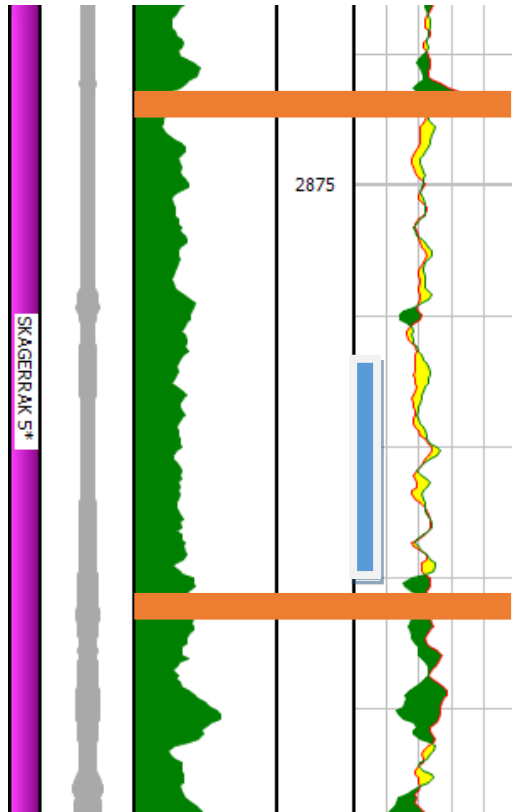


Figure 15-1 CPI from perforated (marked in blue) interval in well 15/9-15

Table 15-1 Perforation interval for DST 1 and DST 2 in well 15/9-15

| Area | DST No | Interval [m] |
|------------------|--------|--------------|
| The Gungne Field | DST 2 | 2830-2850 |
| | DST 1 | 2880-2890 |

The transient pressure analysis was performed in the software Saphir, which is a part of the Ecrin package delivered by KAPPA. Table 15-2 provides the general input data used in Saphir for the pressure interpretation of well 15/9-15. The data are available on NPD's webpage. [1] After the test interpretation three different fault models were established in as attempt to match the test data.

Table 15-2 Input data for the interpretation well test report PL 046 RFT, DST no 1 and No. 2 Well 15/9-15 LET-SVG february 1983. Engineer K.Kviljo

| Parameter | Value |
|-----------------------------------|---|
| Porosity phi | 0.17 |
| Net pay, h (found from CPI plot) | 18 |
| Formation volume factor Bg | $3.868 \cdot 10^{-3} \text{ m}^3/\text{Sm}^3$ |
| Viscosity, myg | $33.91 \cdot 10^{-3} \text{ cP}$ |
| Wellbore radius, rw | 0.107 |
| Gas compressibility, Cg | $1.634 \cdot 10^{-3} \text{ bar}^{-1}$ |
| Formation compressibility, Cf | $5.658 \cdot 10^{-5} \text{ bar}^{-1}$ |
| Water saturation, Sw | 0.6 |
| Well profile | Vertical |
| Perforation length, L | 10 |
| Reservoir temperature, Tres | 107 |
| Reservoir pressure, Pres | 338.74 bar |

15.2 Interpretation of DST 1

Pressure data and rate history was loaded into Saphir for transient pressure analysis. The pressure build-up data and rate history are given in Figure 15-2 and . One can see from the plot that the well is produced at different rates and draw-downs for about 25 hours, before it was shut in for the main build-up which lasted for about 30 hours. The pressure derivative plot for the main build-up including main observations is presented in Figure 15-3. Three distinct behaviours can be interpreted from the plot. In the first period of the test the derivative is dominated by wellbore storage (WBS) effects, before a period of infinite acting radial flow occurs. The permeability and k*h product is estimated from this period. After about 5 hours there is an increase in the derivative, indicating that there are barriers to fluid flow. This corresponds to a distance of about 70 meters. The barriers can be interpreted as one or more sealing faults in the reservoir. Another possible explanation might be that the barrier is the margin of a channel (shale), since the reservoir is deposited in a fluvial environment.

The main observations from the test are summarized in Table 15-3. The test interpreted permeability is estimated 3.1 md, which corresponds fairly well with the permeability of 4 md from the same interval from the core data.

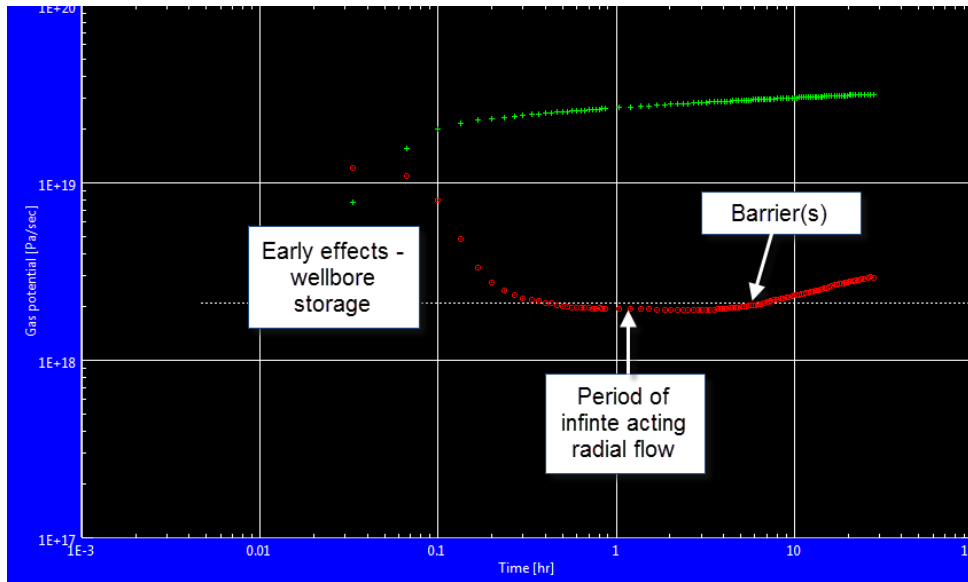


Figure 15-2 Pressure build-up data, well 15/9-15

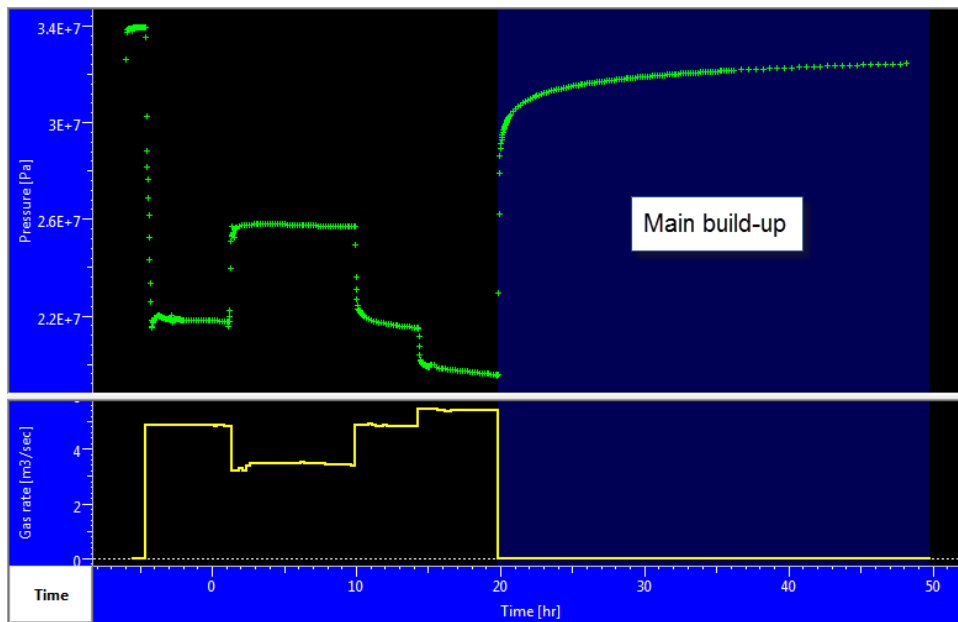


Figure 15-3 History plot

Table 15-3 The results from DST 1

| Standard Gas Test | |
|-----------------------------------|---|
| Well | Vertical |
| Initial Pressure, P_i | $3.3874 \cdot 10^7$ Pa |
| Horizontal permeability, KH | 55.1 md*m |
| Skin factor, S | 0.567 |
| Wellbore storage, C | $4.44 \cdot 10^{-7}$ m ³ /Pa |
| Radius of investigations | 157 m |
| Distance to barriers (increase in | 70 m |

| | |
|--------------|--------|
| derivative) | |
| Permeability | 3.1 md |

15.3 Testing of different fault models

Three different fault models were tested in order to try to match the pressure data from the DST, since this could give indications about the structural setting of the reservoir. In the following plots the dots shows the real test data, while the red and white lines show the modelled response. In all models the wellbore storage is modelled as variable and the reservoir homogeneous.

1. One fault

First a simple model including one single sealing fault (no-flow) 60 meters away from the well was made. Figure 15-6 shows a simple sketch of the model. From Figure 15-4 and Figure 15-5 one can see that that the model matches both the pressure derivative pretty well, and the pressure history match is relatively poorly. The system also seems too open since the modelled pressure in the history plot (Figure 17-5) is higher than the real test data.

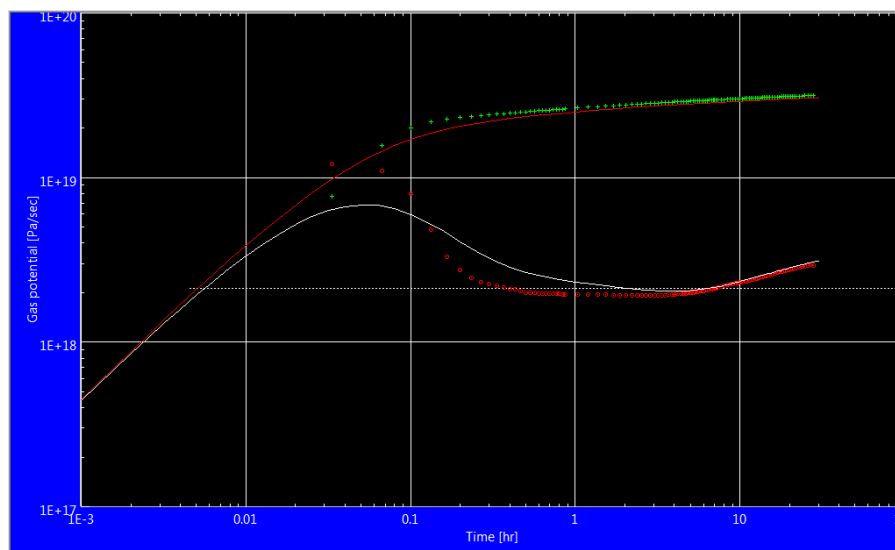


Figure 15-4 Log-log plot of the main build-up (red and white lines represents the model)

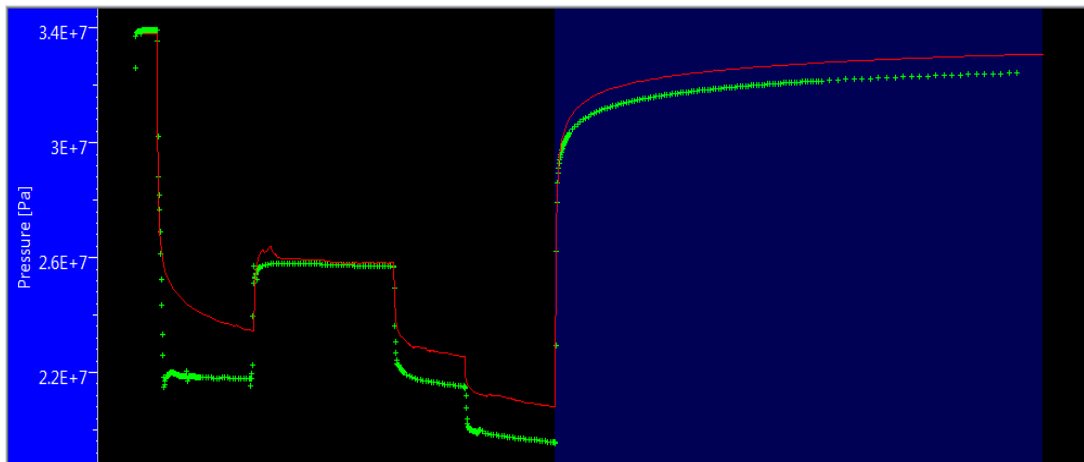


Figure 15-5 Pressure History plot of the main build-up (Green dots are measured data and red line is modelled)

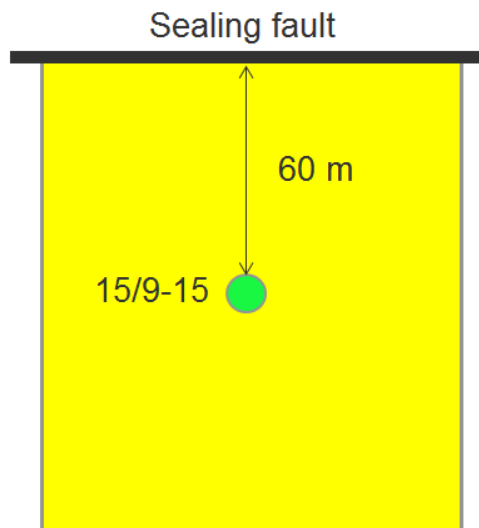


Figure 15-6 Sketch of the well and distance to barrier, one fault

2. Two parallel faults

Since the system seems to be too open with only one sealing fault, another fault was added. Figure 15-9 shows a simple sketch of the model, where two sealing parallel faults are included. This model gives a better match to the pressure history (Figure 15-7), indicating that the system is more compartmentalized. The pressure derivative match is much the same as for the model with one fault (Figure 15-8).

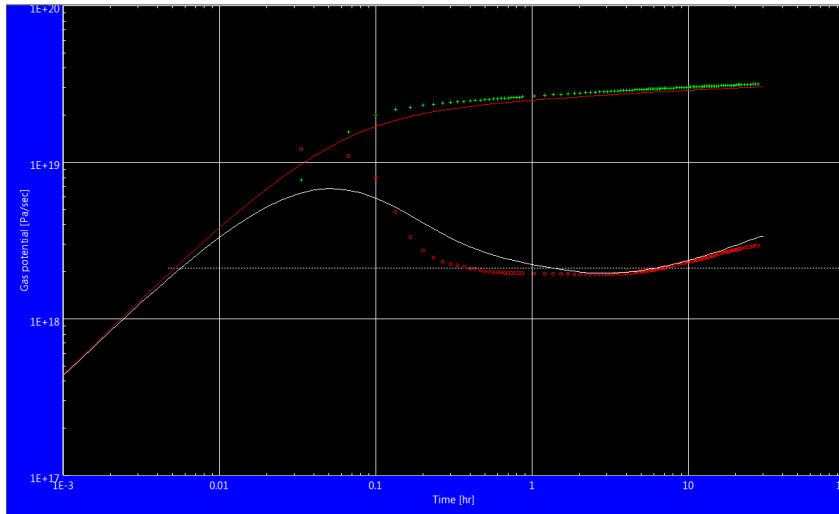


Figure 15-7 Log-log plot of the main build-up (red and white lines represents the model)

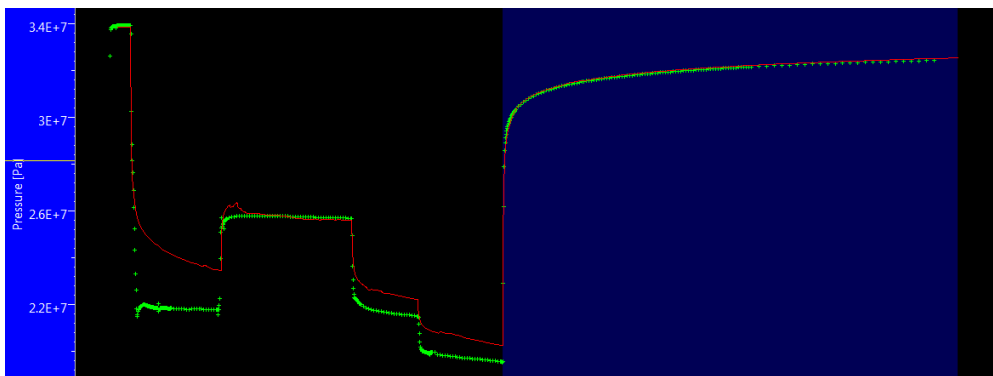


Figure 15-8 Pressure History plot of the main build-up (green dots are measured data and red line is modelled)

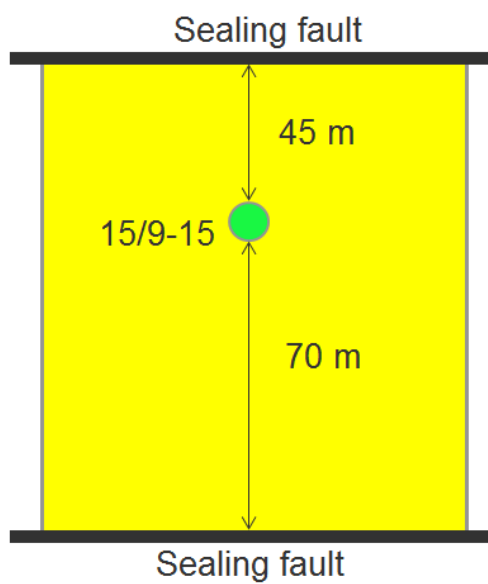


Figure 15-9 Sketch of the well and distance to the two parallel faults

3. Intersecting faults

A final model involving two sealing intersecting faults was tested. Figure 15-12 shows a sketch of the model, and where the well is located with respect to the faults. Figure Figure 15-10 and Figure 15-11 show the model match to pressure derivative and pressure history plot. Like the parallel faults model, this model also gives a fairly good match to the measured data.

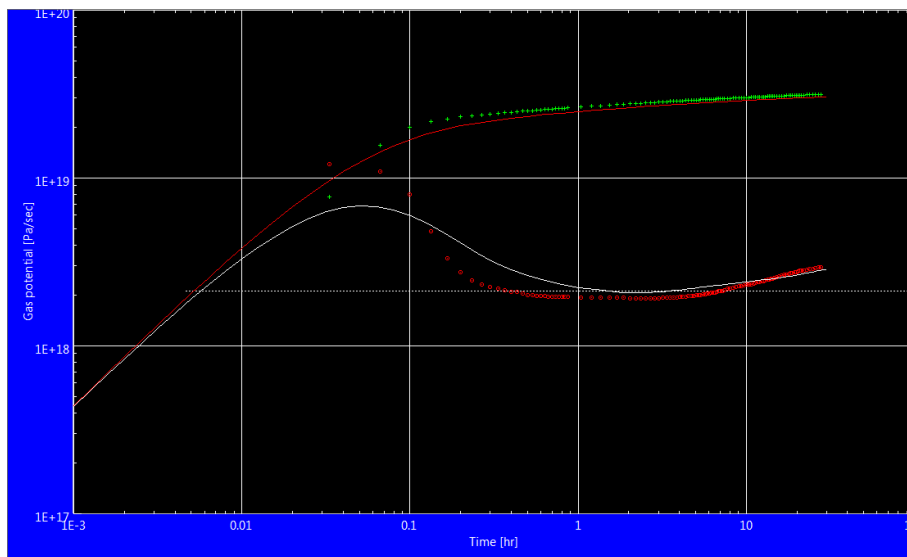


Figure 15-10 Log-log plot of the main build-up (red and white lines represents the model)

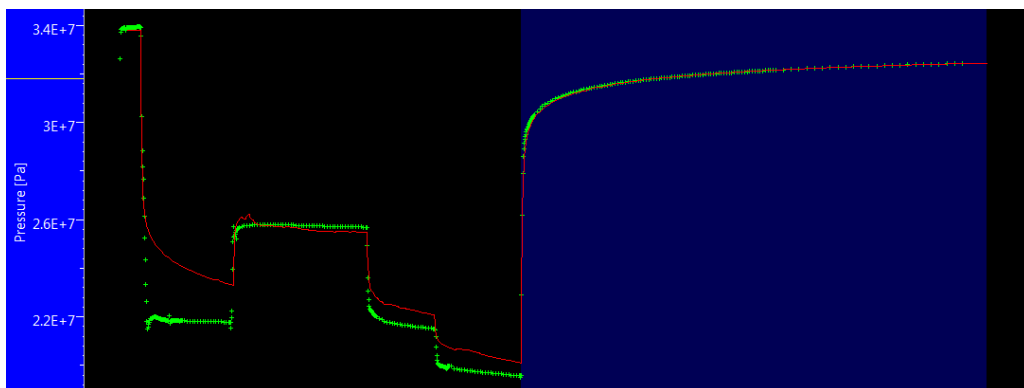


Figure 15-11 Pressure History plot of the main build-up (green dots are measured data and red line is modelled)

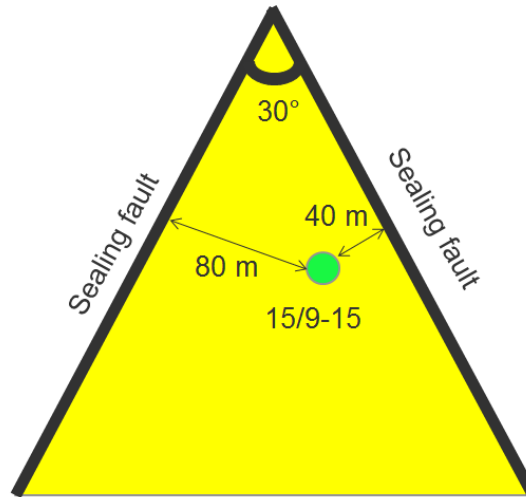


Figure 15-12 Sketch of the well and distance to the two intersecting faults

16 Result

The results of the reservoir characterization of the Skagerrak wells are listed by topics.

16.1 Geology

The Skagerrak Formation can be interpreted as fluvial deposits mainly from braided and meandering river systems. The correlation between 15/9-9, 15/9-15 and 15/9-17 wells shows a clear difference in thickness where Skagerrak was ranging from 96.7-231.1 meters in the wells. The formation is strongly influenced by the fluvial depositions and the gamma ray log pattern are frequently changing from sand and shale intervals. These frequent rapid changes makes it difficult to make a detailed correlation between the wells.

The shaly deposits consisting of silt, shale and clay, are interpreted to be deposits from overbank of the flood basin with considerably lower permeability compared to the channel sandstone sequences.

The porosity and permeability show a large variation within a relatively short depth intervals. The petrophysical parameters are affected by factors like the grain size, the sorting, and the degree of clay volume.

The bottom part (Zone 1 and Zone 2) in both wells 15/9-15 and 15/9-17 shows similarities in gamma ray and density/neutron logs. The well 15/9-9 has not been correlated with the other wells due to lack of finding correlating zones.

The top Skagerrak Formation in well 15/9-15 and well 15/9-17 comprises sequences of sands with fairly to good permeability and porosity properties. They are both comprising hydrocarbons.

The well 6510/7-2 comprising Red Beds from the Norwegian Sea show similar features with the Triassic Formation Skagerrak from well 15/9-9, 15/9-15 and 15/9-17. The rapid changes in lithology of sandstones separated by the massive fine materials of shale and mud is indicating a fluvial system. The main difference from 6510/7-2 compared to the other wells located in the Central North Sea was the porosity properties due to a higher content of clay volume.

16.2 Porosity, Permeability and Cut offs

Porosity

The porosity is the result of calibrating core porosity with the density log and corrected with clay volume and combine this with a clay corrected neutron log to create an effective

$$\text{porosity. } \phi_E = \frac{7*\phi_{DC}+2*\phi_{NC}}{9} \quad \text{Equation 13-1} \quad \phi_E = \frac{7*\phi_{DC}+2*\phi_{NC}}{9} \quad \text{Equation 13-1}$$

The result of the porosity calculations shows a fair to fairly good correspondence between the porosity from logs and core in the wells. (Figure 20-1, Figure 20-2, in Appendix 20) The effective porosity curve show usually lower values than the total porosity model but in some areas they are converging which implies low clay volume causing higher porosity.

There will always be some uncertainties in the calculation of the porosity. The uncertainties will be depending on the various errors in the core data like overburden correction, error in depth shifting, error in the measurements. The quality of the log data due to wash out effects will affect the density/neutron logs.

Well 15/9-9 (Sleipner Øst) has no hydrocarbons and the core coverage is very good. The effective porosity is created from the combined core and density/neutron log. Due to some measurement problems of the neutron log from about 2665 to 2705 m RKB, the porosity is calculated only by use of Density and Core porosity in this interval. The porosity in this interval may be considered as uncertain. The porosity is in the span of 21 % in Upper

Skagerrak while it is about 15 % in Lower Skagerrak. Table 16-2, Table 16-3, Table 16-4. If Vclay is included with cutoff of 0.5 , Table 20-1, Table 20-2, Table 20-3

Well 15/9-15 (Gungne) has hydrocarbon filled Skagerrak Zone 5 and down to 2920 in Skagerrak Zone 4. The average porosity is 14-15 %. Skagerrak has good core coverage and the porosity matches well. The zones (Skagerrak 1-3) without core coverage show a porosity of 17-22 %

Well 15/9-17 (Loke) has Skagerrak with hydrocarbon through the whole formation. The porosity range is 16-23 %

Permeability

The average permeability of Skagerrak Formation is relative low, Table 16-1.

Table 16-1 Average permeability values for the Skagerrak Formation

| Well | Permeability, k [md] |
|---------|----------------------|
| 15/9-9 | 2.5-17 |
| 15/9-15 | 3.8-29 |
| 15/9-17 | 1 -37 |

The permeability obtained from regression analysis matched poorly with the core permeability exhibiting wide scatter in several areas. The mismatch was very evident in the well 15/9-17. (Figure 20-3 in Appendix 20) This was a challenging task in the heterogeneous Skagerrak Formation, and several attempts were made to be able to achieve a satisfying match when plotting the core permeability vs. the core porosity. The use of this method including several permeability correlations from cores were working fairly good in well 15/9-17, but this will make the utilisation of the correlation less universal for adjacent wells. Further improvements are recommended, like for instance introducing the clay volume as a third parameter in the regression analysis due to the formations heterogeneity.

Vertical Permeability

The ratio between horizontal and vertical is showing a very wide spread, referring to the Figure 13-7, Figure 13-8, Figure 13-9 which gave no indication how the vertical permeability is related to the horizontal permeability .

Cut off

Cut off values applied are $k > 0.05$ and a corresponding $\phi > 0.1$, which is applicable to a formation containing gas. (Figure 16-2) In addition a sensitivity is run with including a cut off of $V_{clay} < 0.5$. The results is shown in Table 20-1 to Table 20-3.

The gamma ray method was utilised in the estimation of the clay volume, V_{cl} . The estimated GR max and GR min are given in table 13.1 , section 13.1. In the Skagerrak Formation the amount of clay content is high and has thus an inhibitory effect on the permeability which is causing a restriction of the flow in the Skagerrak Formation when the clay is in contact with other fluids.

In section 10 it was mentioned that the Skagerrak Formation contained heavy minerals. This will be a important factor to take this into consideration when performing a clay volume estimation of formations like the Skagerrak Formation.

The same GR max and GR min were used for the whole interval in each area where the Skagerrak Formation was located. An improvement in this estimation would be to utilise different GR max and GR min in the zones the formation is divided in.

The average values of the clay volume for the Skagerrak formation showed that well 15/9-17 had the highest clay volume content of around 0.50. As Figure 16-1 show, the distribution show large variation compared with well 15/9-9 which has a average value of 0.14. Well 15/9-15 showed a average of 0.33. The well 15/9-9 and 15/9-15 are displayed in Figure 20-12 and in Figure 20-13 in section 20.2.3.

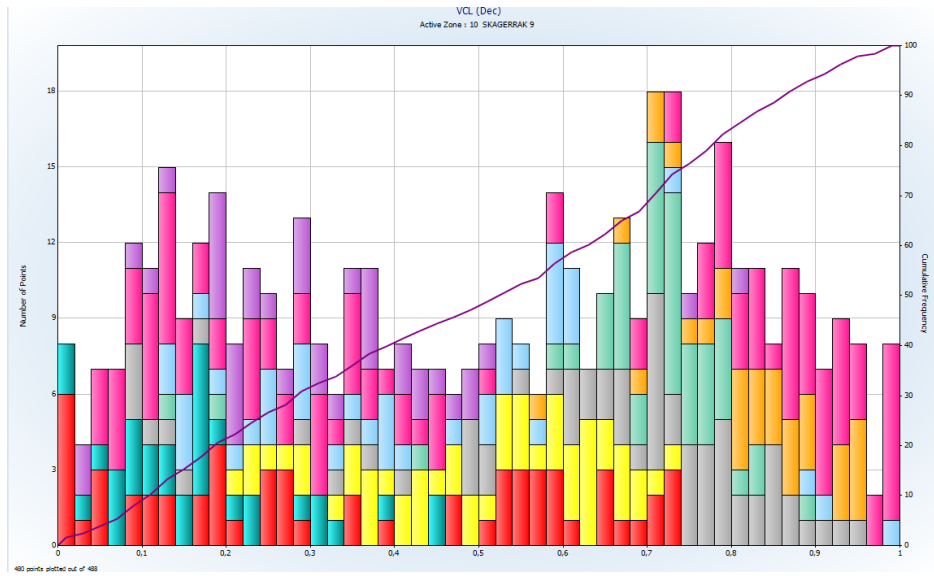


Figure 16-1 Vclay distribution in well 15/9-17

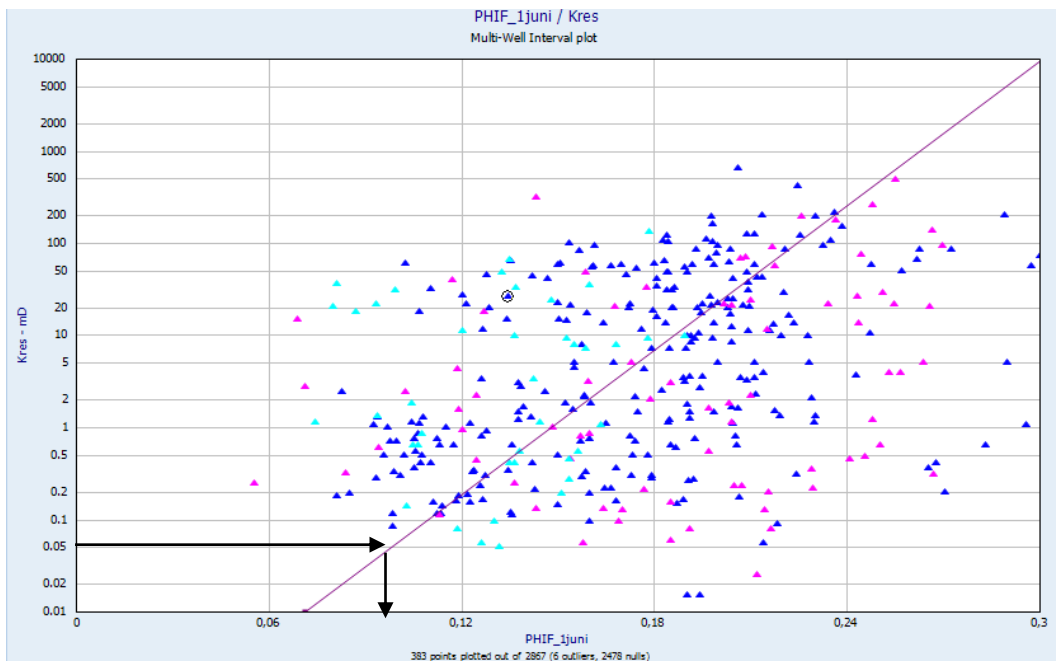


Figure 16-2 Core permeability vs. Effective porosity for all wells

16.3 Averages from Cut offs

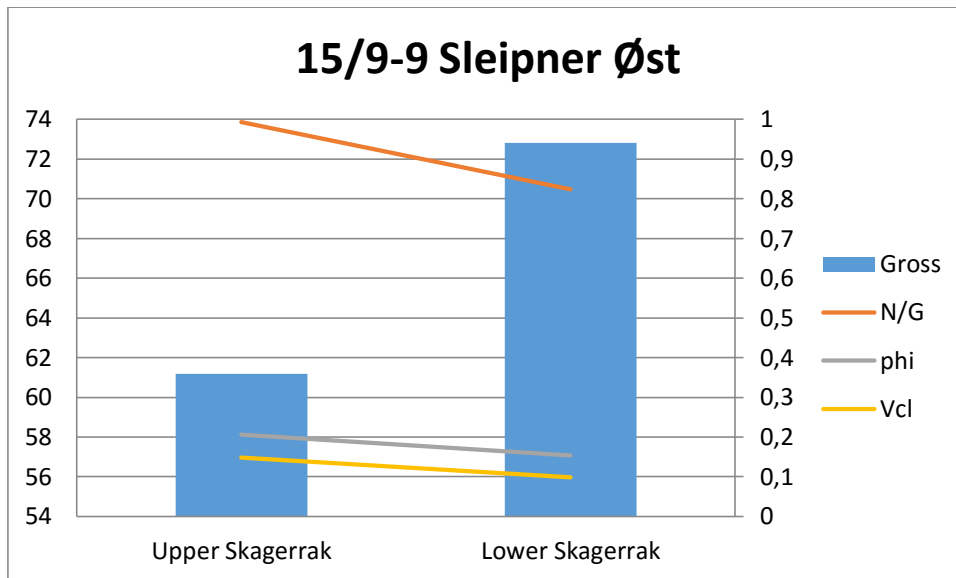


Figure 16-3 Average values from well 15/9-9, Cut offs: $k=0.05$ md and $\phi=0.1$

Table 16-2 Average values by using cut off values $k>0.05$ and $\phi>0.1$

| 15/9-9 | Gross | N/G | phi | Sw | Vcl | KLOGHgeo | KLOGHharit |
|-----------------|-------|-------|-------|-------|-------|----------|------------|
| Upper Skagerrak | 61,17 | 0,993 | 0,206 | 0,85 | 0,148 | 17,192 | 31,223 |
| Lower Skagerrak | 72,83 | 0,824 | 0,153 | 0,782 | 0,099 | 2,555 | 10,104 |

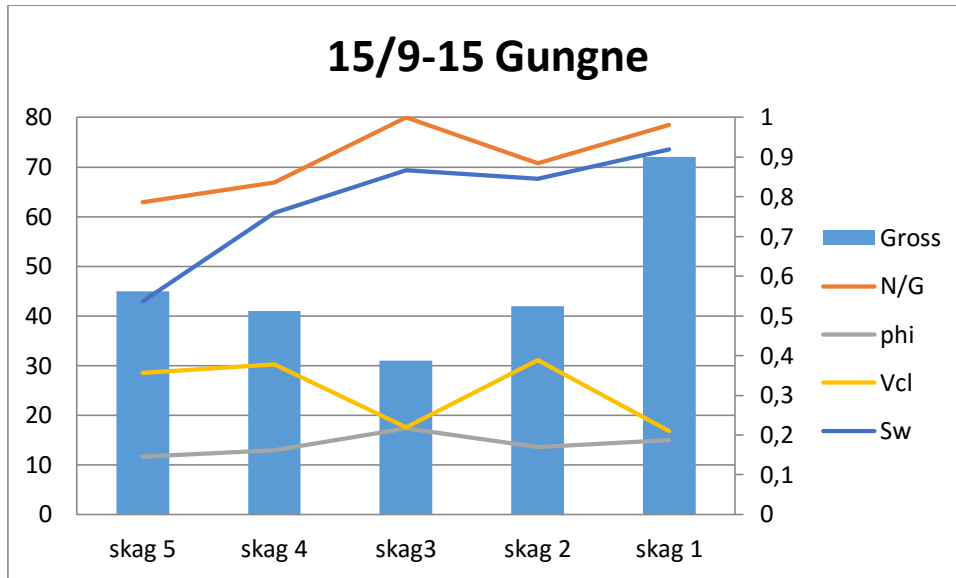


Figure 16-4 Average values from well 15/9-15, Cut offs: $k=0.05$ md and $\phi=0.1$

Table 16-3 Average values by using cut off values $k>0.05$ and $\phi>0.1$

| 15/9-15 | Gross | N/G | phi | Sw | Vcl | KLOGHgeo | KLOGHarit |
|---------|-------|-------|-------|-------|-------|----------|-----------|
| skag 5 | 45 | 0,787 | 0,146 | 0,536 | 0,357 | 7,388 | 15,333 |
| skag 4 | 41 | 0,836 | 0,161 | 0,759 | 0,378 | 3,872 | 16,367 |
| skag 3 | 31 | 1 | 0,217 | 0,867 | 0,22 | 29,985 | 71,275 |
| skag 2 | 42 | 0,884 | 0,17 | 0,845 | 0,389 | 5,305 | 14,479 |
| skag 1 | 72 | 0,981 | 0,187 | 0,919 | 0,21 | 9,893 | 19,683 |

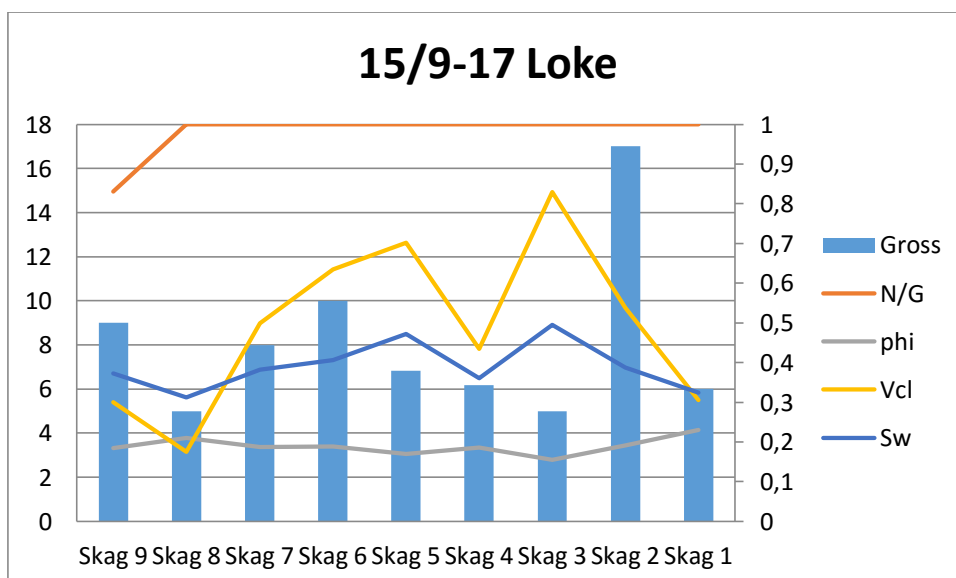


Figure16-5 Average values from well 15/9-17, Cut offs: $k=0.05$ md and $\phi=0.1$

Table 16-4 Average values by using cut off values $k>0.05$ and $\phi>0.1$

| 15/9-17 | Net | N/G | phi | Sw | Vcl | KLOGHgeo | KLOGHarit |
|---------|------|-------|-------|-------|-------|----------|-----------|
| Skag 9 | 7,48 | 0,831 | 0,184 | 0,372 | 0,3 | 8,511 | 34,316 |
| Skag 8 | 5 | 1 | 0,21 | 0,312 | 0,175 | 22,264 | 41,14 |
| Skag 7 | 8 | 1 | 0,187 | 0,382 | 0,499 | 9,344 | 28,238 |
| Skag 6 | 10 | 1 | 0,188 | 0,406 | 0,634 | 9,732 | 47,835 |
| Skag 5 | 6,82 | 1 | 0,17 | 0,472 | 0,702 | 1,743 | 4,615 |
| Skag 4 | 6,18 | 1 | 0,186 | 0,36 | 0,434 | 3,05 | 8,005 |
| Skag 3 | 5 | 1 | 0,155 | 0,495 | 0,829 | 1,033 | 1,34 |
| Skag 2 | 17 | 1 | 0,191 | 0,388 | 0,538 | 3,654 | 17,899 |
| Skag 1 | 6 | 1 | 0,23 | 0,324 | 0,306 | 37,194 | 50,119 |

16.4 Results from Water Saturation Modelling

- There is not a consistent pattern of one specific method is lowest or highest water saturation
- The water saturation determined from core only-method shows the highest water saturation
- Adjusting $\sigma\cos\theta$ in the core method doesn't make it possible to match the log methods
- The method that is varying the most is Waxman Smits which is significantly lower in 15/9-15 while it is significantly higher in 15/9-17 compared with the Indonesia method. This method is probably suffering due to the Qv model that is established

with the existing measurements. The Waxman Smits is not considered suitable for these wells.

- Archie is only included to show the effect on water saturation if no clay is taken into account.
- The only method that can match the Indonesia method is combining Swirr from Indonesia with Sw_n established from cores with modification of $\sigma\cos\theta$ from 72 (lab) to 150 (res).
- The method using only logs to establish the J, Sw_n, Sw show a consistency to high water saturation compared with the Indonesia Equation.
- The best method is to use core data to establish the shape of J-function combined with Swirr from logs. In this method the final tuning can be done with the $\sigma\cos\theta$. It requires less subjective interpretation.

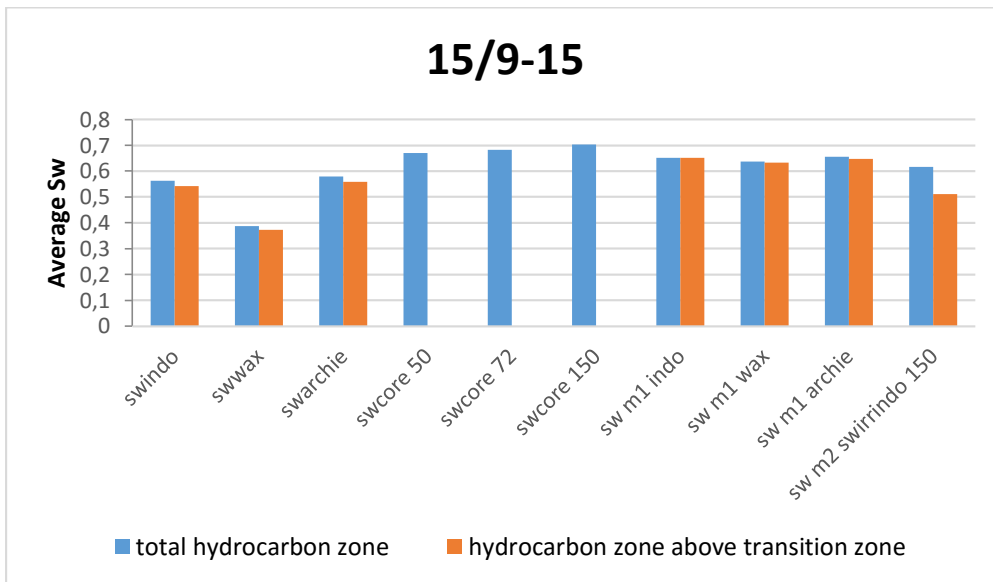


Figure 16-6 Comparing the water saturation methods 15/9-15

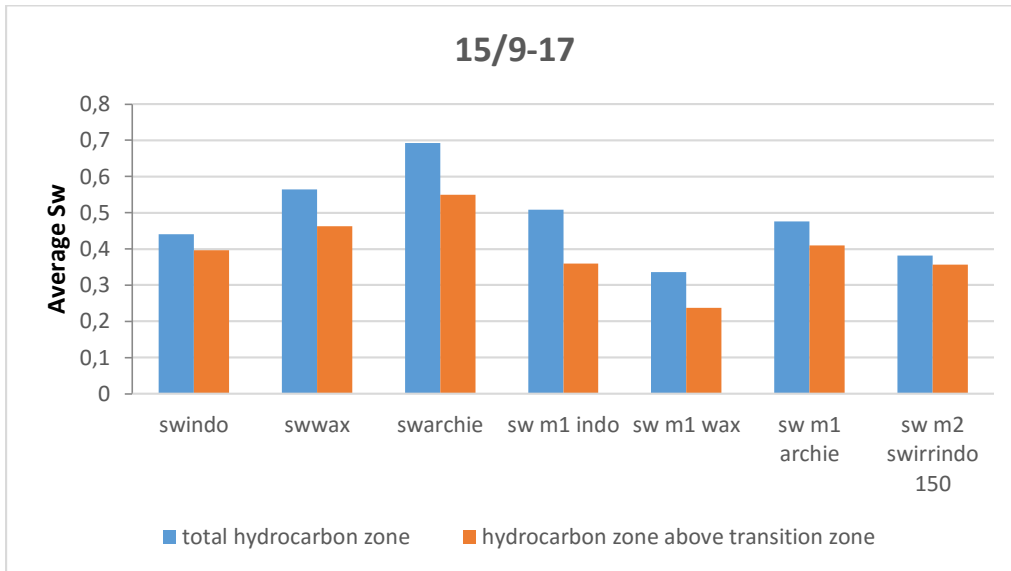


Figure 16-7 Comparing the water saturation methods 15/9-17

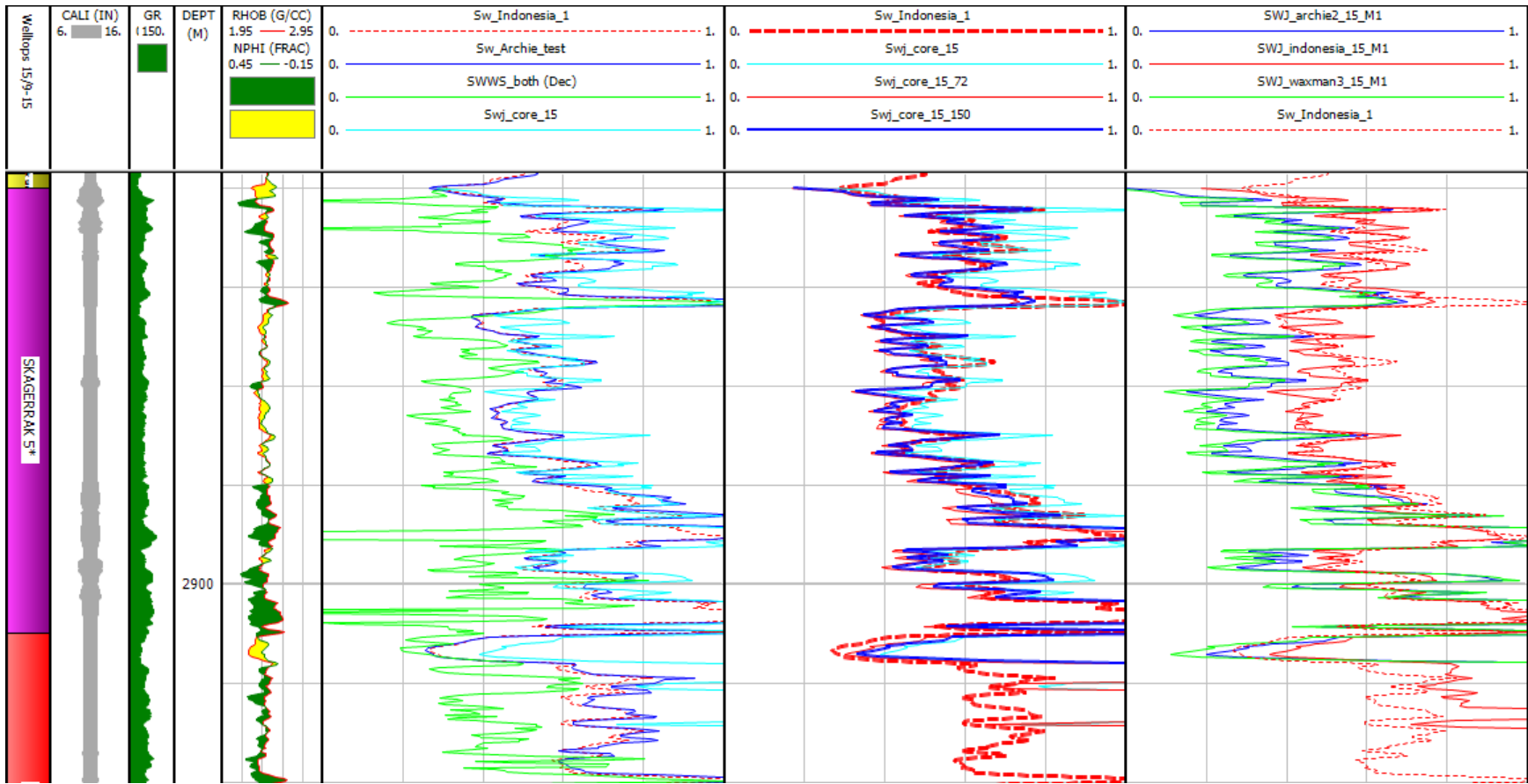


Figure16-8 Comparison of water saturation well 15/9-15

Explanation to the tracks in Figure 16-8

Track 6: Sw_Indonesia_1 = Standard Indonesia method, Sw_Archie=Standard Archie method, SWWS_both=Standard Waxman Smits method. : Swj_15_core= well 15/9-15 watersaturation from core with irreducible watersaturation from cores.

Track 7: Sw_Indonesia_1 = Standard Indonesia method, : Swj_15_core_150 = well 15/9-17 watersaturation from core with irreducible watersaturation from Indonesia and sigmacosØ=150, : Swj_15_core_15 = well 15/9-15 watersaturation from core with irreducible watersaturation from kjerne, Swj_15_core_72 = well 15/9-15 watersaturation from core with irreducible watersaturation from cores sigmacosØ=72

Track 9: Track Swj_indonesia2_M1 = method section 14.7 well 15/9-15, Track Swj_archie2_M1 = method section 14.7 well 15/9-15, , Track Swj_waxman2_M1 = method section 14.7, Sw_Indonesia_1 well 15/9-15, Sw_Indonesia_1 = Standard Indonesia method.

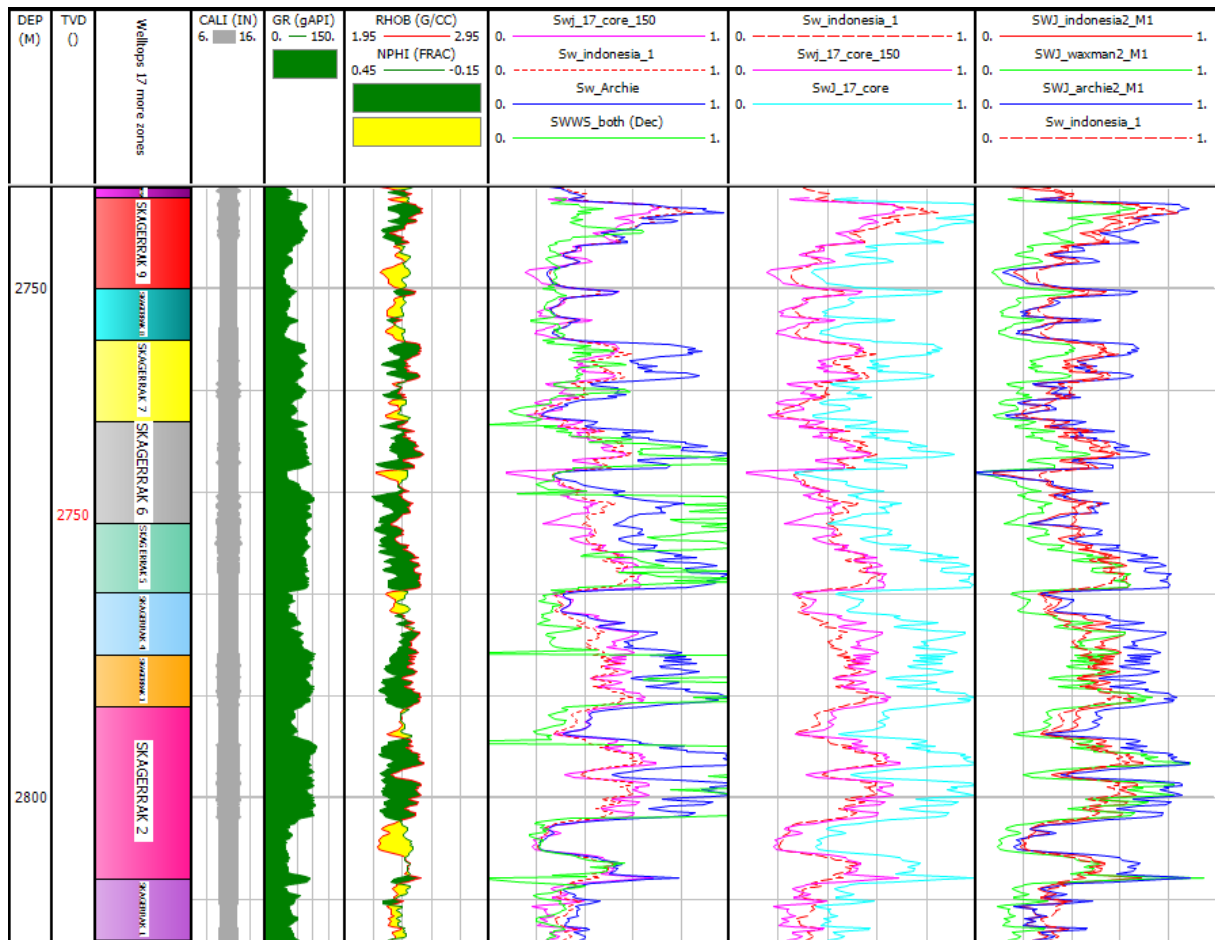


Figure16-9 Comparison of water saturation well 15/9-17

Explanation to the tracks in Figure 16-9

Track 7: Swj_17_core_150 = well 15/9-17 water saturation from core with irreducible watersaturation from Indonesia and sigmacosØ=150, Sw_Indonesia_1 = Standard Indonesia method, Sw_Archie=Standard Archie method, SWWS_both=Standard Waxman Smits method.

Track 8: Sw_Indonesia_1 = Standard Indonesia method, : Swj_17_core_150 = well 15/9-17 watersaturation from core with irreducible watersaturation from Indonesia and sigmacosØ=150, : Swj_17_core_15 = well 15/9-17 watersaturation from core with irreducible watersaturation from cores,

Track 9: Track Swj_indonesia2_M1 = method section 14.7, Track Swj_archie2_M1 = method section 14.7, Track Swj_waxman2_M1 = method section 14.7, Sw_Indonesia_1

Archie, Indonesia, Waxman Smits

The water saturation methods show similar results in the clean sandstone sections due to the fact that the shale conductivity is negligible. The clay related equations, Indonesia and Waxman Smits are converging to the Archie equation in these areas. Despite of this the results illustrate the need for clay correction in the Skagerrak Formation.

The Archie's equation shows a tendency of overestimating the water saturation in gas bearing wells 15/9-15 and 15/9-17. This will lead to potentially hydrocarbon bearing zones being missed due to its ability to suppress the resistivity when the clay distributions are present.

The Indonesia equation and the Waxman Smits method were used to compensate for the clay effect. These method shows a lower water saturation compared to the Archie's equation. Despite of these methods being more correct to utilise in this type of formation it need to be taken into consideration the content of minerals like glimmer and feldspar that will make the clay determination more difficult.

Overall the Waxman Smits equation are showing lower water saturation compared to the other two methods. Poor correlation of Q_v factor can be a critical point in this method. It must also be taken into consideration that the special core analysis data are old measurements and these may only be based on good zones in the formation. This will contribute in a misleading result by the Waxman Smits equation

The use of Indonesia Equation should be satisfying in the Skagerrak Formation due to its ability to operate with salinities over 50 000 ppm NaCl. The Waxman Smits is not calibrated good enough in the water bearing zones.

Swirr

1) The irreducible saturation, Sw_{irr} , from cores is higher than for logs. The plugs measured on labs will be depressurized. These measuring conditions can explain the difference in the Sw_{irr} from cores and logs. The pore volume under lab conditions will be greater due to the atmospheric conditions. This means that new pores can be formed and this will be imbibed in the cores. This is the reason for higher Sw_{irr} in cores compared to the Sw_{irr} from logs.

2) This water saturation is additionally independent of resistivity log which can easily be affected by neighbouring layers. This will result in too high value of water saturation S_w in current zone. Differences appearing in cored zones of the formation will be better described by the S_{wJ} .

16.5 Result of DST Evaluation

Test derived permeability was compared with the permeability from cores in the same interval and they correspond relatively well. The test derived permeability was estimated to 3.1 md while the permeability from cores is estimated to 4 md.

The transient pressure analysis of DST 1 in well 15/9-15 indicates that there are barriers in the reservoir at a distance of about 70 meters from the well. A model including a sealing fault about 60 meters away from the well gave a relatively poor match to the measured data. The system seems too open, and two other fault models, which included one additional sealing fault, were established. Both of these models gave a better match to the measured data, indicating that the well is located in a more compartmentalized area. This might be due to sealing faults present in the reservoir, or that the test sees the margins of a sand channel since the well is located in a fluvial environment. The DST evaluation shows that there is not one unique model that matches the data. Different fault scenarios can give a fairly good match to the data, and it is therefore important to have an idea of the geological -and stratigraphic setting of the reservoir (ie. faults and depositional environment) when interpreting a well test.

17 Conclusion

The Skagerrak Formation can be interpreted as fluvial deposits mainly from braided and meandering river systems. The comparison between 15/9-9, 15/9-15 and 15/9-17 wells shows a clear difference in thickness where Skagerrak was ranging from 96.7 - 231.1 meters in the wells. The transient pressure analysis of DST 1 in well 15/9-15 indicates that there are barriers in the reservoir at a distance of about 70 meters from the well. The permeability from the test indicates a permeability of 3.1 md representing gas permeability while the average permeability from log- core correlation is about 4.0 md, representing total permeability. (including the Swirr term)

The combination core and log properties is challenging in these environment with rapid changing lithology, and extrapolating the correlation outside cored interval must be handled with care.

The Red Bed well 6510/7-2 is comparable with the 15/9-17 (Loke Field) changes in gamma ray pattern and how the changes in shale and sand deposits are made, but the porosity is much lower in 6510/7-2.

The average porosity of Skagerrak Formation is ranging between 14-23% with a permeability cutoff of 0.05 md. The average Net to Gross within a cutoff of 0.05 md is generally high, ranging from 0.8-1.0.

The average saturation in the hydrocarbon column is 31-53%. The best method is assumed to be the Indonesia- method within the current lithology, clay content and water salinities. Alternative a combined method with core can be suggested with the shape of J from core and the irreducible part from logs.

18 Nomenclature

a: Tortuosity factor

dL: Length Interval

dP: Pressure Difference

GR: Gamma Ray Log

GRmax: Maximum Gamma Ray log value

GRmin: Minimum Gamma Ray log value

haFW L: Height above Free Water Level

HCPV: Hydro Carbon Pore Volume

EOR : Enhanced Oil Recovery

FF: Formation Resistivity Factor

FW L: Free Water Level

k: Permeability

kres : Permeability at Reservoir conditions

m: cementation exponent

T VDSS: meters True Vertical Depth Sub Sea

n: Saturation exponent

N/G: Net to Gross

NGL: Natural Gas Liquids

Pc: Capillary Pressure

Pnw : Pressure of non wetting phase

Pw: Pressure of wetting phase

PD: Displacement Pressure

ppm: Parts Per Million

q: Volumetric Flow rate

r: Pore Throat Radius

Rt: Formation Resistivity

Rw : Water Resistivity

rw: radius of well bore

Sw: Water Saturation

Swr : Residual Water Saturation
Swirr: Irreducible Water Saturation
Vcl: Clay Volume/Fraction,
 $\Delta\rho$: Density Difference
 θ : Contact Angle
 μ : Viscosity
 v : Apparent Fluid Velocity
 ρ_{fl} : Fluid Density
 ρ_{log} : Density Log readout
 ρ_{ma} : Matrix Density
 σ : Surface Tension, Interfacial Tension
 ϕ :Porosity
 ϕ_D :Porosity from Density log
 ϕ_e = Effective Porosity
 ϕ_N = Porosity from Neutron log
 ϕ_{tot} = Total Porosity

19 References

Most of the theory that deals with petrophysical theory, geology, well testing and the general information about the Skagerrak Formation including the wells is based on written literature. In the petrophysical interpretation part it has been used computer softwares like Microsoft Excel and Interactive Petrophysics to be able to treat the data. Karl Audun Lehne has handed out important input to some of the calculations and interpretations. Some of the figures have been drawn or modified in Paint.

19.1 Written references

1. NPD, <http://factpages.npd.no/default.aspx?culture=no>
2. bin T.T. Nguyen, Stuart J. Jones, Neil R. Goult, Alexander J. Middleton, Neil Grant, Alison Ferguson, and Leon Bowen. "The role of fluid pressure and diagenetic cements for porosity preservation in Triassic fluvial reservoirs of the Central Graben, North Sea"
3. Neil Grant, Alexander J. Middleton and Stuart Archer. Porosity trend in the Skagerrak Formation central Graben, United Kingdom Continental Shelf: "The role of compaction and pore pressure history"
4. CE Deegan and BJ Scull "A Standard Lithostratigraphic nomenclature for the central and northern North Sea"
5. Kjell Sigve Lervik, "Triassic Lithostratigraphy of the Northern North Sea Basin"
6. Terence C. Blair and John G. McPherson, "Alluvial fan processes and forms"
7. GY 111 Lecture Note series sedimentary environments 1: "Alluvial Fans"
8. Recognition of Fluvial Depositional systems and their Resource potential 1985
9. Brian R. Rust, "Depositional models for braided alluvium"
10. J.G. Richardson, J.B. Sangree, R.M. Sneider, "Braided Streams Reservoirs" SPE 28828 Well test interpretation in a heterogeneous braided fluvial reservoir
11. J.G. Richardson, SPE, Richardson, Sangree & Sneider. J.B. Sangree, SPE, Richardson, Sangree & Sneider, R.M. Sneider, SPE, Richardson, Sangree & Sneider. "Meandering stream reservoirs"
12. Statoil.com, <http://www.statoil.com/no/Pages/default.aspx>

13. Karl Audun lehne, Various of data material
14. Walter H Fertl, George v Chillanger "Determination of volume type and distribution modes of clay minerals from well logging data" SPE 17145 (1988)
15. Harold Vance department of petroleum engineering Texas a&M university Formation evaluation PETE 663 shaly sand evaluation (2010)
16. David Earl Johnson Kathryn E pile. Well logging in nontechnical language second edition (2002)
17. Karl Audun Lehne, lecture notes from the course Formation Evaluation 2015
18. J.H Schön "physical properties of ROcks- A workbook (2011)
19. Lecture Notes From Hans Kleppe, Reservoir Simulation 2015
20. <http://www.glossary.oilfield.slb.com/Terms/p/permeability.aspx>
21. Oberto serra "the well logging handbook" 2008
22. Luca cosentino "integrated reservoir studies" 2011
23. Edited by S.J Mazzullo H.H Rieke, G.V Chilingarian "Carbonate reservoir characterization: A geologic engineering analysis, part 2 (1996)
24. bok lånt på uis bibliotek
25. George Asquith and Daniel Krygowski (with sections by Steven Henderson and Neil Hurley): "basic well log analysis" (2004)
26. Edited by Ward Chesworth "Encyclopedia of Soil Science" (2008)
27. Malcolm Rider & Martin Kennedy: The Geological interpretation of well logs, third edition
28. Jonathan C evenick Introduction to well logs and subsurface maps (2008)
29. Abhijit Y Dandekar: "Petroleum Reservoir ROck and Fluid Properties", second edition (2013)
30. Enhances oil recovery 2 processes and operations redigert av E.C Donaldson G.V Chilingarian, TF. Yen
31. Norman J. Hyne: "dictionary of Petroleum Exploration, Drilling and production (1991)
32. Edited by Bob Harrison, Petrophysical Society, Geological SOciety of London: Russian-style FOrmation Evaluation" (1995)
33. Principles of Mathematical Petrophysics

34. SCAL report lecture notes Karl Audun
35. Well logging and formation evaluation by Toby darling
36. Encycloperdia of Well logging by Robert Desbrandes
37. H. Eshahawi, SPE M. Samir, SPE and K. K Fathy, SPE, Schlumberger Oilfield Services: Correction for wettability and Capillary pressure effects on FOrmation tester measurements, SPE 63075 (2000)
38. Anatoly B Zoolutkhin and Jann Rune Ursin; " Introduction to Petroleum Reservoir Engineering" HØyskoleforlaget (2006)
39. Essentials of reservoir engineering by Pierre Donnez
40. Enhanced Oil Recovery Don W green G Paul willhite SPE textbook series volume 6
41. James W amyx, Daniel M. Bass JR, Robert L WHiting, The Agricultural and mechanical college of texas: Petroleum reservoir engineering- Physical Properties (1960)
42. Natural Gas by Alexandre Rojey
43. Integrated Reservoir studies luca Cosentino
44. Noaman El- Khatib, SPE, King Saud University, "Development of a modified capillary pressure J-function, SPE 29890 (1995)
45. O. Torsæter M abtahi: "Reprints from Laboratory Manual, Reservoir engineering (1994)
46. Frank W. COle, Gulf Publishing company Houston,Texas "Reservoir engineering Manual" (1969)
47. <http://infohost.nmt.edu/~petro/faculty/Engler524/PET524-4-multiphase.pdf>, New mexico institute of mining and technology
48. <https://brage.bibsys.no/xmlui/bitstream/handle/11250/220934/Reservoir%20characterization%20through%20numerical%20models.pdf?sequence=1&isAllowed=y>
49. Alluvial fans and their natural distinction from rivers based on morphology hydraulic processes sedimentary processes and facies assemblages discussion. SEUNG BUM KIm
50. Chapter 5 Modern alluvial fans and fan deltas frank G Ethridge department of earth resources colorado state university
51. Alluvial fans formed by channelized fluvial and sheet flow. 1 theory by gary parker, member , ASCE, chris Paola Kelin X Whipple and David Mohrig
52. From depositional systems to sedimentary successions on the norwegian

53. Petroleum Geoscience: From sedimentary environments to Rocks Physics by Knut bjørlykke 51
54. landet blir til norges geologi ivar B ramberg, inge bryhni arvid nøttvedt
55. The sleipner A platform: an efficient gas and condensate installation by OT gudmestad and JWA Coker, Statoil A/S
56. Karl Audun Lehne Geologisk brønnlogging
57. William Lyons, Gary J Plisga, BS Michael Lorenz, "Standard Handbook of Petroleum and Natural Gas Engineering."
58. http://www.glossary.oilfield.slb.com/Terms/t/total_porosity.aspx

19.2 Oral References

- 59 Karl Audun Lehne, advisor at the Master thesis
- 60 Geir Byberg, Specialist in Reservoir Technology, Statoil

19.3 Software

- Microsoft Excel
- Microsoft Word
- Microsoft Paint
- Interactive Petrophysics, A Senergy Software, developed by PGL, Technical and marketing support by GeoQuest
- Microsoft Power Point
- Saphir by Ecrin

19.4 Illustrations used in the thesis

- Maps over Central North Sea from NPD.no
- Lithostratigraphy diagram from NPD.no
- Braided river diagram from <http://www.ucpress.edu> (University of California Press)
- Meandering river diagram http://www.geocaching.com/geocache/GC1TGAY_menomonee-river-straight-sinuous-or-meandering?guid=b89306b0-083e-427e-94be-f4bo367b47fd
- excess conductivity diagram from "Essentials of Modern Open Hole for interpretation by John. T Dewan.

20 Appendix CPI-Plot

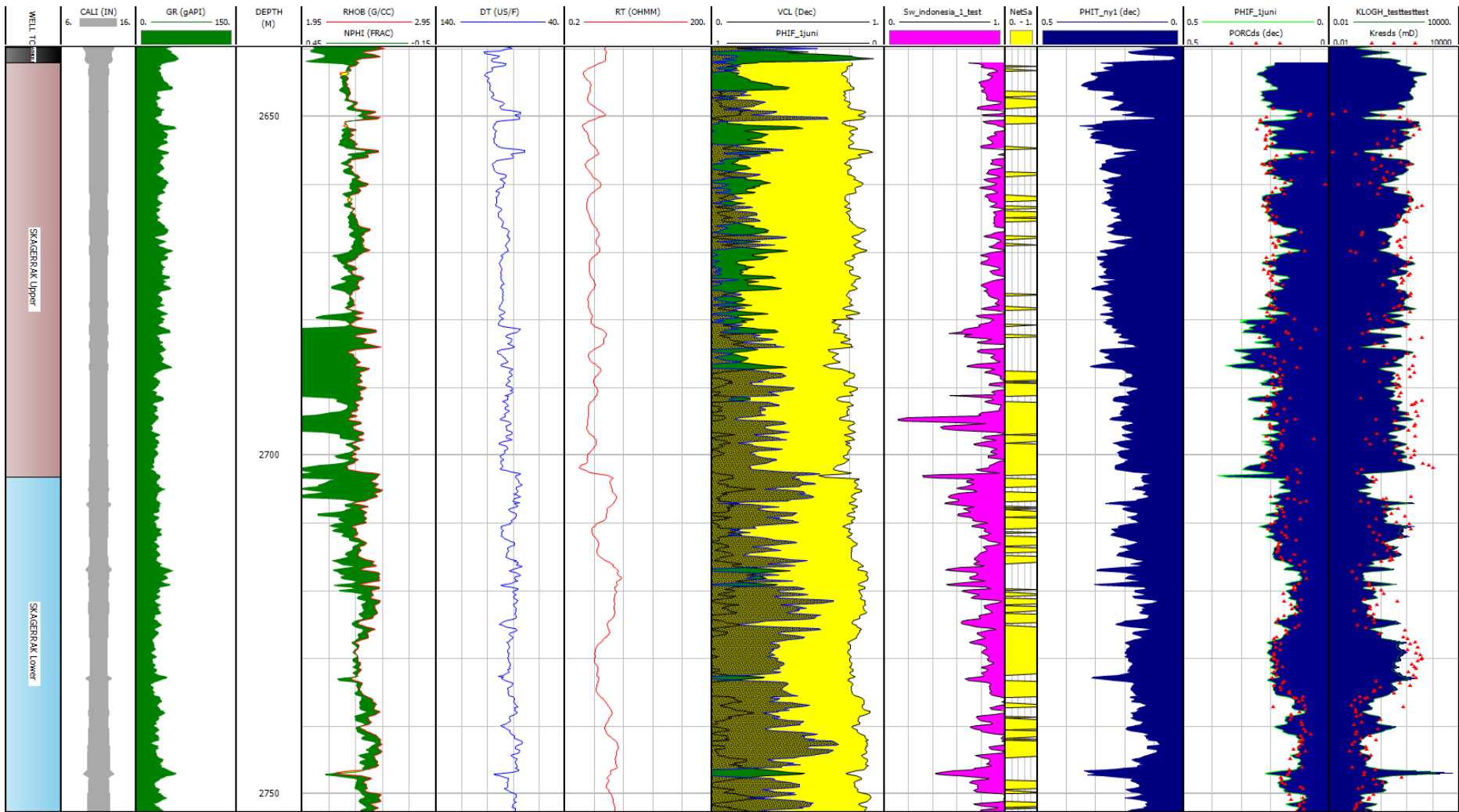


Figure 20-1 CPI-plot of well 15/9-9, Skagerrak Formation

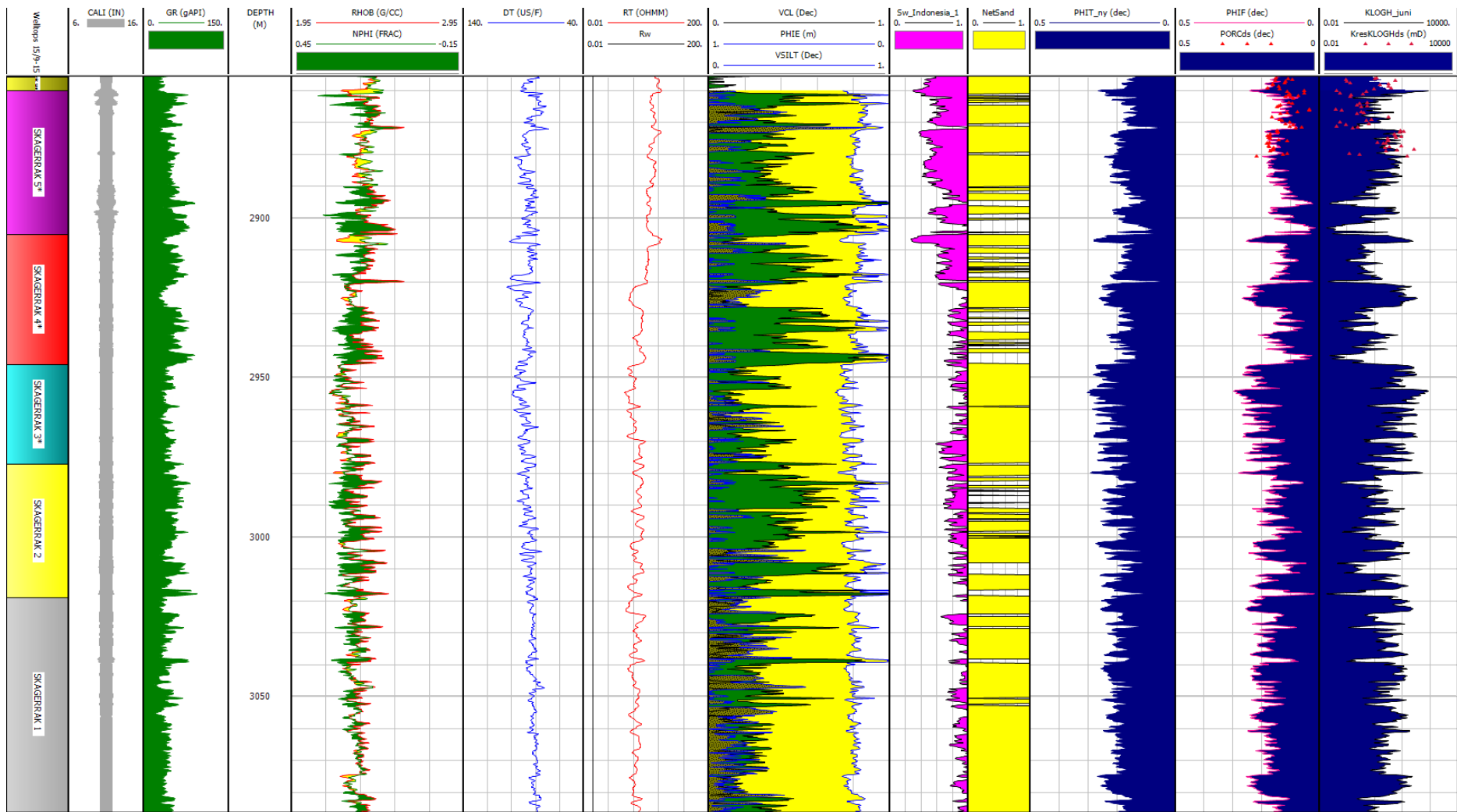


Figure 20-2 CPI- Plot, well 15/9-15, Skagerrak Formation

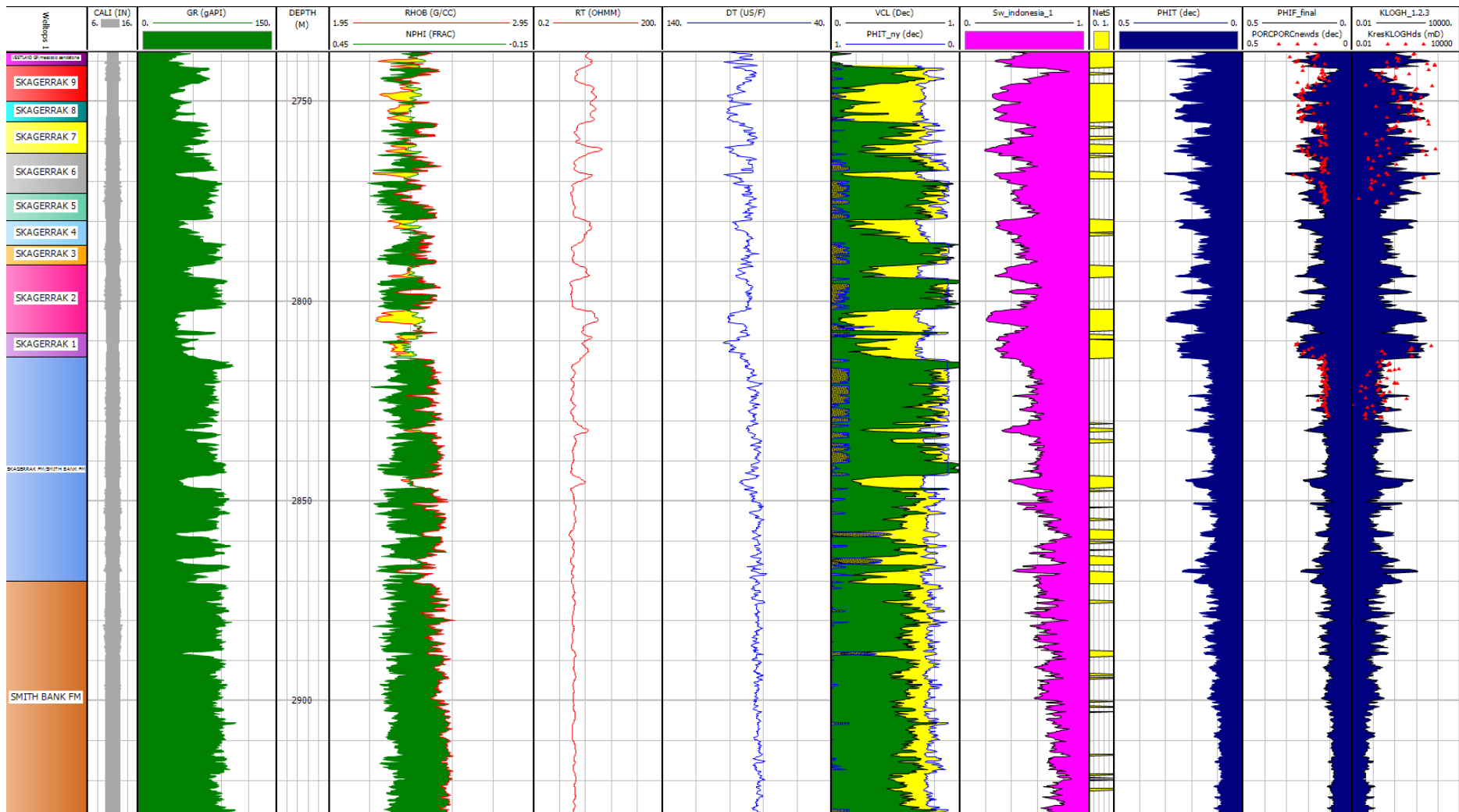


Figure 20-3 CPI- Plot, well 15/9-17, Skagerrak

20.1 Appendix Geological Data

20.1.1 Correlation of the Skagerrak Formation

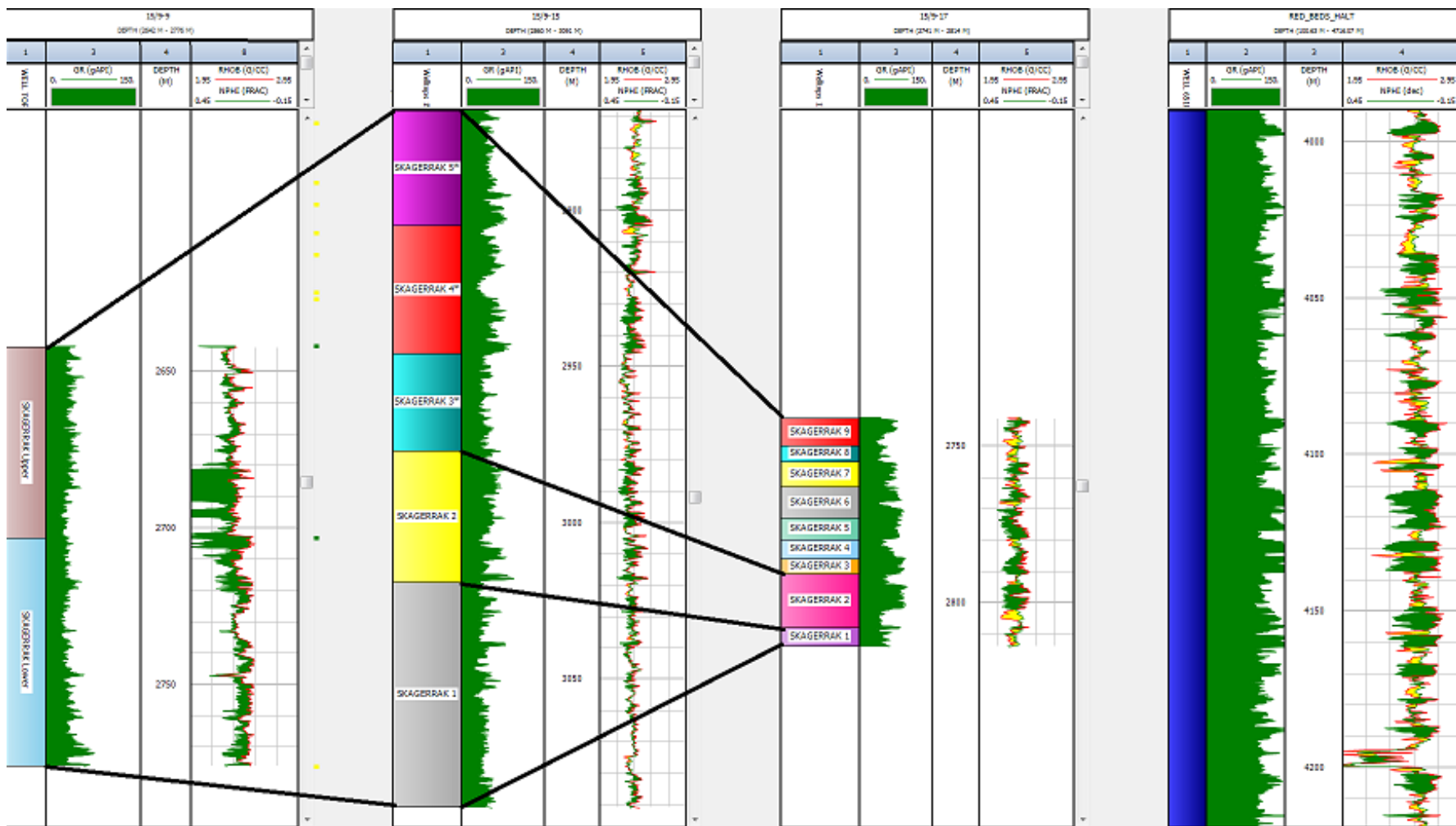


Figure20-4 Correlation of Zone 1 and 2 in well 15/9-15 and 15/9-17

20.2 Appendix Petrophysical Data

20.2.1 Plots of Core Porosity vs. Permeability with Vclay

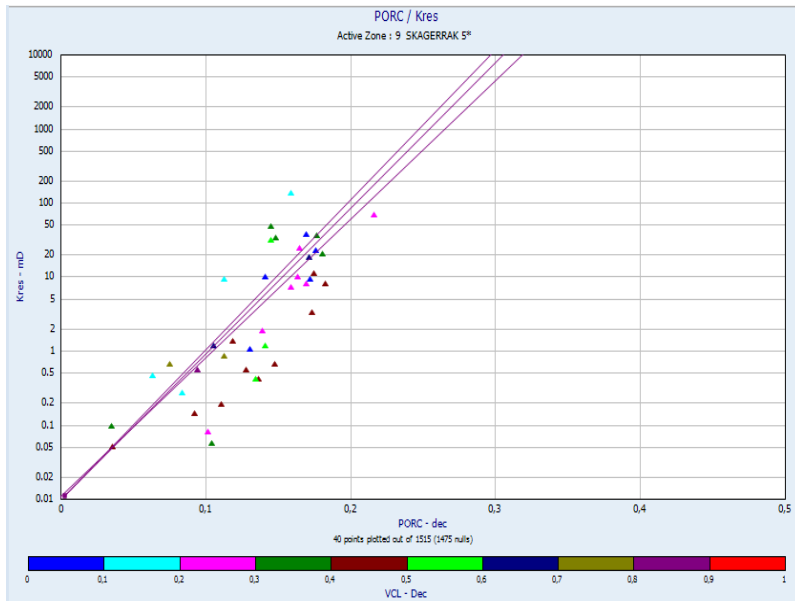


Figure 20-5 Core permeability vs. core porosity vs. Vcl, well 15/9-15

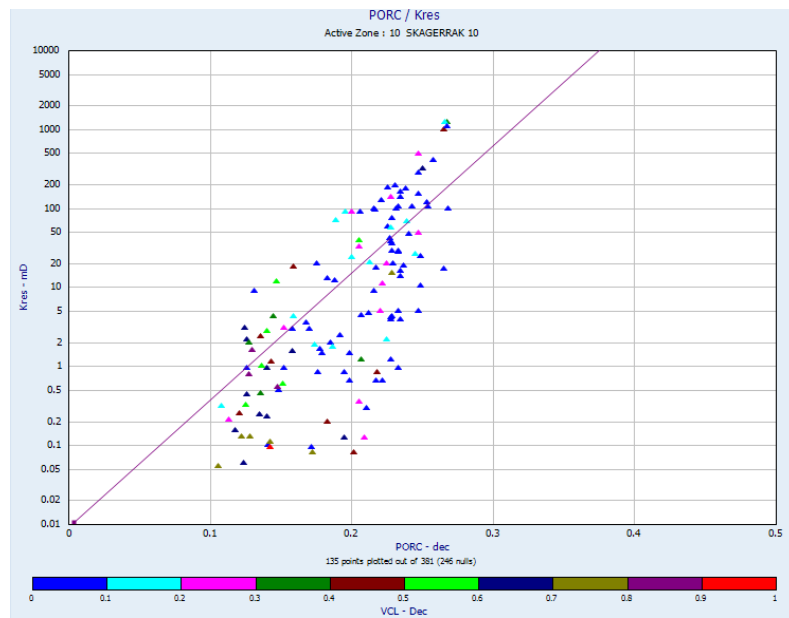


Figure 20-6 Core permeability vs. core porosity vs. Vcl, top part of well 15/9-17

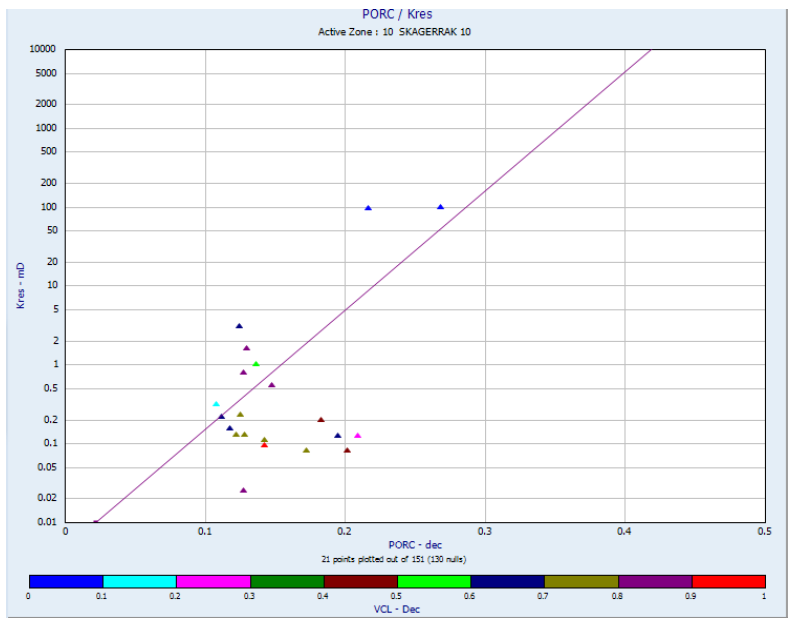


Figure 20-7 Core Permeability vs. core porosity vs. Vcl, middle part of well 15/9-17

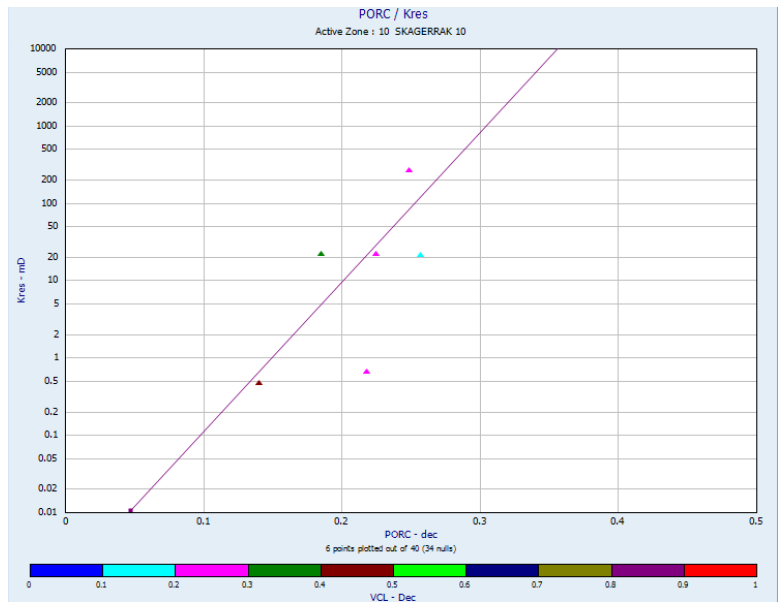


Figure 20-8 Core Permeability vs. core porosity vs Vcl, lower part of well 15/9-17

20.2.2 Averages from Cut off

Table 20-1 Average values by using cut off values $k>0.05$, $\phi>0.1$, $Vcl=0.5$, well 15/9-9

| well 15/9-9 | Gross | Net | N/G | phi | Sw | Vcl | KLOGHgeo | KLOGHarit |
|-----------------|-------|-------|-------|-------|-------|-------|----------|-----------|
| Upper Skagerrak | 61,17 | 60,56 | 0,99 | 0,206 | 0,85 | 0,147 | 17,143 | 31,166 |
| Lower Skagerrak | 72,83 | 59,57 | 0,818 | 0,152 | 0,785 | 0,095 | 2,481 | 6,874 |

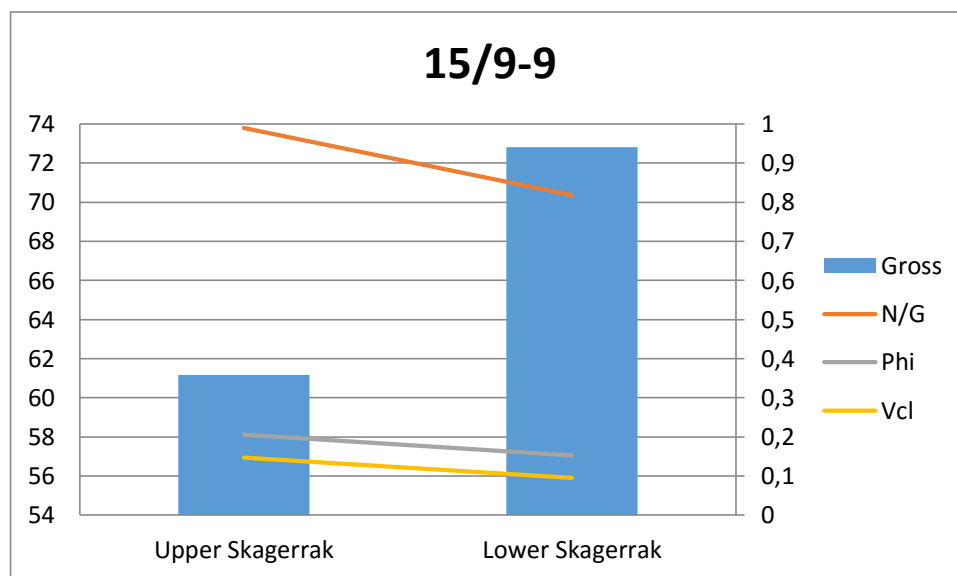


Figure 20-9 Average values from well 15/9-9, Cut offs: $k=0.05$ md, $\phi=0.1$, $Vcl=0.5$

Table 20-2 Average values by using cut off values $k>0.05$, $\phi>0.1$, $Vcl=0.5$ 15/9-15

| Well 15 | Gross | Net | N/G | phi | Sw | Vcl | KLOGHgeo | KLOGHarit |
|-------------|-------|-------|-------|-------|-------|-------|----------|-----------|
| Skagerrak 5 | 45 | 29,78 | 0,662 | 0,15 | 0,528 | 0,308 | 8,919 | 17,366 |
| Skagerrak 4 | 41 | 23,61 | 0,576 | 0,178 | 0,764 | 0,275 | 7,229 | 23,257 |
| Skagerrak 3 | 31 | 30,34 | 0,979 | 0,219 | 0,867 | 0,212 | 32,36 | 72,79 |
| Skagerrak 2 | 42 | 25,74 | 0,613 | 0,183 | 0,86 | 0,296 | 8,588 | 19,654 |
| Skagerrak 1 | 72 | 68,34 | 0,949 | 0,189 | 0,921 | 0,197 | 10,607 | 20,285 |

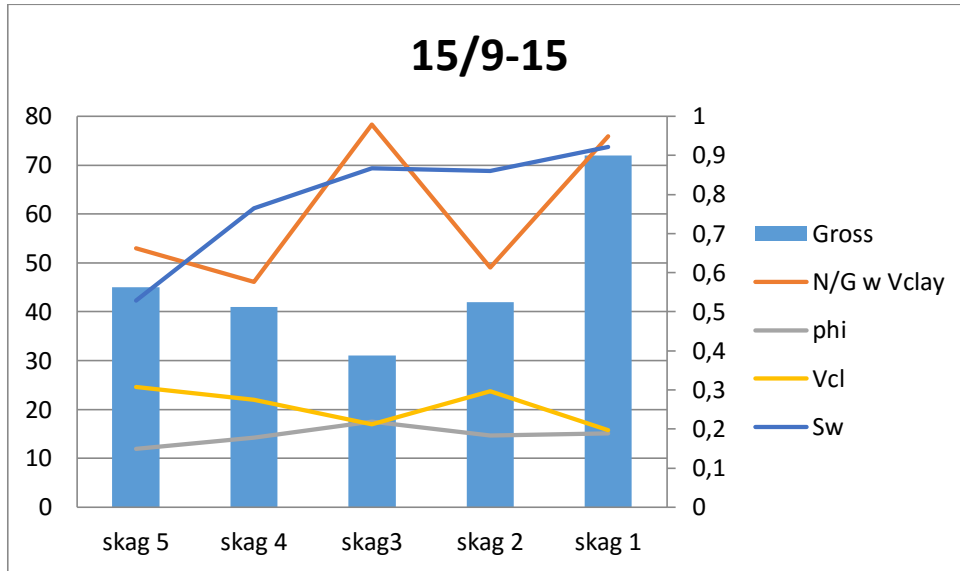


Figure 20-10 Average values from well 15/9-15, Cut offs: $k=0.05$ md, $\phi=0.1$, $Vcl=0.5$

Table 20-3 Average values by using cut off values $k>0.05$, $\phi>0.1$, $Vcl=0.5$ 15/9-17

| Well 15/9-17 | Gross | Net | N/G | phi | Sw | Vcl | KLOGHgeo | KLOGHarit |
|--------------|-------|------|-------|-------|-------|-------|----------|-----------|
| Skagerrak 9 | 9 | 5,34 | 0,594 | 0,206 | 0,328 | 0,172 | 19,337 | 47,505 |
| Skagerrak 8 | 5 | 5 | 1 | 0,21 | 0,312 | 0,175 | 22,264 | 41,14 |
| Skagerrak 7 | 8 | 3,72 | 0,465 | 0,211 | 0,318 | 0,366 | 23,4 | 51,856 |
| Skagerrak 6 | 10 | 2,29 | 0,229 | 0,236 | 0,318 | 0,27 | 58,885 | 175,982 |
| Skagerrak 5 | 6,82 | 0,38 | 0,056 | 0,225 | 0,351 | 0,278 | 11,925 | 17,17 |
| Skagerrak 4 | 6,18 | 3,43 | 0,555 | 0,215 | 0,319 | 0,273 | 8,471 | 13,651 |
| Skagerrak 3 | 5 | 0 | 0 | 0 | 0 | 0 | 0 | 0 |
| Skagerrak 2 | 17 | 8,53 | 0,502 | 0,226 | 0,317 | 0,223 | 12,464 | 33,341 |
| Skagerrak 1 | 6 | 5,6 | 0,933 | 0,233 | 0,323 | 0,28 | 42,804 | 52,935 |

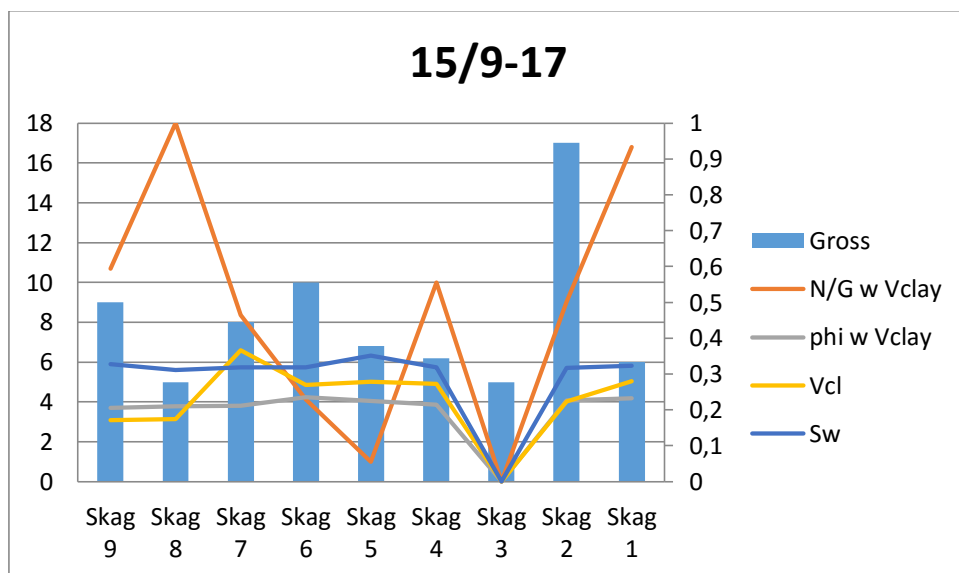


Figure 20-11 Average values from well 15/9-17, Cut offs: $k=0.05$ md, $\phi=0.1$, $Vcl=0.5$

20.2.3 Vclay Averages

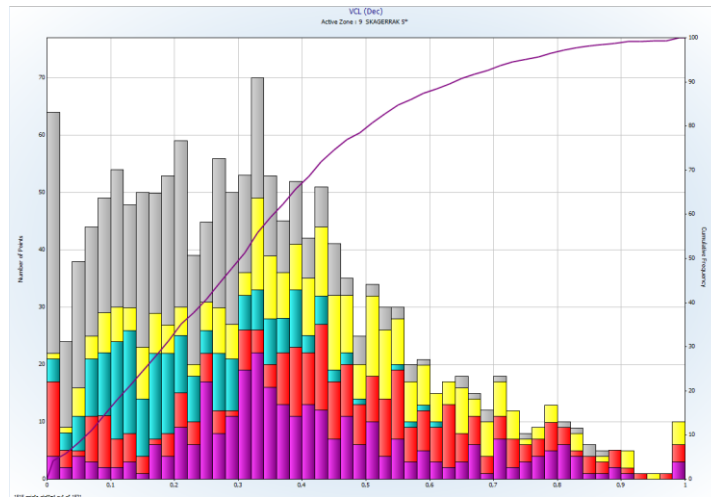


Figure 20-12 Vclay distribution in well 15/9-15

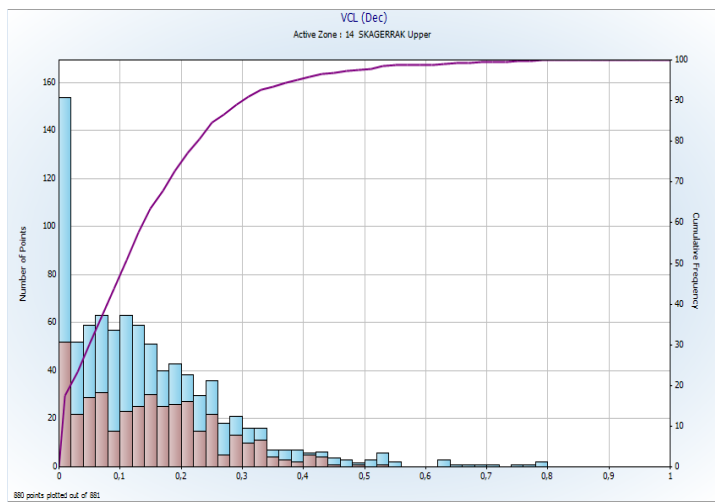


Figure 20-13 Vclay distribution in well 15/9-9

20.3 Water saturation methods

20.3.1 Swirr from Indonesia, Archie and Waxman Smits

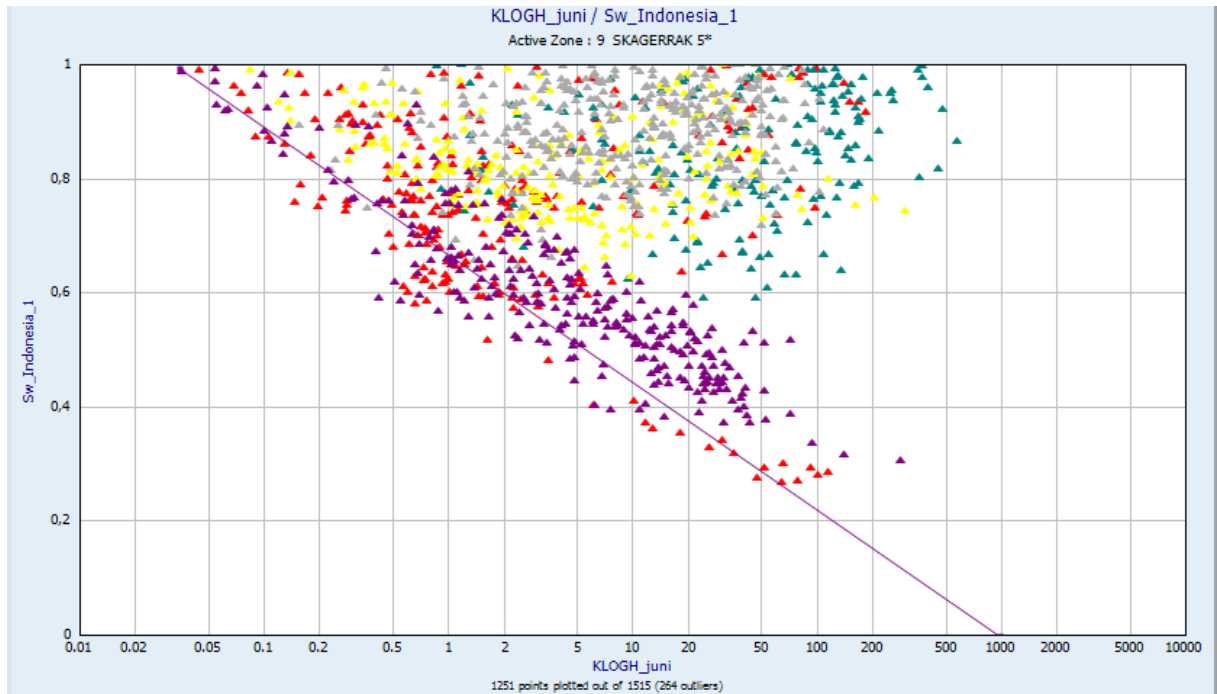


Figure 20-14 Watersaturation from Indonesia vs KLOGH 15/9-15

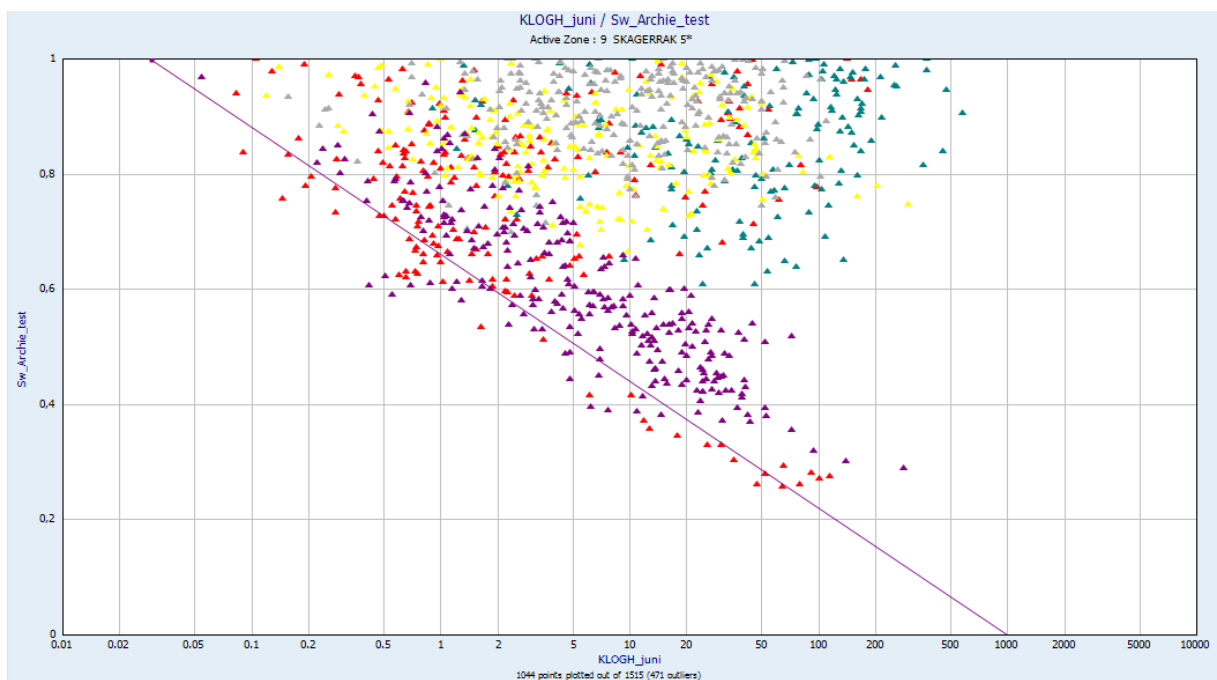


Figure 20-15 Water saturation from Archie vs.KLOGH well 15/9-15

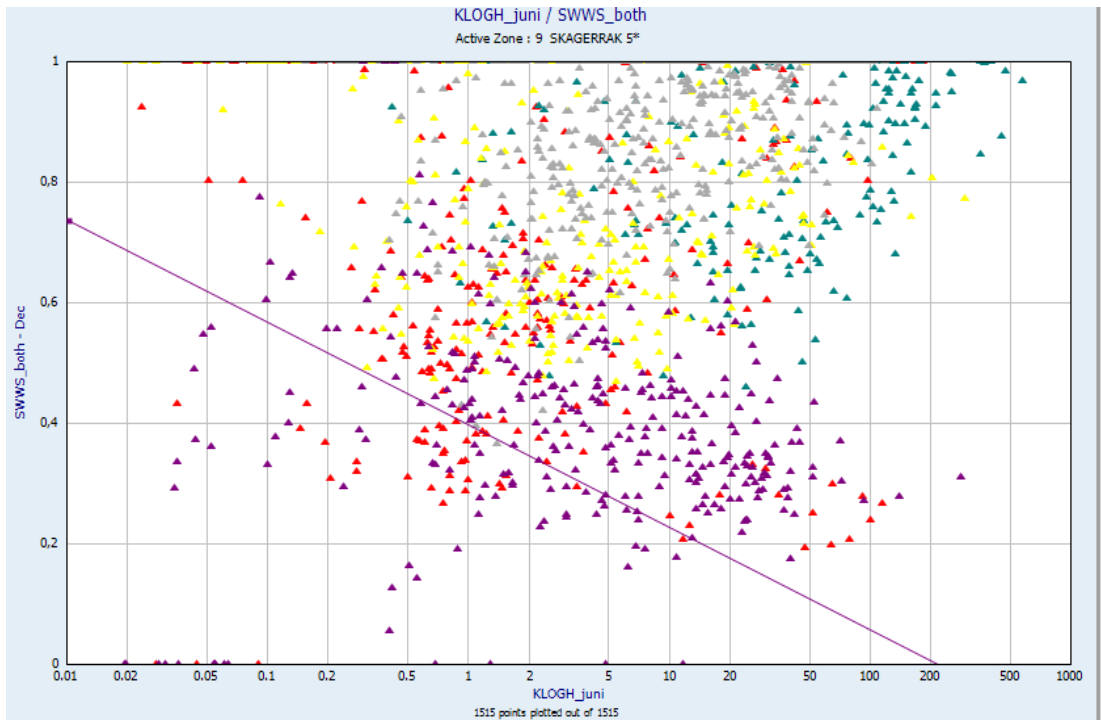


Figure 20-16 Water saturation from Waxman Smits vs KLOGH, well 15/9-15

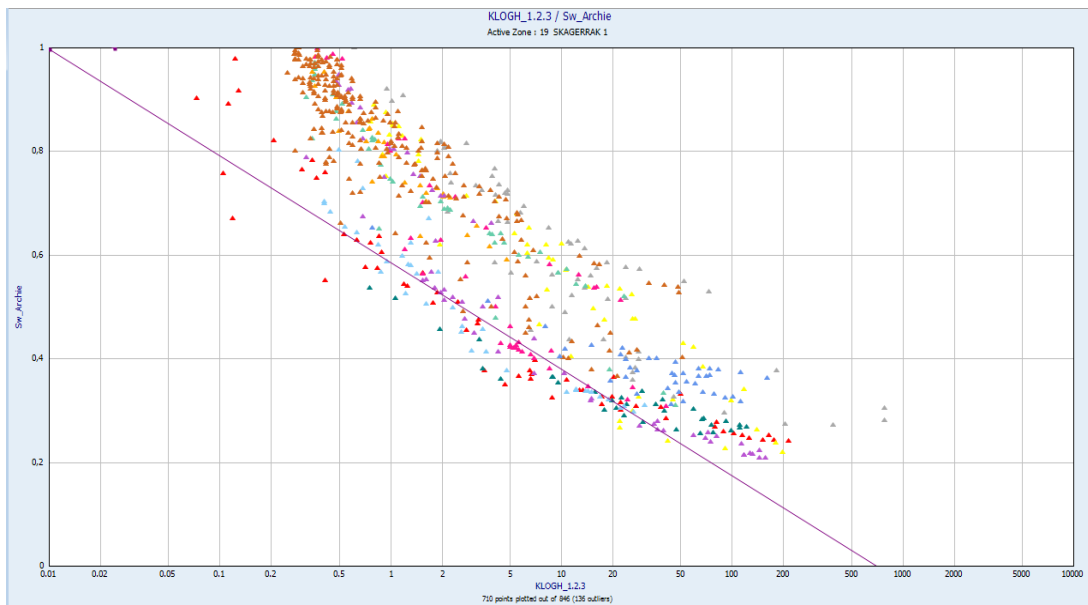


Figure 20-17 Water saturation from Archie vs. KLOGH, well 15/9-17

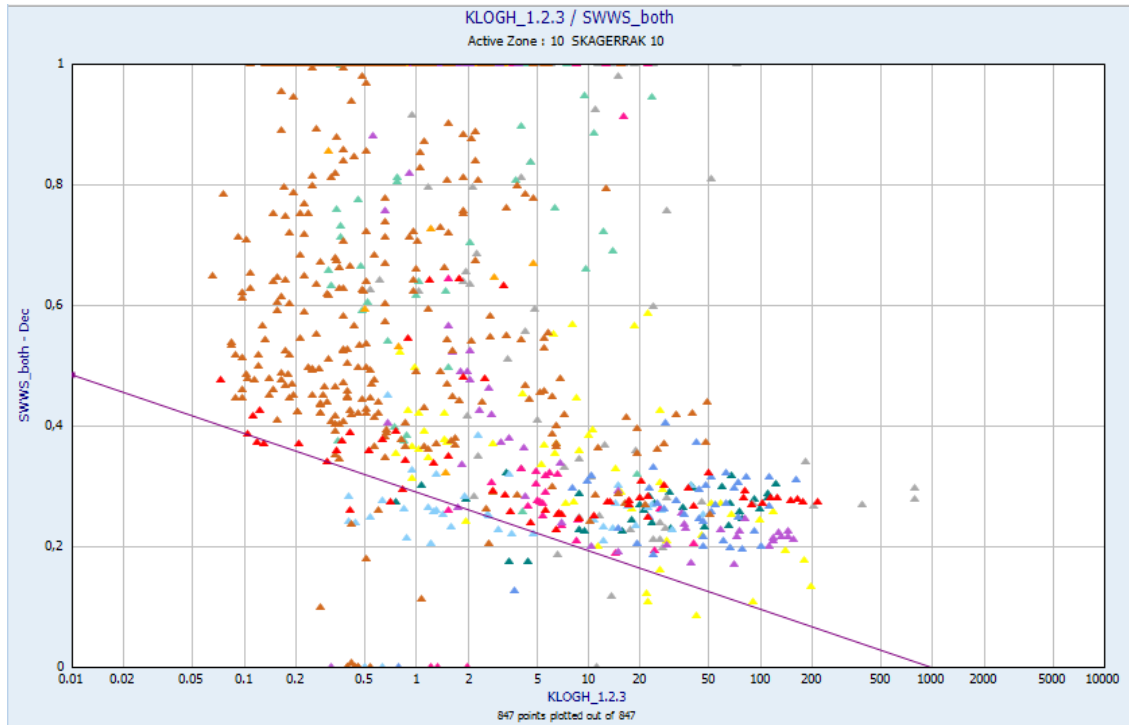


Figure 20-18 Water saturation from Waxman Smits vs. KLOGH well 15/9-17

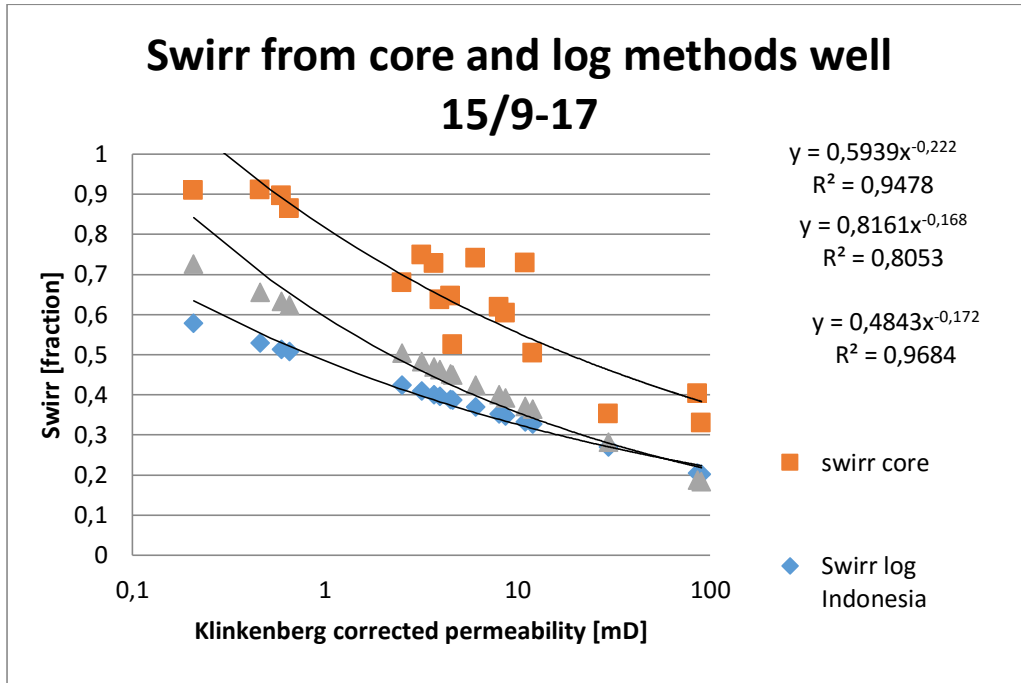


Table 20-4 Swirr determined from core and log methods

| Well 15/9-17 | Swirr log= a-b*log(permeability) swirr core=a*perm^(-b) | |
|--------------|---|-----------|
| Method | a | b |
| Cores | 0.8161 | -0.168 |
| Indonesia | 0.481336 | -0.143018 |
| Archie | 0.58586 | -0.205775 |
| Waxman Smit | 0.290844 | -0.097107 |

20.3.2 Swn determined from logs

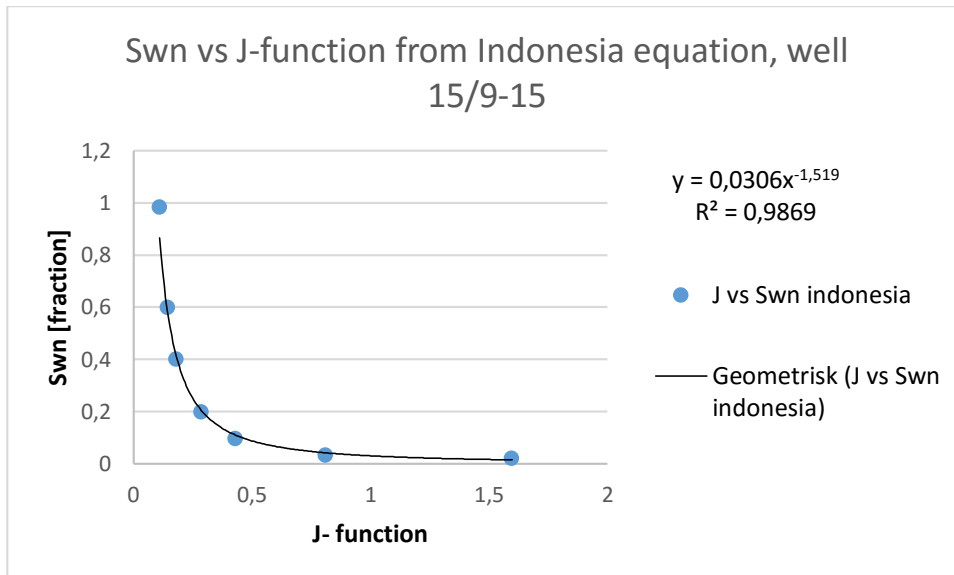


Figure 20-19 Swn vs J-function from Indonesia Equation, well 15/9-15

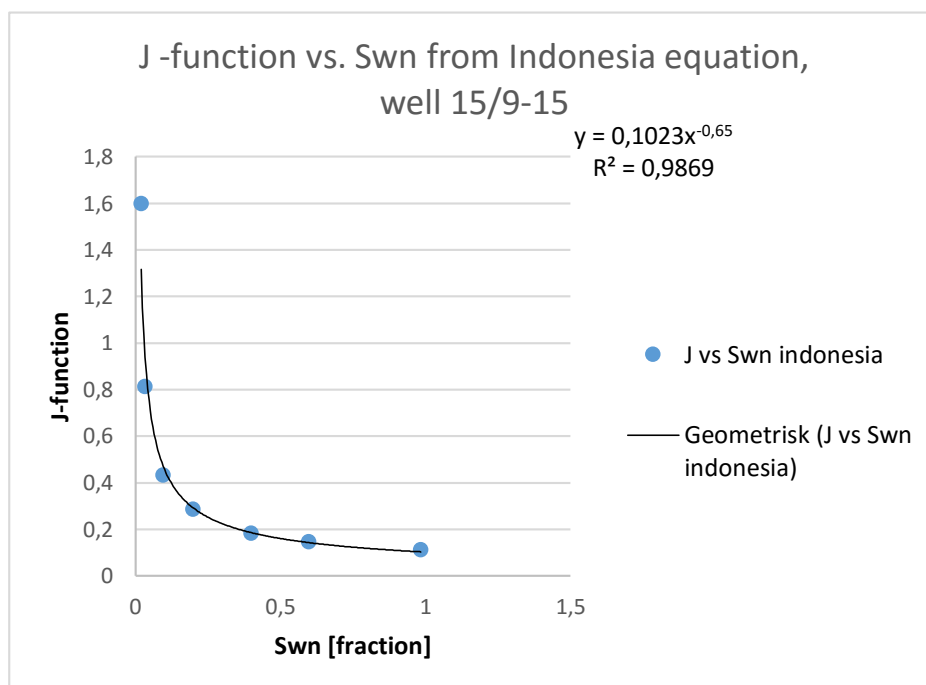


Figure 20-20 J-Indo from Indonesia Equation, well 15/9-15

Table 20-5 a and b determined from log methods, well 15/9-15

| Well 15/9-15 | $S_{wn} = a * J^{-b}$ | |
|---------------------------|-----------------------|--------|
| Water saturation equation | a | b |
| Indonesia | 0.0306 | -1.519 |
| Waxman Smits | 0.0533 | -1.565 |
| Archie | 0.2636 | -1.002 |
| Core | 0.0297 | -1.076 |

20.3.3 Determination of B in the Waxman Smits Method

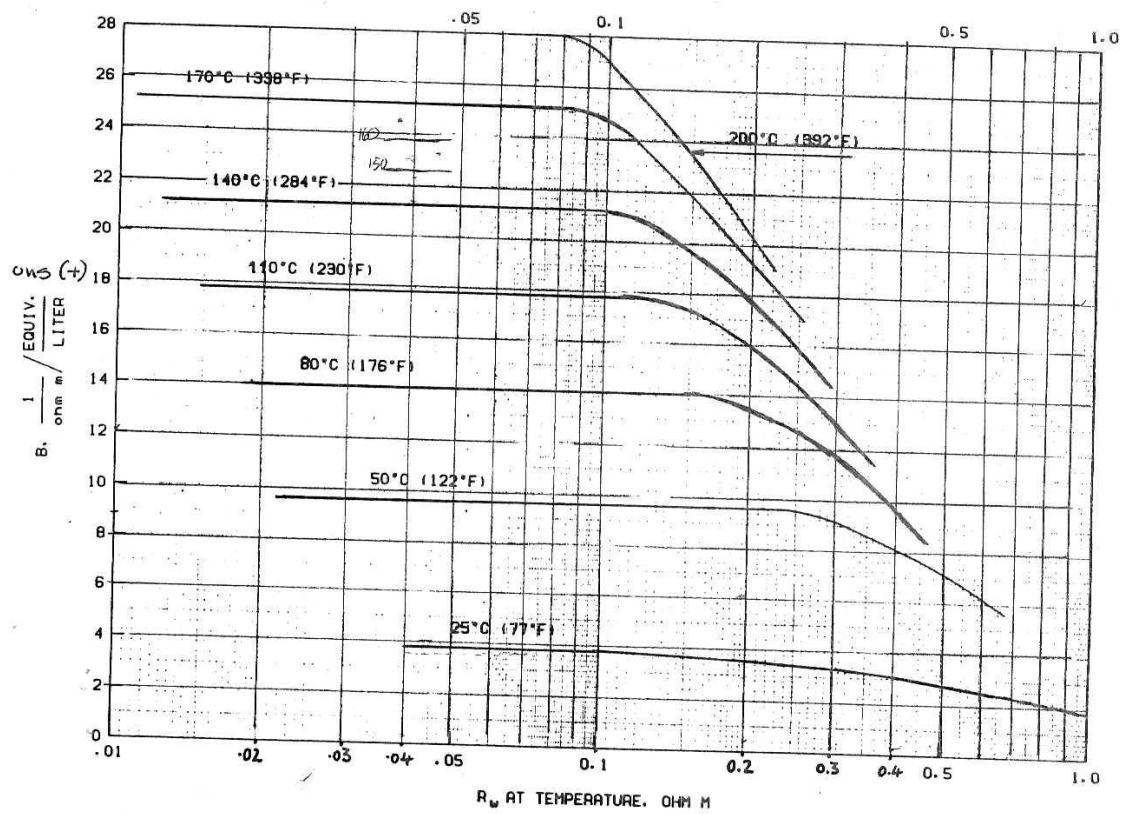


Figure 20-21 Waxman Smits B $R_w T$